NV CENTERS IN DIAMOND AS A PLATFORM FOR QUANTUM TECHNOLOGIES

Sergei Kilin
Center of quantum optics an quantum information ,
B.I.Stepanov Institute of Physics NASB, Minsk

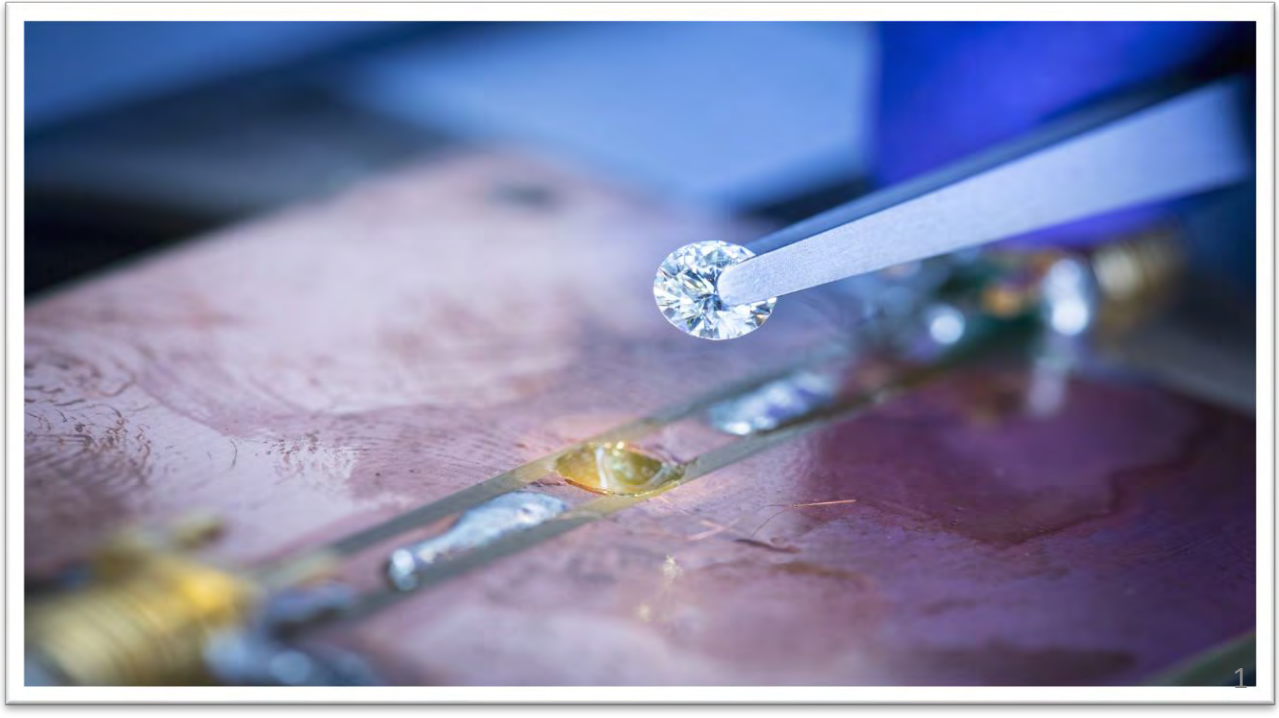

Квантовая суперпозиция

Случайность

Хоста

Миасс

?????

Квантовая перепутанность

Прогноз отдельного события возможен только вероятностно

Why NV

Quantum objects are automatically fixed in the solid, and the qubits maintain their position even in the case of the failure of technical devices.

The defect-free isotopic ^{12}C diamond crystal, with its large bandgap of 5.4 eV, has properties similar to those of a vacuum; thus, a point defect center can be compared to an atom in a trap.

The large bandgap ensures that even at room temperature, the conduction band remains unoccupied and no free electrons can unintentionally interact with the qubits.

A high Debye temperature of over 1800K so that few phonons disturb the system.

The low diffusion constants of almost all elements enable the atoms to retain their positions even at temperatures of several hundred Kelvin.

Because of the well-defined properties of defects based on single atoms, all quantum devices have similar electronic structures, spectral lines, and spin properties.

NV ID (2021)

Quantum chips:	Value	Refs.	Remarks
Number of qubits demonstrated	7 qubits	75	Entangled GHz state
	10 qubits	75	Fully connected
	29 qubits	76	Rudimentary qubits controlled
Chip linked	2	120	Optical interconnection
Coherence			
T_2 (e qubit)	2.4 ms	69	Temperature 300 K
	0.6 s	121	77 K
	1.5 s	70	4 K
T_2 (n qubits)	2 s	9	300 K
	1 min	75	4 K
T_1 (e qubits)	>1 h	70	4 K
T_1 (n qubits)	>6 min	75	4 K
Control gates			
Fidelity: single qubit gate	99.995%	78	300 K
Fidelity: two qubit (e-e)	>97%	122	300 K
Fidelity: (e-n)	99.2%	78	300 K
Speed: single qubit gate (e)	<10 ns	38	300 K
Speed: two qubit gate (e-n)	700 ns	78	300 K
Measurement			
Fidelity (e)	98%	120	
Projectiveness	>99%	123	Post-measurement state
Measurement time	3 μs	120	
Fidelity three-qubit parity measurement	0.63	123	
Initialization			
Fidelity	99.9%	124	Excitation of electron
Speed	200 ns	88	Excitation of electron
Chip to chip interconnection			
Entanglement fidelity	92%	120	
Distance	>1 km	120	
Sub routines			
Algorithm: Q-search		125	Temperature 300 K
Algorithm: Q simulation		126	300 K
Quantum error correction	3-qubit code	91	300 K
Logical qubits		92	4 K

Sebastien Pezzagna and Jan Meijer, Appl. Phys. Rev. 8, 011308 (2021); doi: 10.1063/5.0007444

SINGLE SPINS HARNESSING: NV CENTERS IN DIAMOND

A. Gruber,
Ch. von Borczyskowski
Chemnitz, 1997

Wrachtrup, 97
→ single NV centers

Wrachtrup, Kilin, Nizovtsev, 01
→ WKN paper: ^{13}C nuclear spins, Q memory & Q reristers

Jelezko, 04
Lukin 06, 07, 08
Awshalom
.....
EQUIND (FP6), 06-10

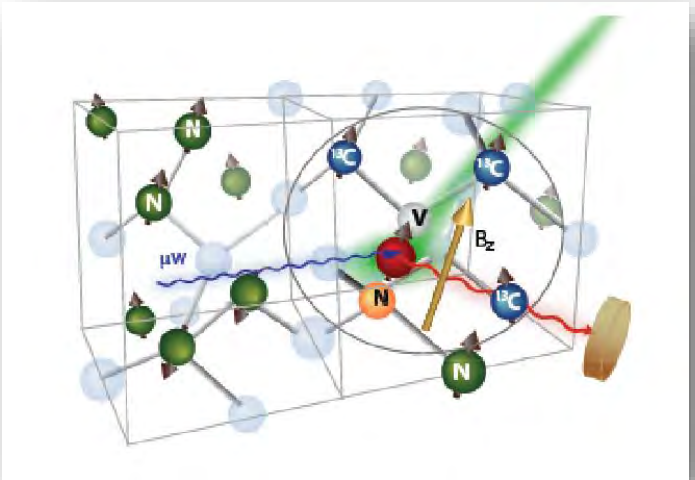

Grand Challenges:

→ to manipulate coherently with individual nuclear spins (Q physics)
→ to suppress spin decoherence (Material science)
→ to understand properties of NV+n^{13}C spin systems (Q chemistry).

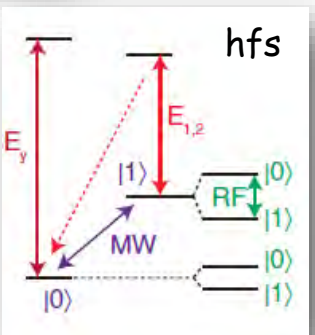

NV ID

✔ **Structure**

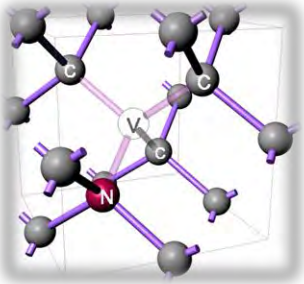

✔ **Single NV photo**

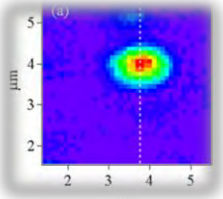

✔ **Simple Energy diagram**

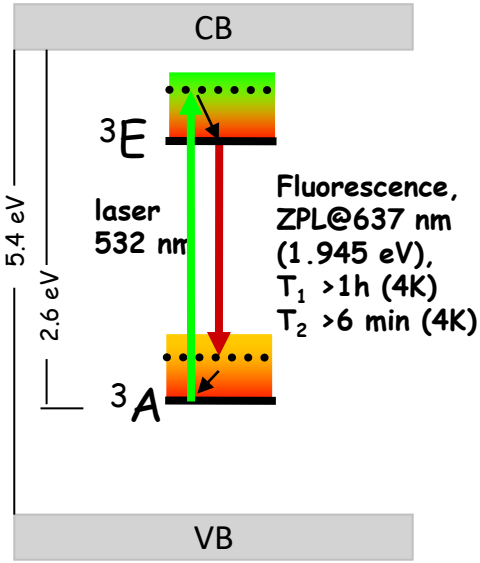

✔ **Configurational diagram**

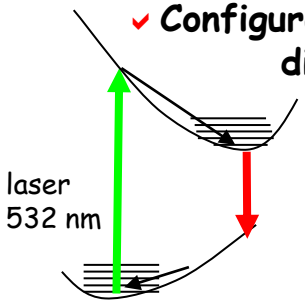

✔ **Abs./ Em. Spectra**

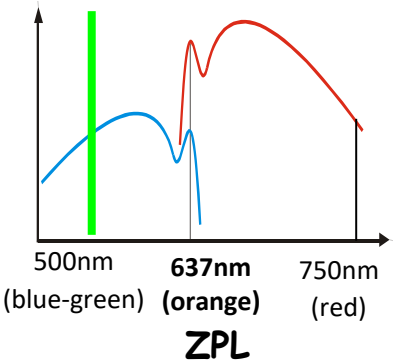

- C_{3v} symmetry, 6 e^- model,
- Paramagnetic ground state (S = 1)
- Perfectly photostable

NV GROUND STATE CONFIGURATION AND ODMR SPECTRA

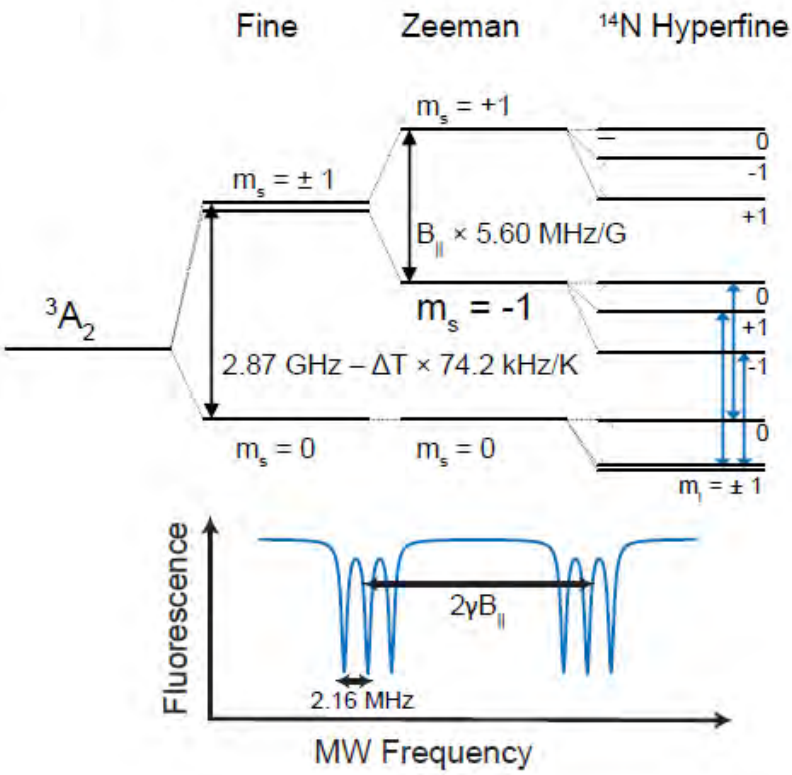

NV RADIATIVE AND NON-RADIATIVE STATE TRANSITIONS

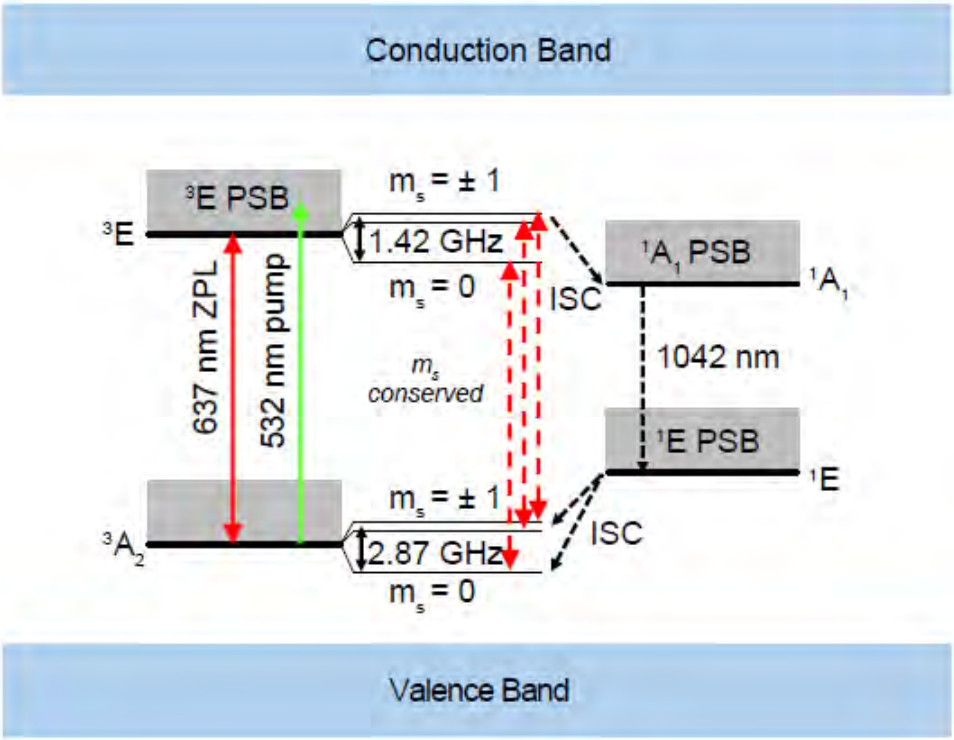

ПРИРОДНЫЕ АЛМАЗЫ

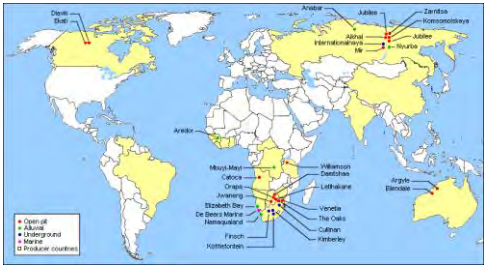

Старейшая шахта – Южная Африка, Кимберли

Крупнейшая шахта – Россия, Мирный (h=525 m, D=1.2 km) 1957-2001

PROGRESS IN DIAMOND ENGINEERING

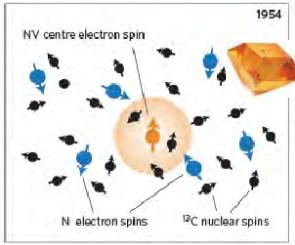

HTHP

CVD '56

GDTFWvB (1997)

WKN (2001)

Man beats Nature

CVD

Element 6

T_2~ 1μs,
^{13}C~ 1,1%,
N > 1000 ppb

T_2~ 100μs,
^{13}C~ 1,1%,
N < 10 ppb

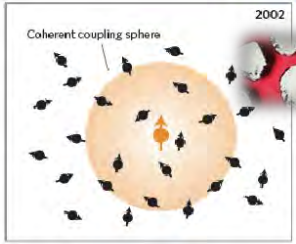

2006 EQUIND

ULTRA-PURE CVD

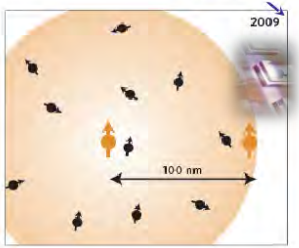

T_2~ 1,8 ms
^{13}C~ 0,3%
N < 0,05 ppb
<10^{13} cm^{-3}

Towards Large Scalable QC:
Progress in diamond engineering

Recent (E6)

T_2> 10 ms
^{13}C~ 0,01%

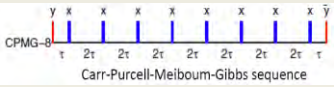

Plus dynamical control (CPMG-8) → T_2~ 1sec
Lukin et.al. 2012

10

NANODIAMONDS

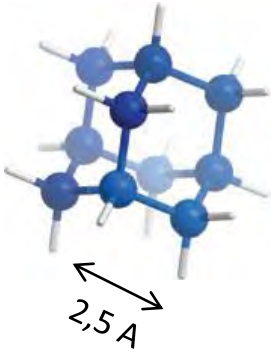

Adamantane

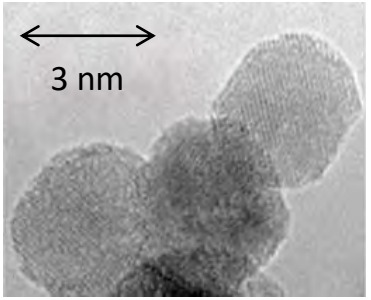

Detonation nanodiamonds

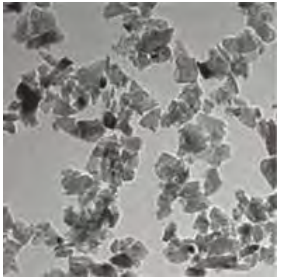

ND produced by mechanical grinding

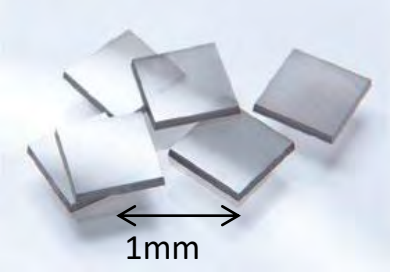

Millimeter-sized single-crystal CVD diamond

АЛМАЗ КВАНТОВОЙ ЧИСТОТЫ

Изотоп: 99.999% ^{12}C

Концентрация примесей:
ниже 10^{12} cm^{-3}

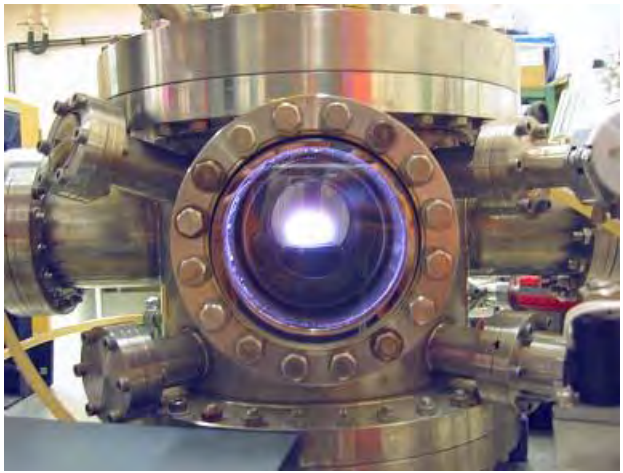

University Paris XIII (Villtaneuse) J. Achard

D. Twitchen, Element 6 Ltd

CHEMISTRY: SPACE STRUCTURE

NV^-

The electronic structure of the NV center involves six electrons. Two are provided by the nitrogen atom, and another three are dangling bonds from the three carbon atoms surrounding the vacancy.

Углерод – $1s^2 2s^2 2p^2$ (двухвалентен)
В кристалле – sp^3 гибридизация -
$1s^2 1s 2p^3$ (четырехвалентен)

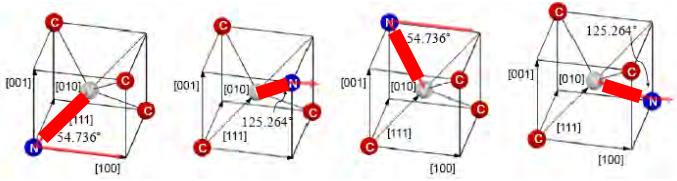

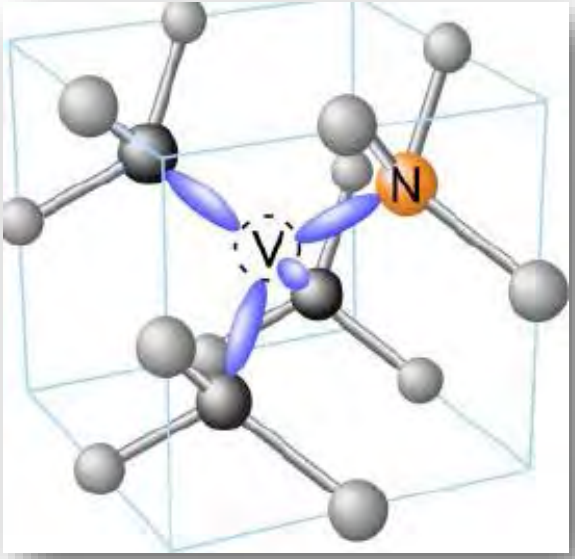

The sixth electron is captured from the lattice (typically, nitrogen donors), making the overall charge state NV^-.

DIAMOND LATTICE

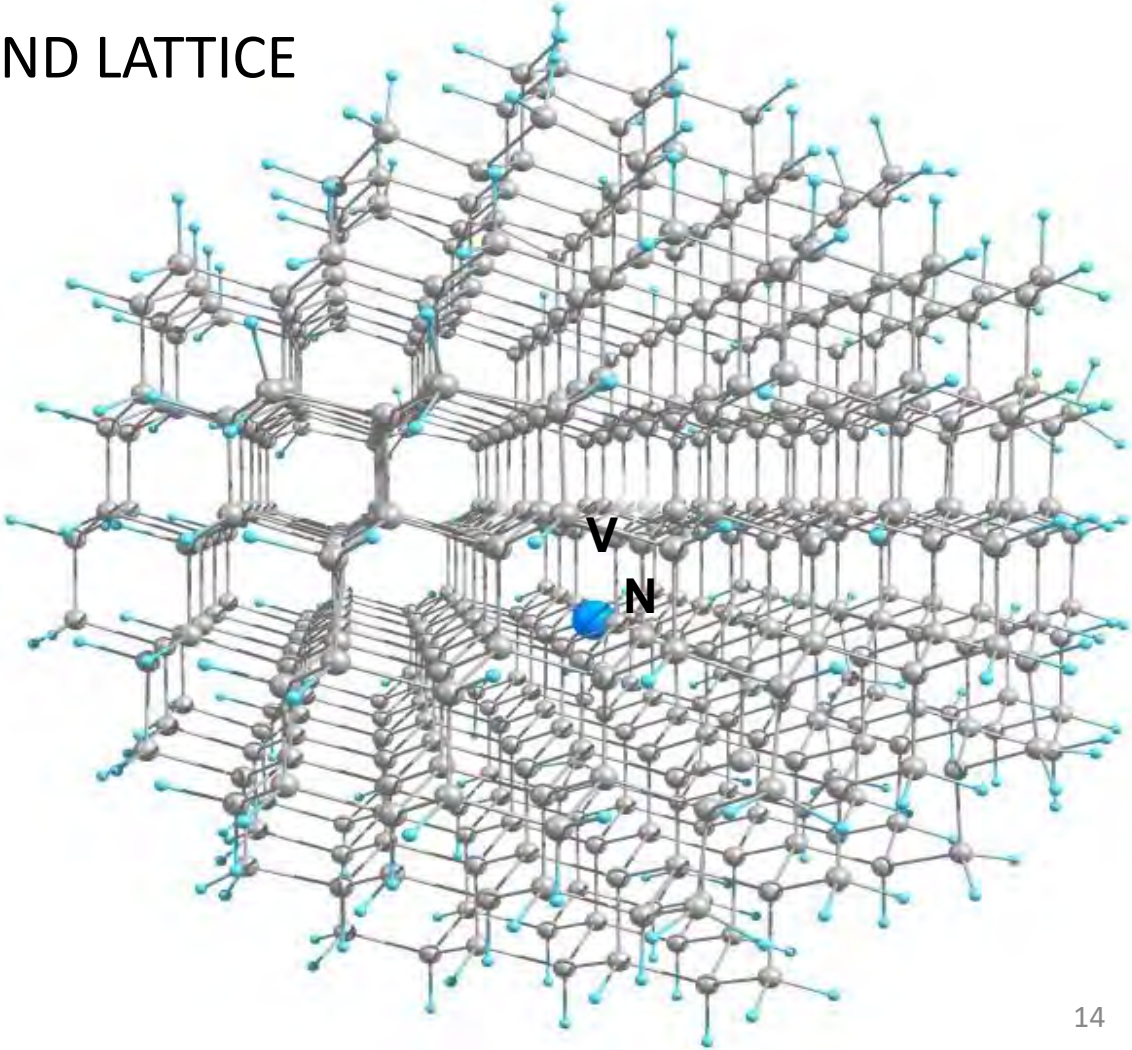

DIAMOND LATTICE RELAXATION AROUND NV CENTER

(By simulation of the cluster $C_{291}[NV]H_{172}$)

Unrelaxed

8C element
of diamond lattice

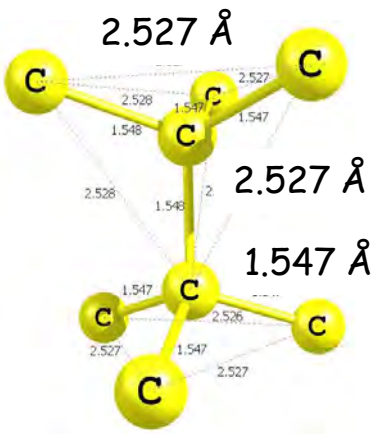

Remove one C atom and change
the other one for the N atom

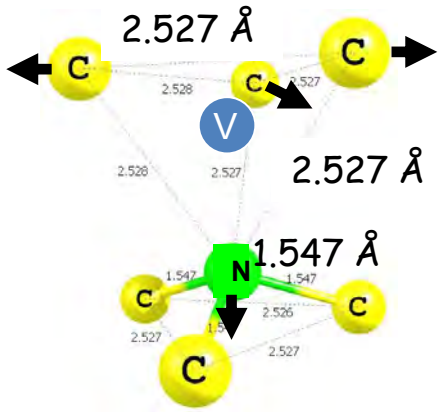

Relaxed

NV+6C element
of diamond lattice

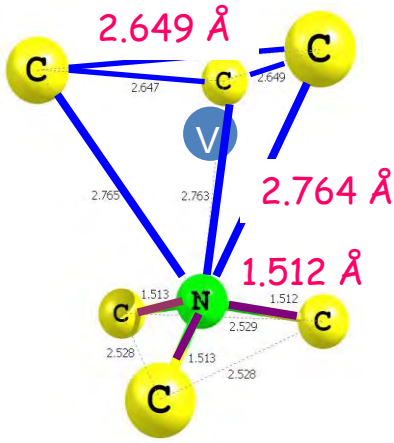

Due to relaxation:

- atom N moves to the plane where the three nearest C atoms are disposed resulting in the reduction of the distance between N atom and nearest C atoms;
- three C atoms, being nearest neighbors of the vacancy, moves away from each other and from the N atom

SPIN DENSITY

TOP VIEW

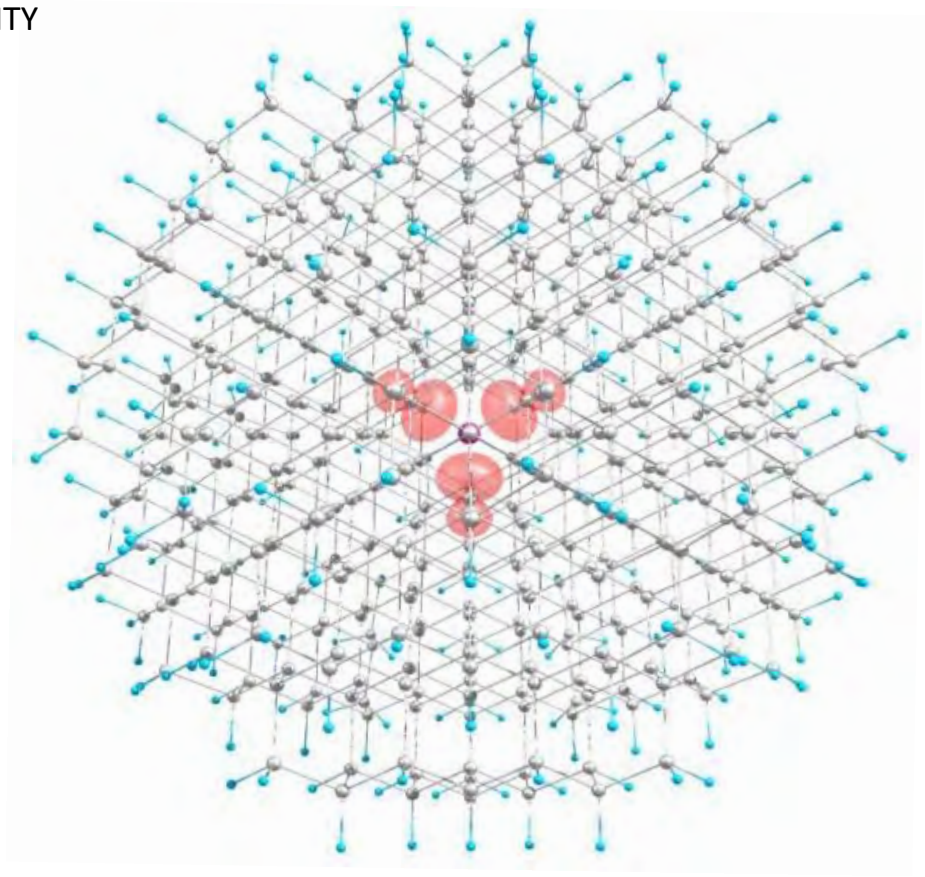

SPIN DENSITY

TOP VIEW

X 100

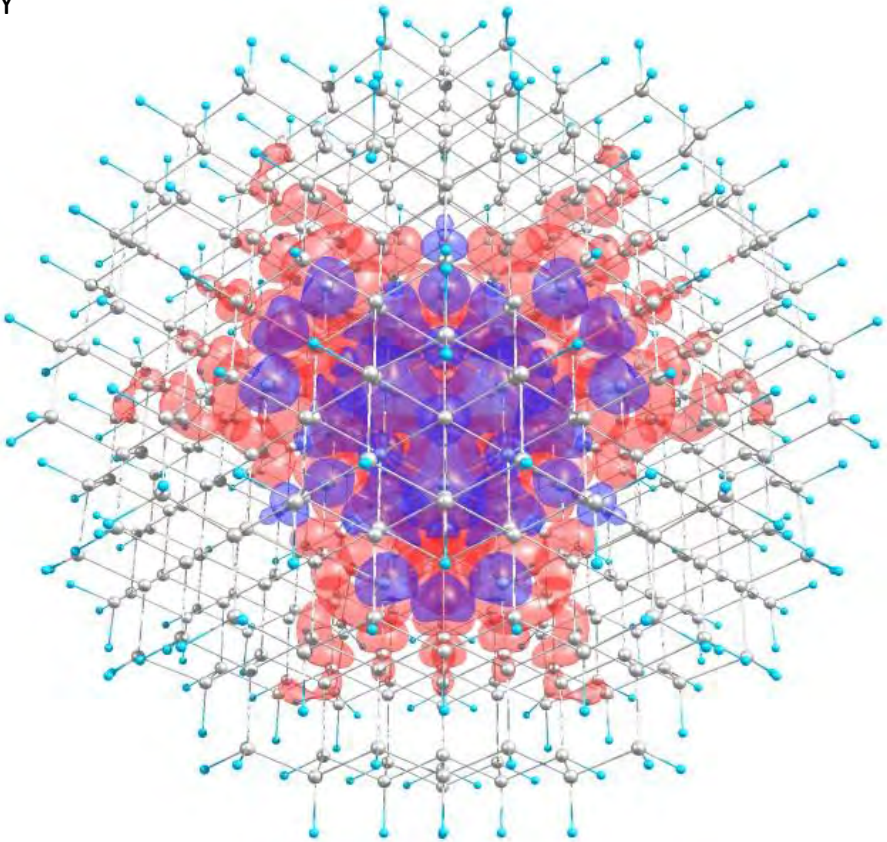

SPIN DENSITY

SIDE VIEW

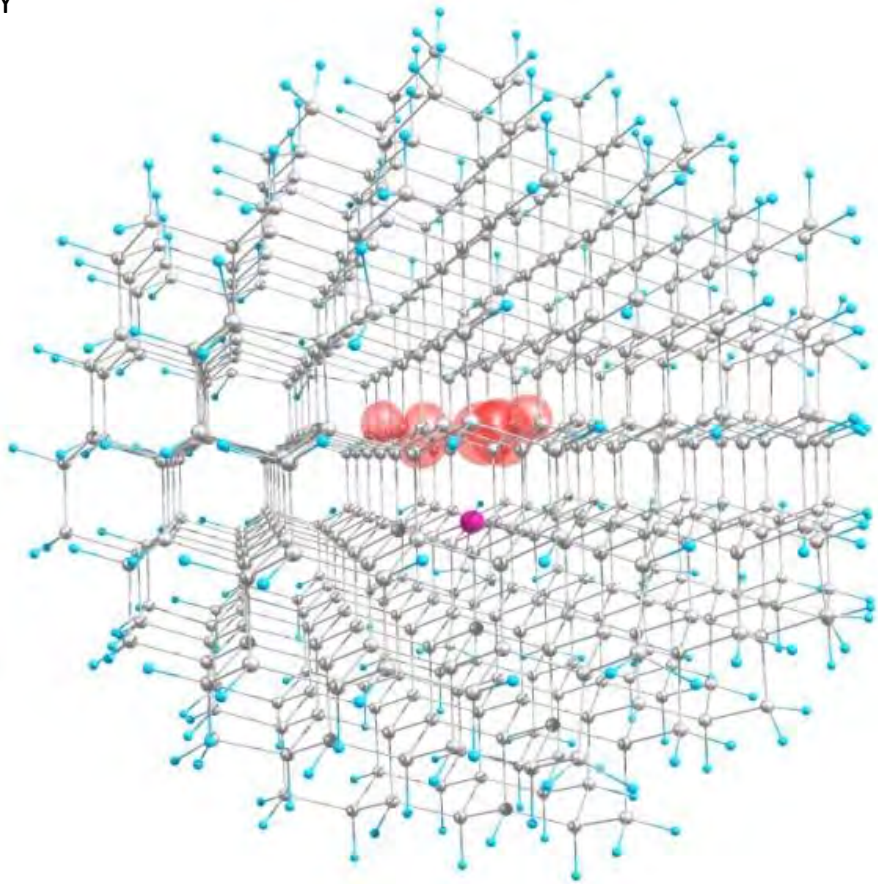

SPIN DENSITY

SIDE VIEW

X 100

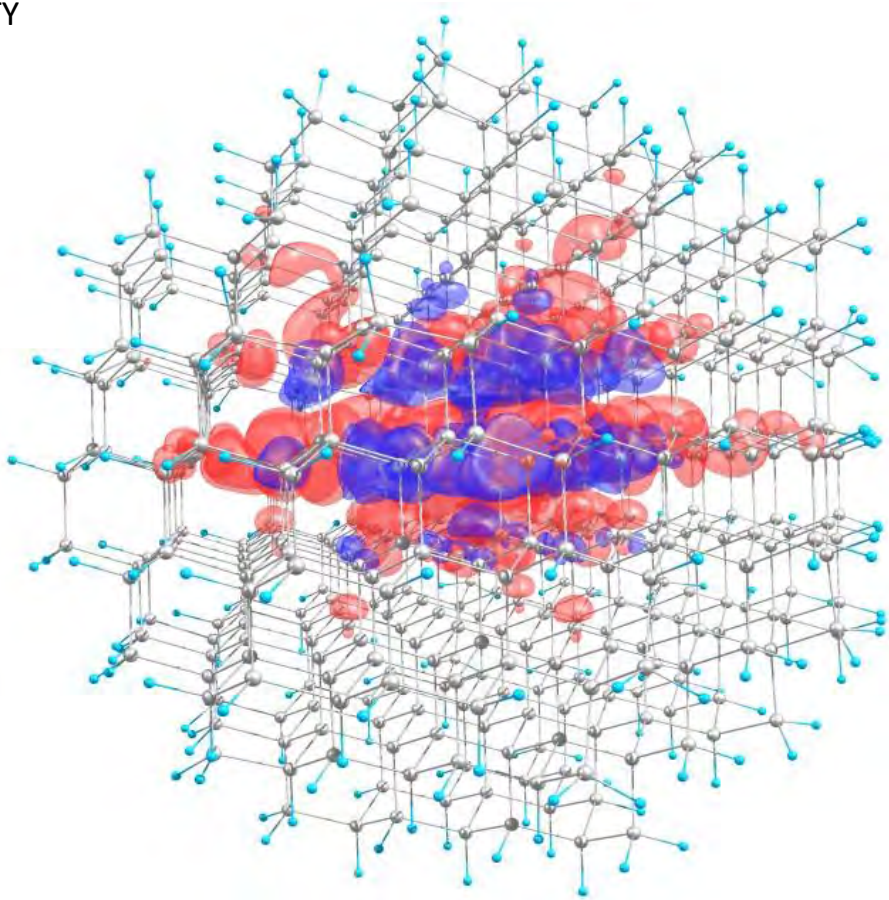

PHYSICS: HAMILTONIAN OF NV INTERACTIONS

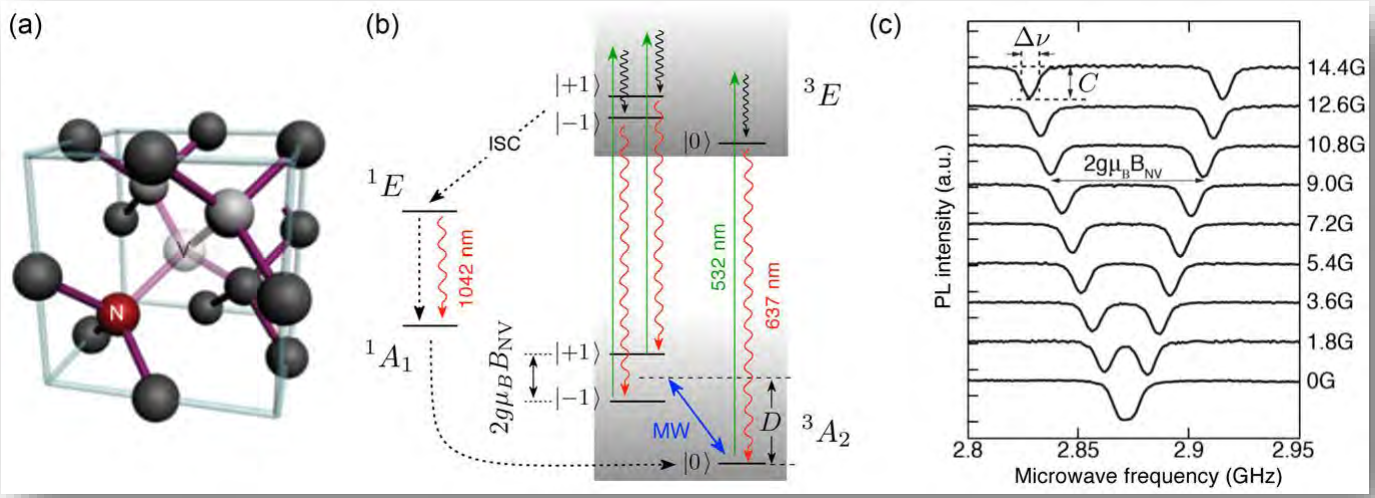

$$\frac{\mathcal{H}}{\hbar} = \underbrace{D\left(S_z^2 - \tfrac{2}{3}\right)}_{\text{zfs}} + \underbrace{\gamma \mathbf{B}\cdot\mathbf{S}}_{\text{magnetic}} + \underbrace{\epsilon_z E_z\left(S_z^2 - \tfrac{2}{3}\right) + \epsilon_{xy}\left\{E_x\left(S_x S_y + S_y S_x\right) + E_y\left(S_x^2 + S_y^2\right)\right\}}_{\text{electric}}$$

D ← spin–spin interaction between the two unpaired electrons of the defect

e_{xy} ← strain

Coupling coefficients and typical sensitivities

$$\frac{\mathcal{H}}{\hbar} = \underbrace{D\left(S_z^2 - \tfrac{2}{3}\right)}_{\text{zfs}} + \underbrace{\gamma \mathbf{B}\cdot\mathbf{S}}_{\text{magnetic}} + \underbrace{\epsilon_z E_z\left(S_z^2 - \tfrac{2}{3}\right) + \epsilon_{xy}\{E_x\left(S_xS_y + S_yS_x\right) + E_y\left(S_x^2 + S_y^2\right)\}}_{\text{electric}}$$

Property	Coupling coefficient		Typical sensitivity[a]
Magnetic field[b]	γ	28 GHz/T	0.36 μT/$\sqrt{\text{Hz}}$
Electric field[b]	ϵ_z	0.17 Hz/(V/m)	5.8 kV cm^{-1}/$\sqrt{\text{Hz}}$
Electric field[c]	ϵ_{xy}	3.5×10^{-3} Hz/(V/m)	280 kV cm^{-1}/$\sqrt{\text{Hz}}$
Strain[d]	$\sim\epsilon_{xy}/d$[c]	$\sim 10^{11}$ Hz/($\delta l/l$)	$\sim 10^{-7}/\sqrt{\text{Hz}}$
Orientation[e]	γB	100 kHz/°	0.1°/$\sqrt{\text{Hz}}$
Temperature	$\partial D/\partial T$	−74 kHz/K	0.13 K/$\sqrt{\text{Hz}}$
Pressure	$\partial D/\partial P$	1.5 kHz/bar	6.8 bar/$\sqrt{\text{Hz}}$

[a]Typical sensitivity for DC detection assuming a frequency resolution of 10 kHz/$\sqrt{\text{Hz}}$.
[b]Longitudinal ($\theta = 0°$), where θ is the angle between the nitrogen-vacancy axis and the electric field.
[c]Transverse ($\theta = 90°$).
[d]$d \approx 3 \times 10^{-13}$ (V/m)$^{-1}$ is the local piezoelectric coupling coefficient (67).
[e]At a transverse magnetic field of 1 mT.

EXPERIMENTS

GROWTH

CVD

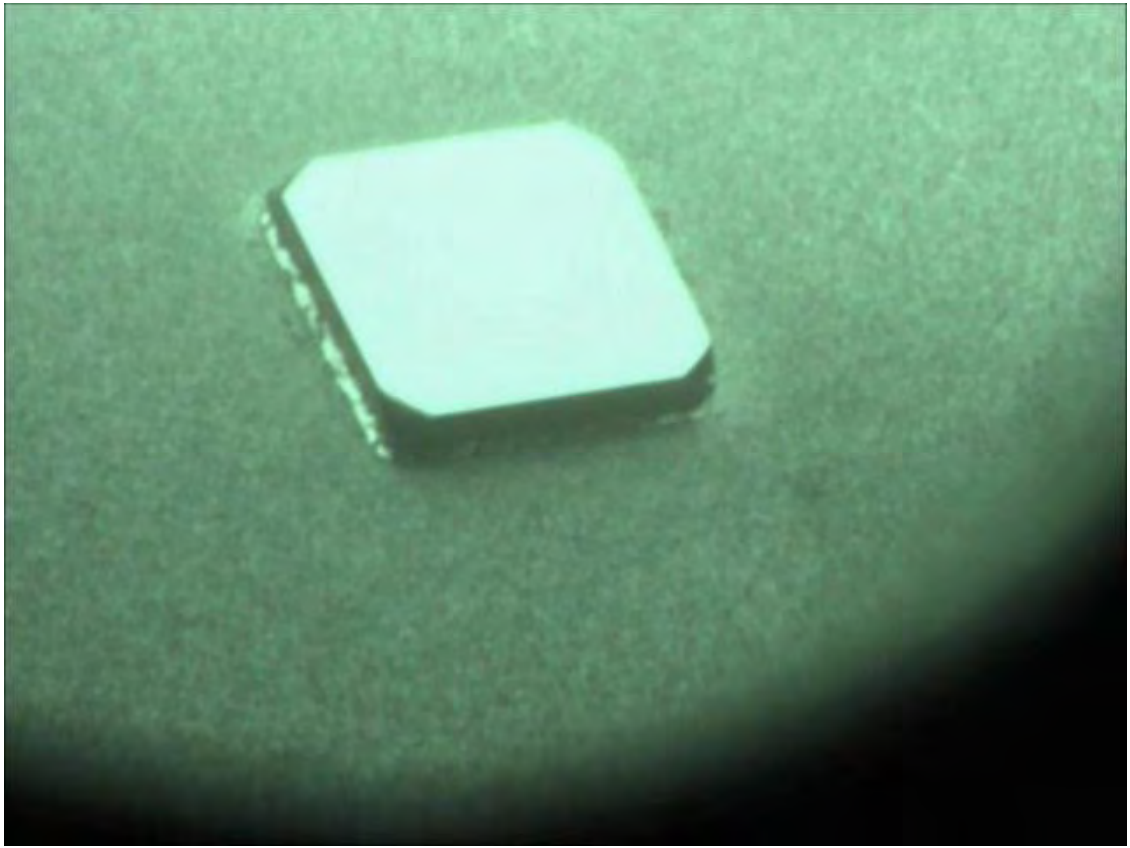

Courtesy of D. Twitchen, E6 Ltd

ISOTOPIC AZA-ADAMANTANE – A SEED OF NANODIAMOND

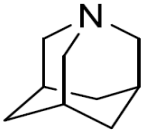

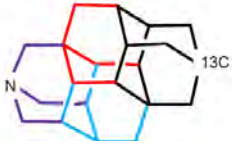

ACS Photonics

Article

Cite This: ACS Photonics 2019, 6, 1266−1271

pubs.acs.org/journal/apchd5

Growth of High-Purity Low-Strain Fluorescent Nanodiamonds

Masfer Alkahtani,[*,†,‡] Johannes Lang,[¶] Boris Naydenov,[¶,§] Fedor Jelezko,[¶] and Philip Hemmer[†,∥,⊥]

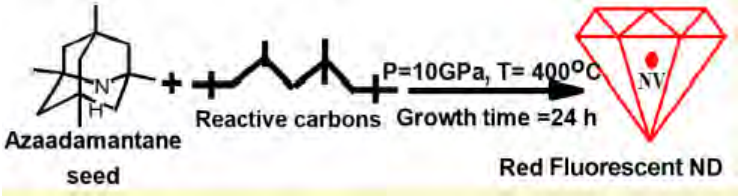

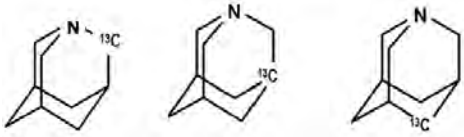

1-AZA-ADAMANTANE +^{13}C -> THE NV-^{13}C SYSTEM

Precursors –
1,2 aza-adamantane

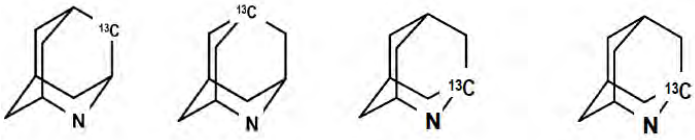

2-AZA-ADAMANTANE +^{13}C -> THE NV-^{13}C SYSTEM

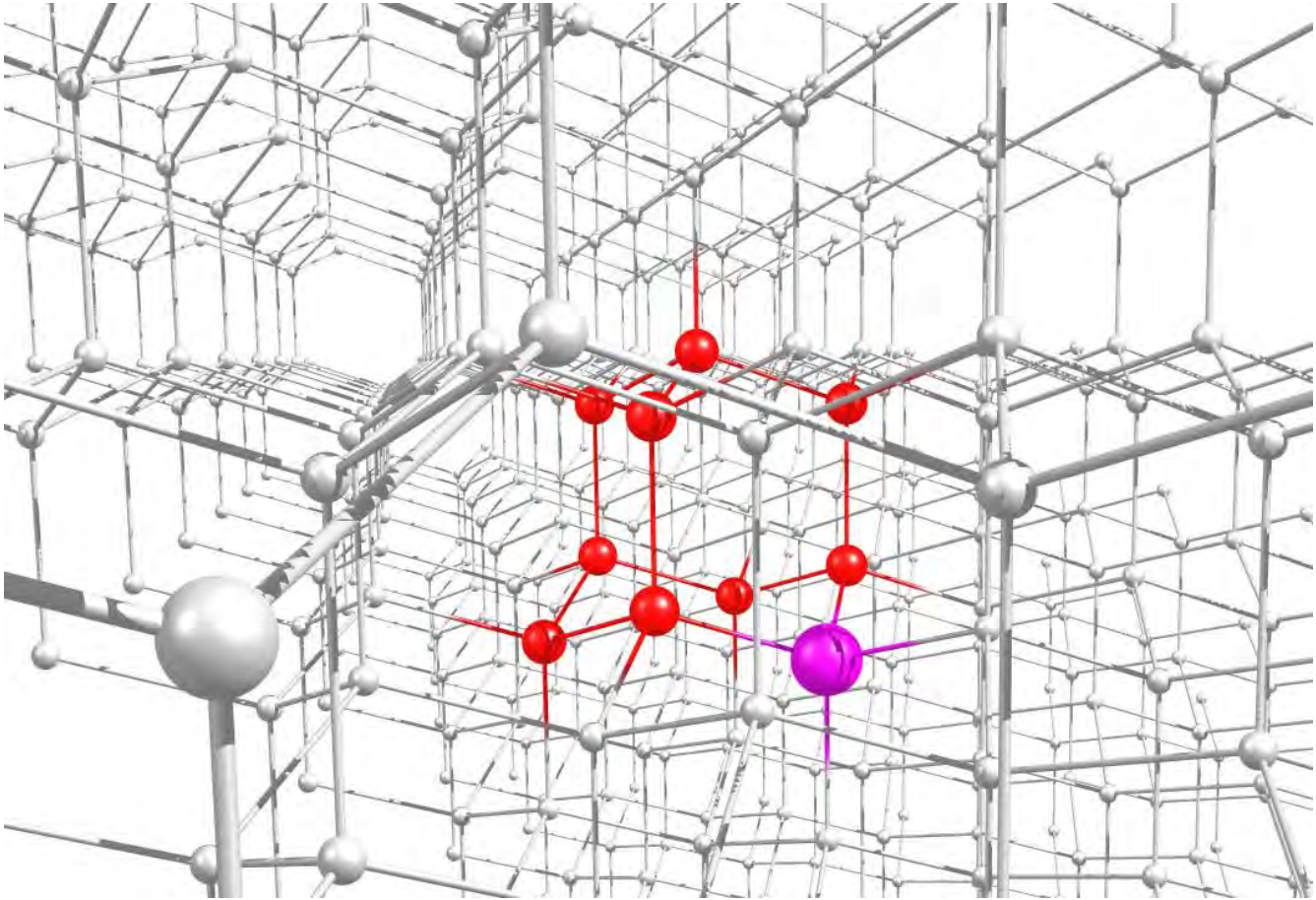

TEST SIMULATION – ADAMANTANE MOLECULE $C_{10}H_{16}$

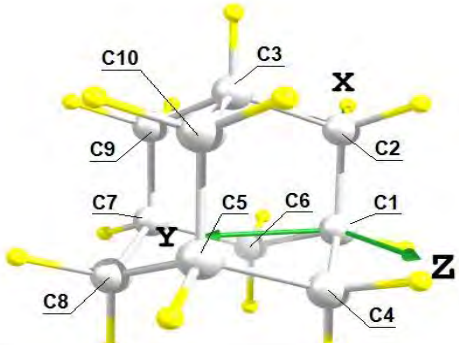

Эксперимент

$^{1}J_{iso}$=31.4±0.5 Гц

JOURNAL OF MAGNETIC RESONANCE **91.** 186–189 (1991)
IAN D. GAY, C. H. W. JONES, AND R. D. SHARMA

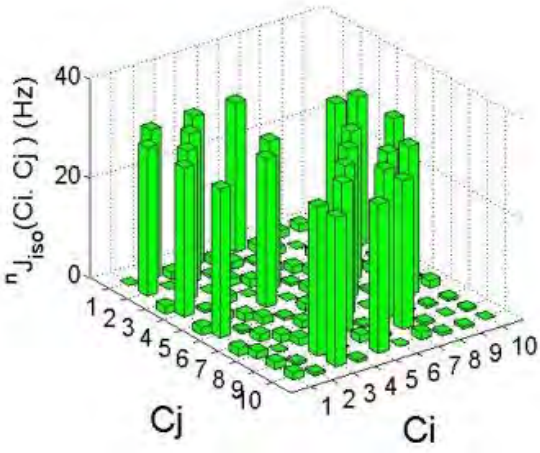

Теория

$^{1}J_{iso}$=29.9 Гц

We have used **ORCA 5.0.2 software package with the B3LYP/def2/J/RIJCOSX level of theory** and then simulated the n-bond *J*-coupling tensors $^{n}J_{KL}$(Ci,Cj) for all possible ^{13}Ci-^{13}Cj pairs in the clusters using B3LYP/TZVPP/AUTOAUX/decontract level of theory. The functional B3LYP in combination with TZVPP basis is recommended for NMR calculations by ORCA [21, 22].

IMPLANTATION

Creation of diamond defects

Ion beam

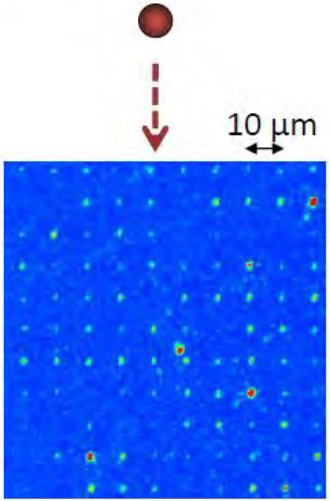

J Meijer APL 2006
J Rabeau APL 2006

Nanoaperture

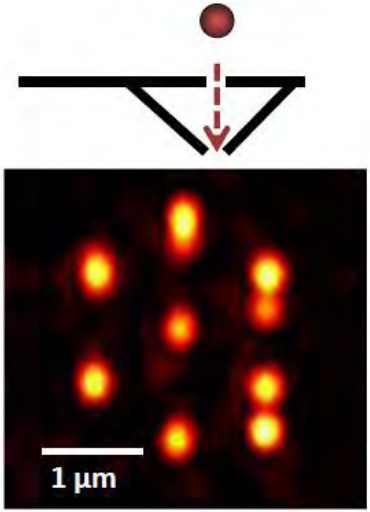

S Pezzagna Small 2010

Large scale nanolithography

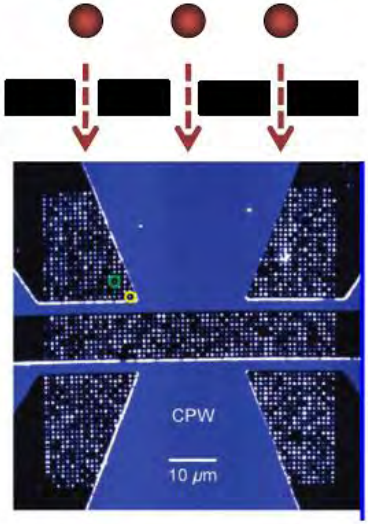

DM Toyli, D. Aschalom Small 2010

Positioning accuracy: 10nm

Nanoapertures assisted implantation

Collaboration: Jan Meijer, Leipzig

- Success chance ~1 %

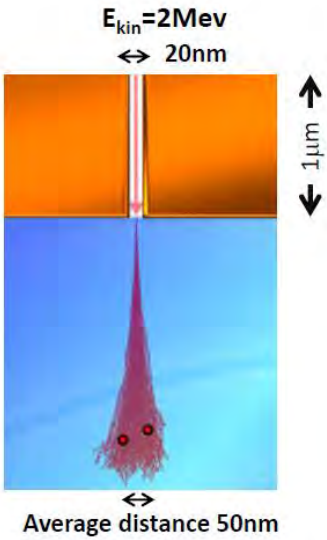

mica

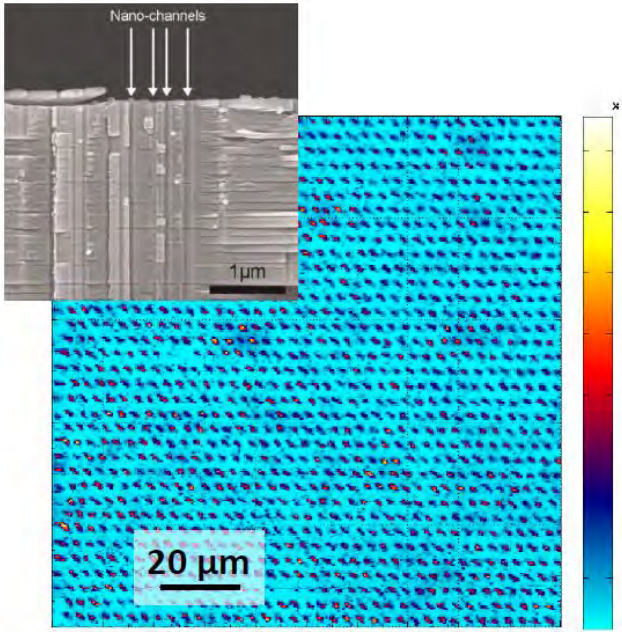

Entanglement between two electron spins, Dolde et al., Nature Physics (2013)

Deterministic single ion implantation out of a Paul trap

Collaboration
J. Meijer, F. Schmidt-Kaler

Proposal J. Meijer *et al.*, Applied Physics A 83, 321 (2006)
Experiment: K. Groot-Berning et al., NJP 23 063067 (2021)

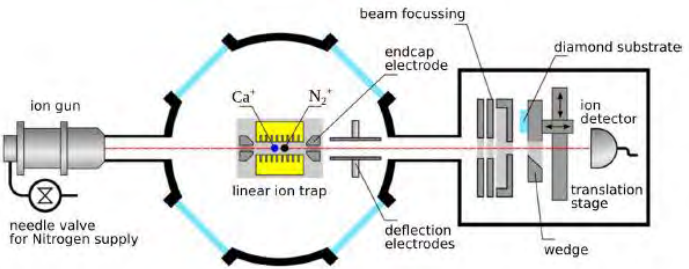

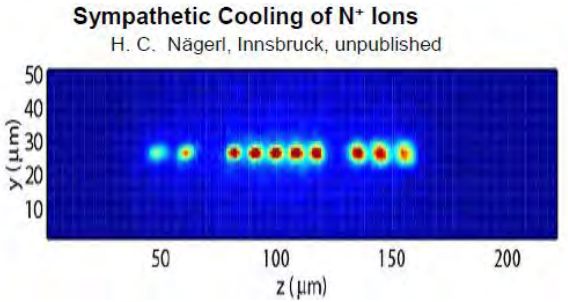

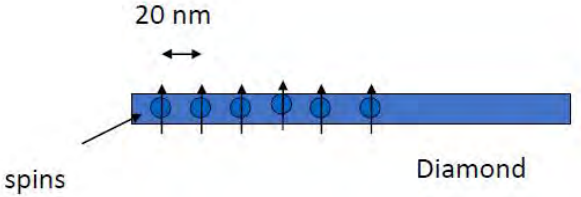

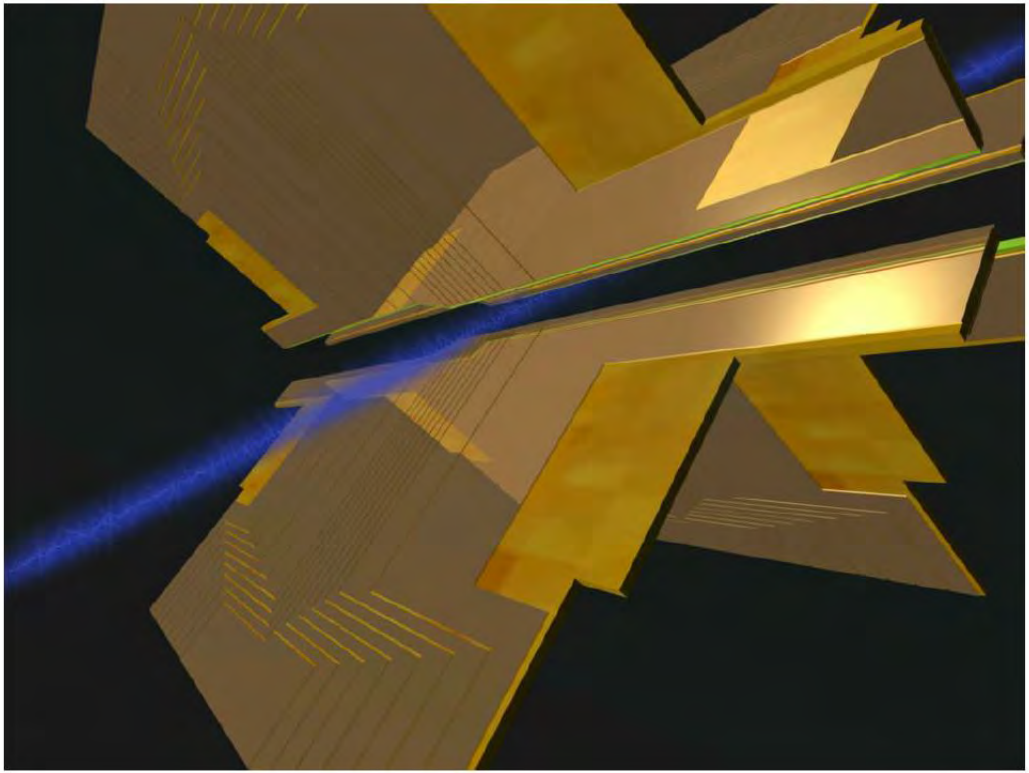

F. Schmidt-Kaler (Mainz)

Deterministic single ion implantation out of a Paul trap

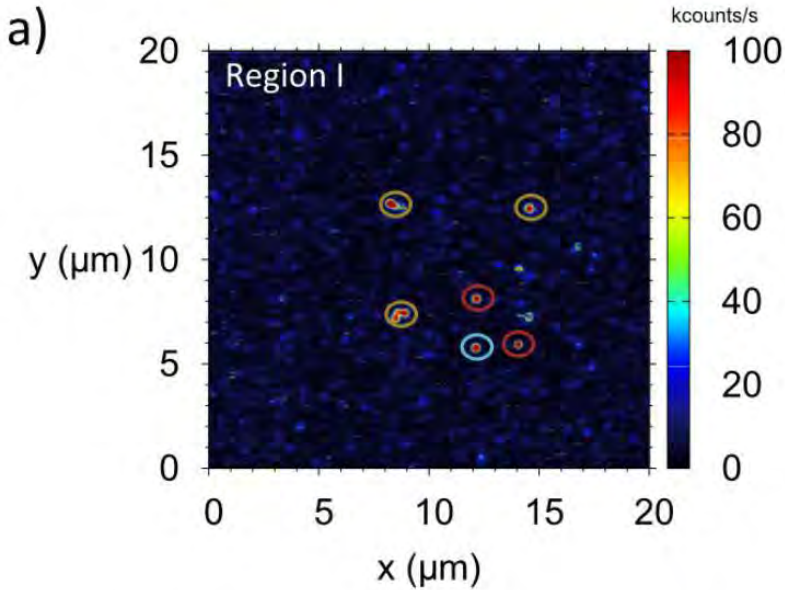

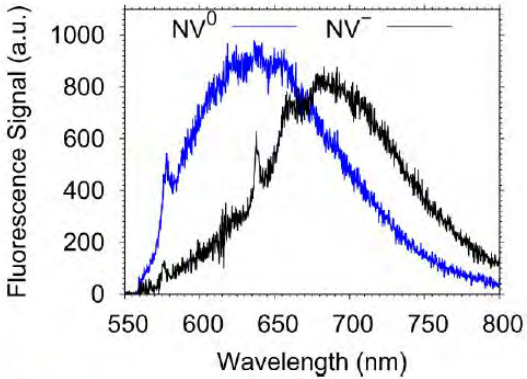

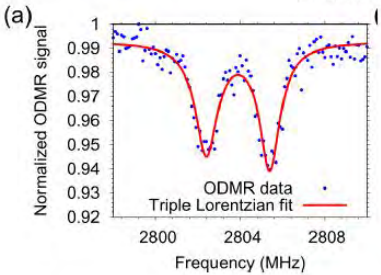

Groot-Berning et al 2021 New J. Phys. 23 063067

Implanting molecules

Collaboration: T. Oshima, S. Onoda (QST), T. Teraji (NIMS)

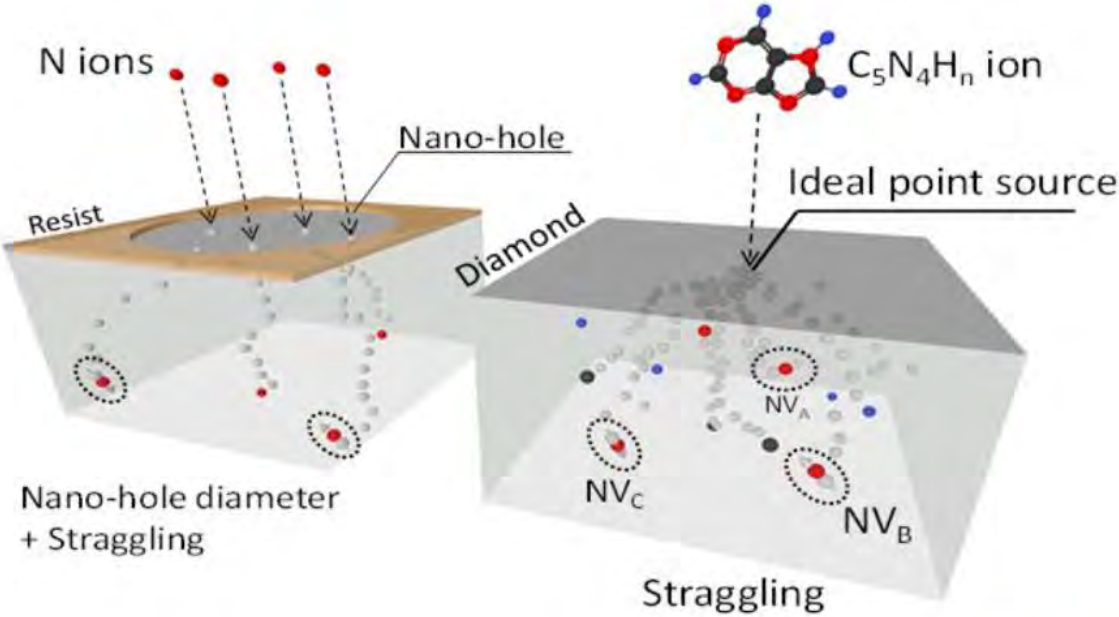

DETECTION AND MEASUREMENTS

Experiment

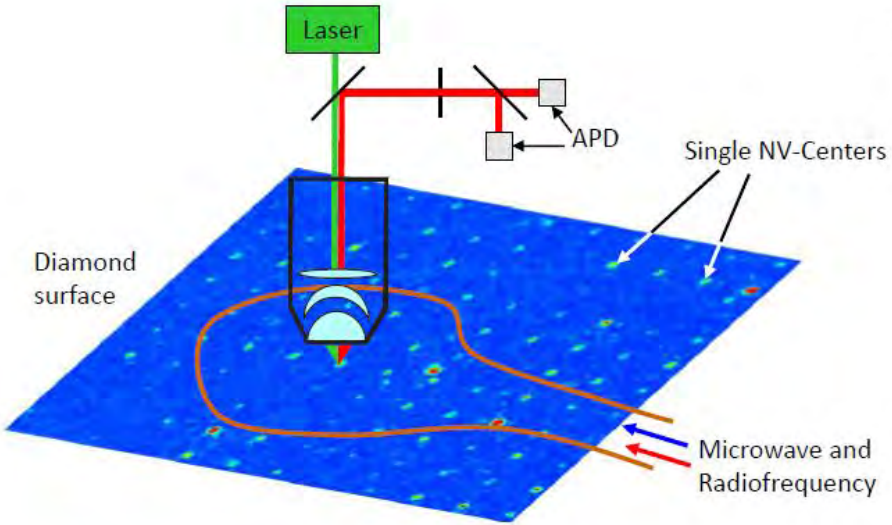
Laser
APD
Single NV-Centers
Diamond surface
Microwave and Radiofrequency

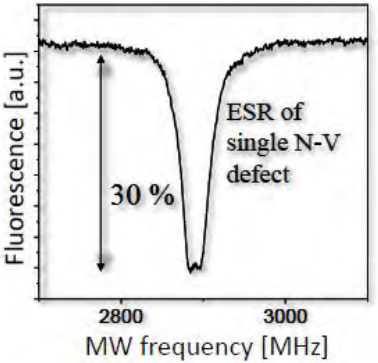
Fluorescence [a.u.]
ESR of single N-V defect
30 %
2800
3000
MW frequency [MHz]

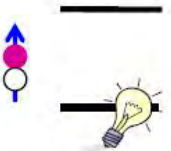

УСТАНОВКА ДЛЯ ИССЛЕДОВАНИЯ NV-ЦЕНТРОВ (ULM)

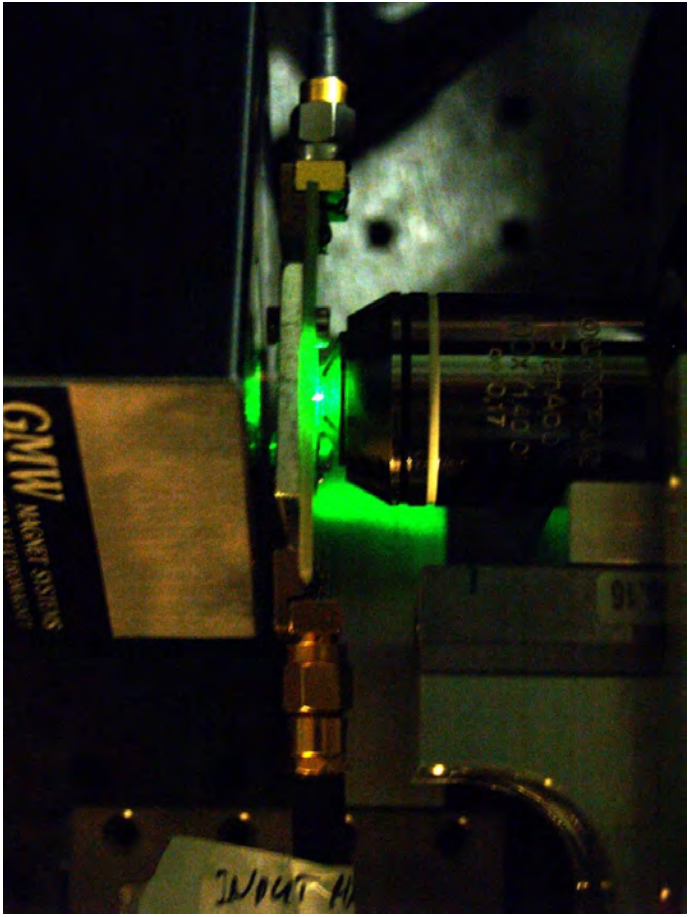

ОПТИЧЕСКОЕ ДЕТЕКТИРОВАНИЕ ОДИНОЧНЫХ NV ЦЕНТРОВ

Источник одиночных фотонов

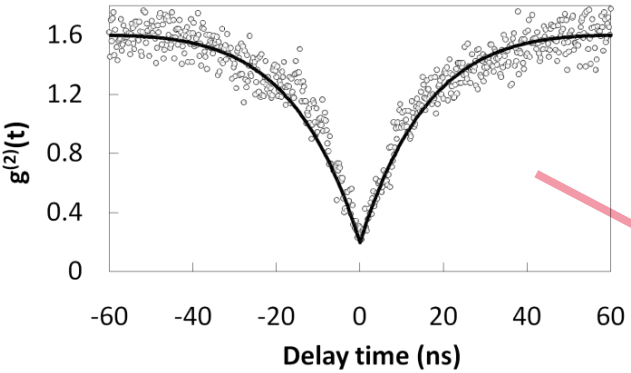

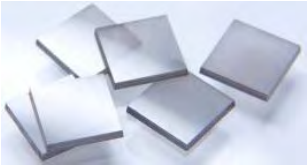

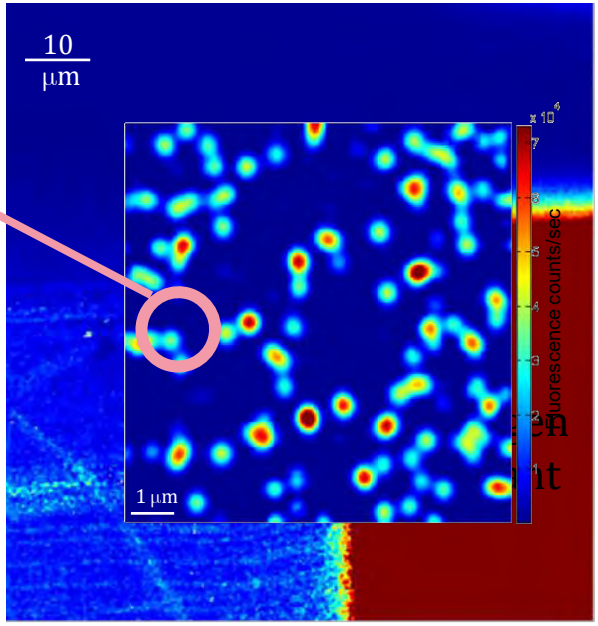

$$g^{(2)}(\tau) = \frac{\langle I(t) I(t+\tau) \rangle}{\langle I(t) \rangle^2}$$

Spin readout enhancement

Reaching high fidelity and spatial resolution

- Better collection efficiency (SILs)
- optical cavities, plasmonics
- Swap and readout via nuclear spins (^{13}C, ^{15}N)
- Spin to charge conversion

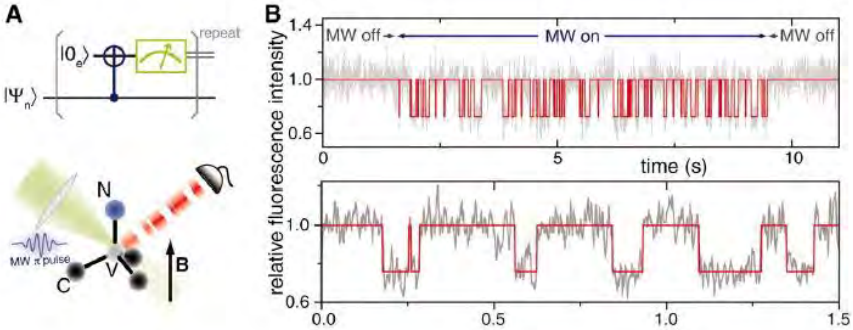

STED-МИКРОСКОПИЯ

Позволяет преодолеть предел дифракции для разрешения

Confocal STED

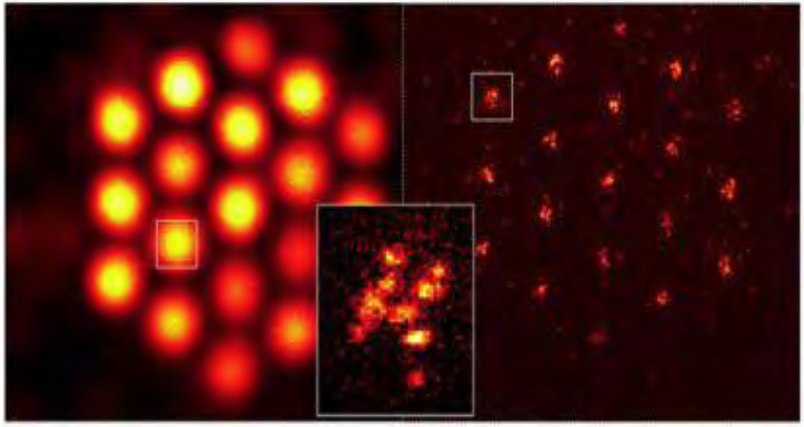

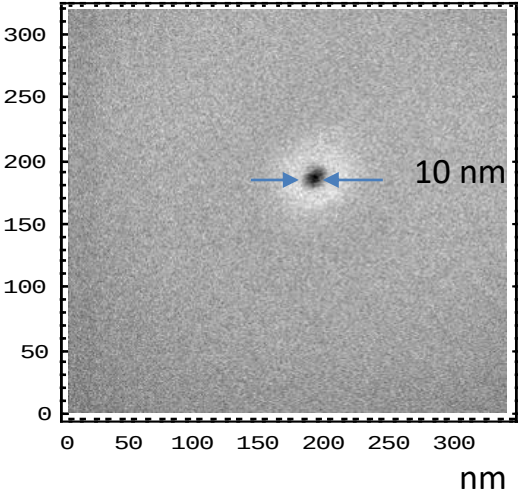

S. Hell (Göttingen), J. Meijer (Bochum)

S. Pezzagna et al., Small 6, 2117 (2010).
K. Y. Han et al., Nano Lett 9, 3323 (2009).

Nanoscale optical addressing of single spins

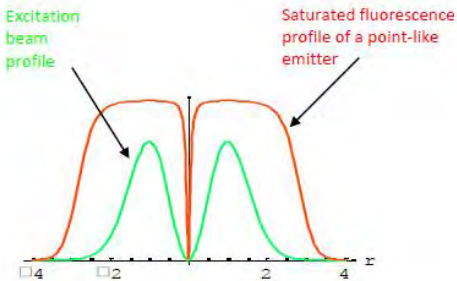

Confocal STED

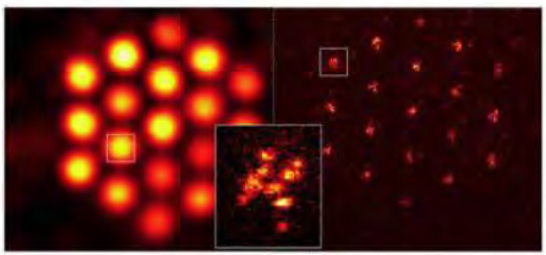

Han, Jelezko, Hell et al., Nano Letters 2009

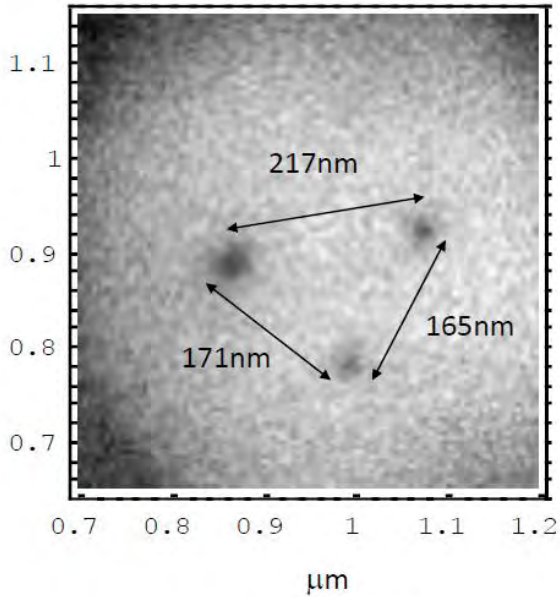

Resolution scaling $\delta x \approx \frac{\lambda}{\Omega \Gamma^{-1}}$

PHOTOELECTRIC IMAGING OF SINGLE SPINS

$$NV^- \rightleftarrows NV^0$$

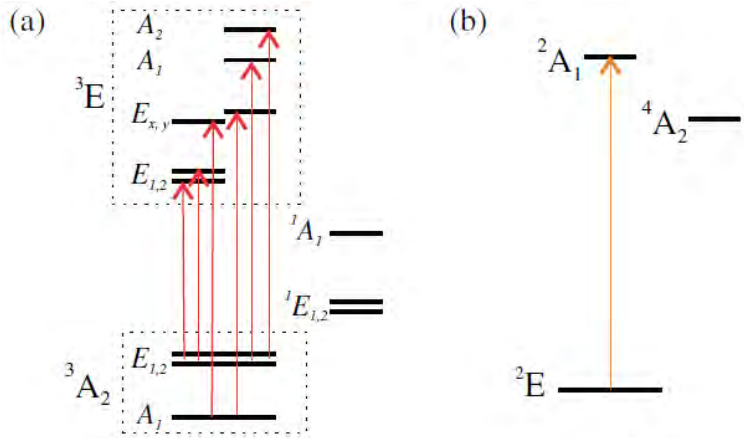

Photoelectric imaging of single spin qubits in diamond

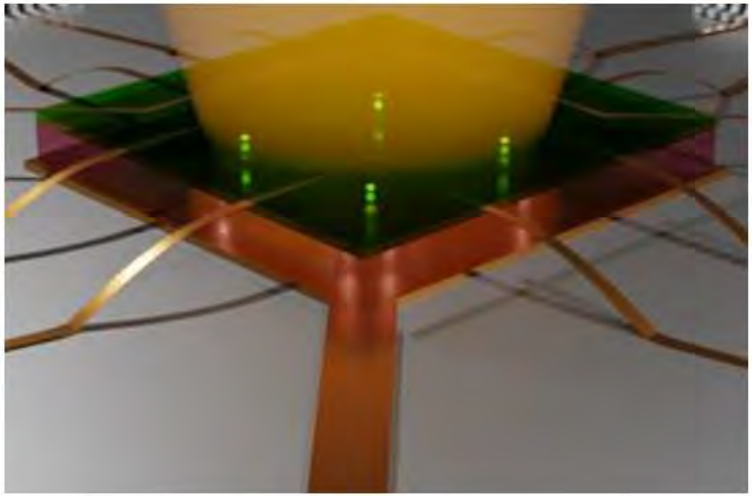

Emilie Bourgeois, Michal Gulka, T. Yamamoto, M. Nesladek
UHasselt & IMEC, Belgium
Michael Trupke, TU Wien, Austria
Adam Gali, Wigner Institute Budapest, Hungary
Toku Teraji, Junichi Isoya, NIMS and Tsukuba University, Japan

Electrical readout of NV spins

State detection based on photoionization

Spin state access:
Shelving into singlet state prevents ionization

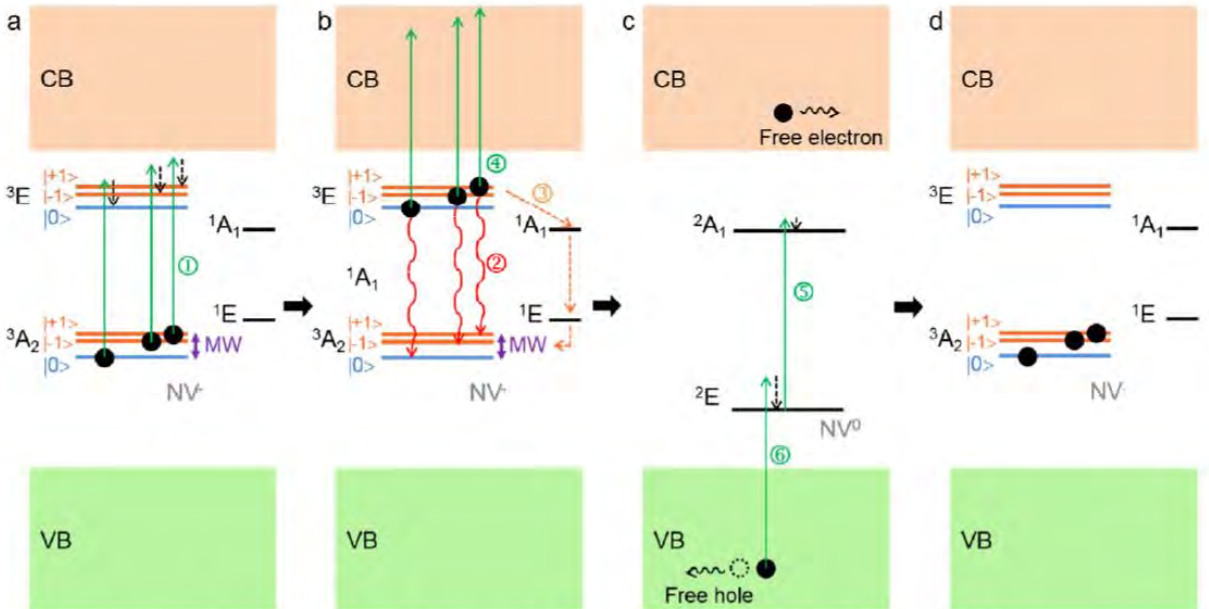

Ionisation pathway : P. Siyushev et al. Phys. Rev. Lett. 110, 167402 (2013)

Photoelectrical imaging of single NV defects

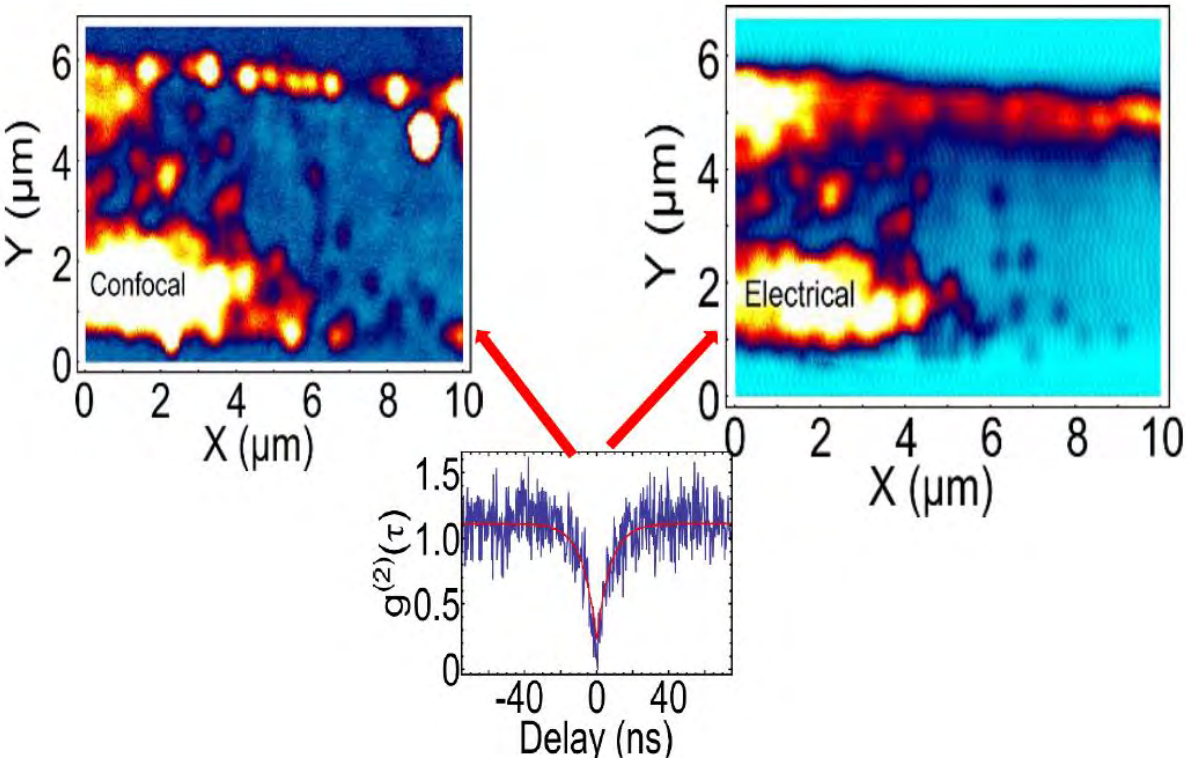

Photoelectric vs optical signals of single NV defects

Siyushev et al, *Science*. 363, 728 (2019)

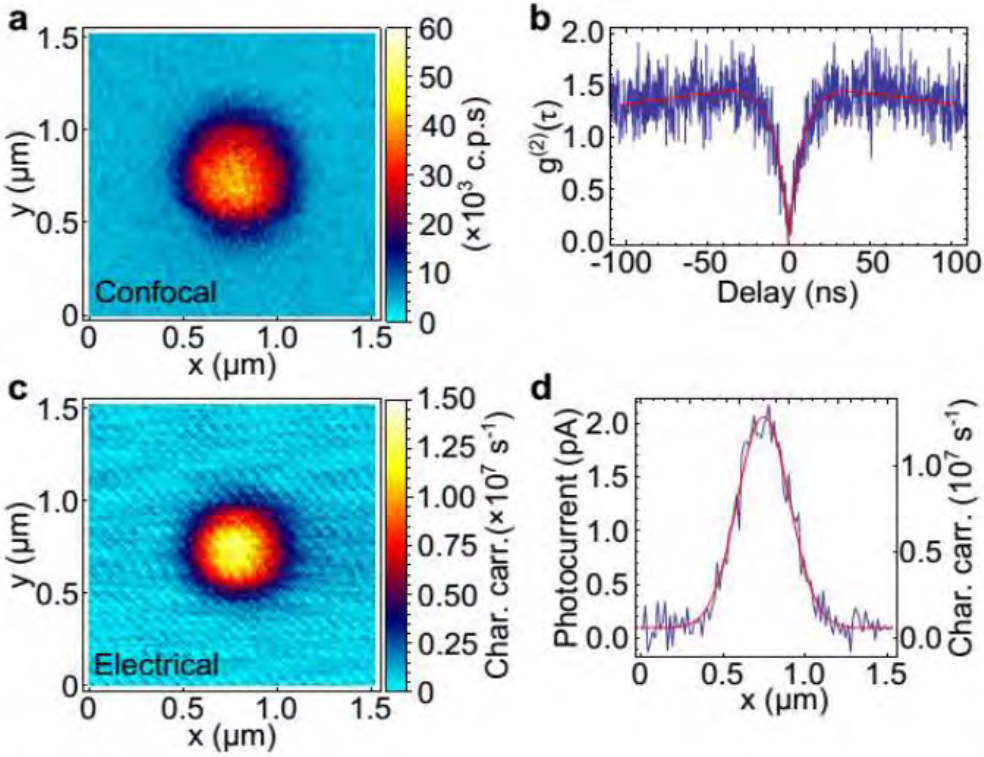

SINGLE ELECTRONIC AND NUCLEAR SPIN MEASUREMENTS

ОПТИЧЕСКОЕ СЧИТЫВАНИЕ ОДИНОЧНЫХ ЭЛЕКТРОННЫХ СПИНОВ

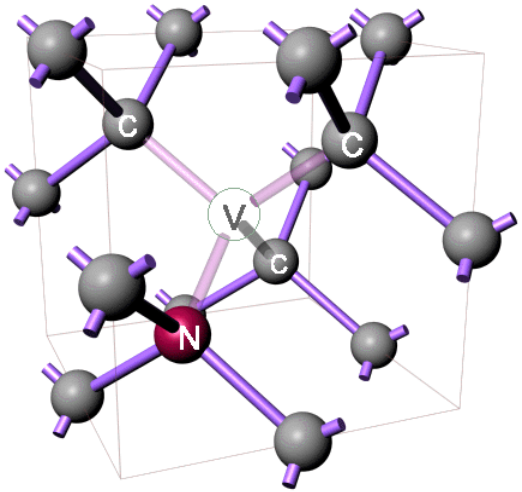

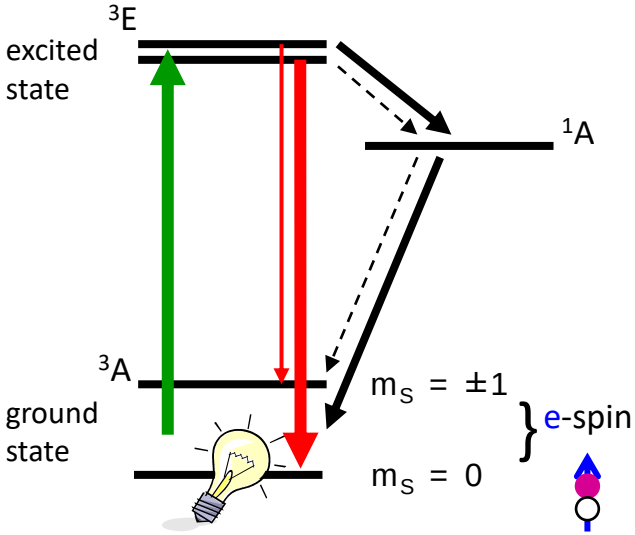

Спиновый триплет основного состояния

$$H = (D - 2/3) S_Z^2 + (g\mu_B/h)\vec{S}\cdot\vec{B}$$

Early work

P. Nizovtsev, *Physica B* **308**, 608 (2001)

Recent review M. W. Doherty et al., Phys Rep 528, 1 (2013).

КОГЕРЕНТНОСТЬ ОДИНОЧНЫХ ЭЛЕКТРОННЫХ СПИНОВ

оптическое детектирование магнитного резонанса

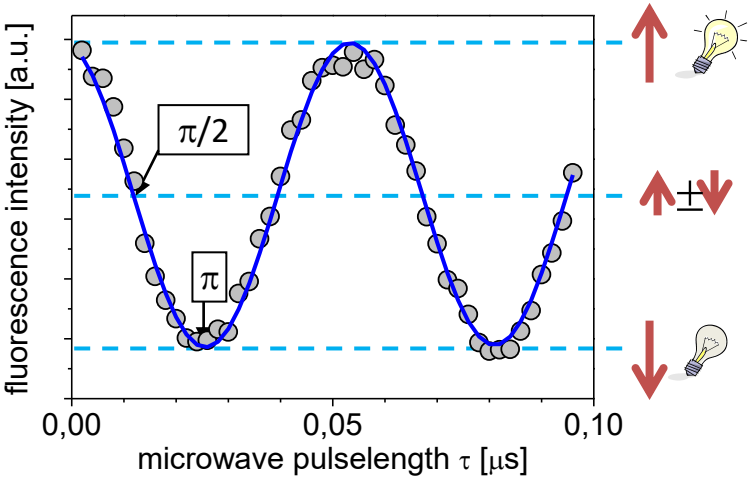

Оптически детектируемый магнитный резонанс на одиночных центрах

Jelezko, F et al., *Phys Rev Lett* **92**, 076401 (2004).
Jelezko, F. *et al. Phys Rev Lett* **93**, 130501 (2004).
Dutt, M. V. G. *et al. Science* **316**, 1312 (2007).
Childress, L. *et al. Science* **314**, 281 (2006).

КОГЕРЕНТНОСТЬ ЯДЕРНЫХ СПИНОВ

Ramsey fringes
99.999 % enriched ^{12}C (Element 6, Tsukuba)
Nuclear spin free lattice

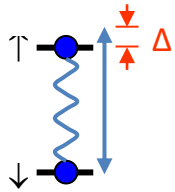

$$\varphi = \frac{1}{\sqrt{2}}\left(|\uparrow\rangle + |\downarrow\rangle\right)$$

$$\rho_\varphi = \frac{1}{2}\begin{pmatrix} 1 & 1 \\ 1 & 1 \end{pmatrix}, \begin{matrix}\uparrow \\ \downarrow\end{matrix}$$

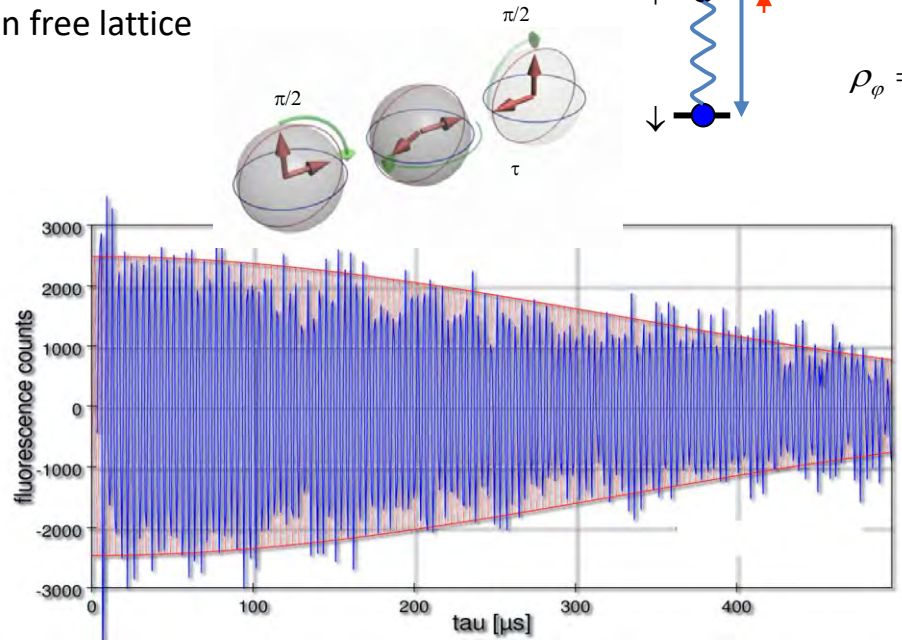

Максимальное время фазовой памяти для твердотельных систем

Jahnke KD et al. Appl Phys Lett, **101**, 012405 (2012)
Balasubramanian G et al. Nat Mater, **8**, 383 (2008).

РЕГИСТРАЦИЯ ЯДЕРНЫХ СПИНОВ, СВЯЗАННЫХ С NV

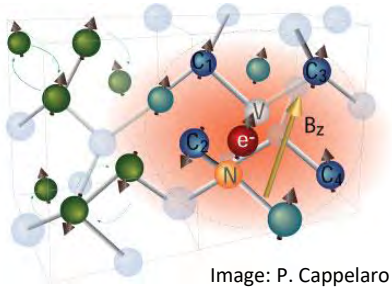

Image: P. Cappelaro (MIT)

Квантовая память

Квантовые скачки одиночного ядерного спина при комнатной температуре

Ядерный спин
Большое время когерентности
Ресурс

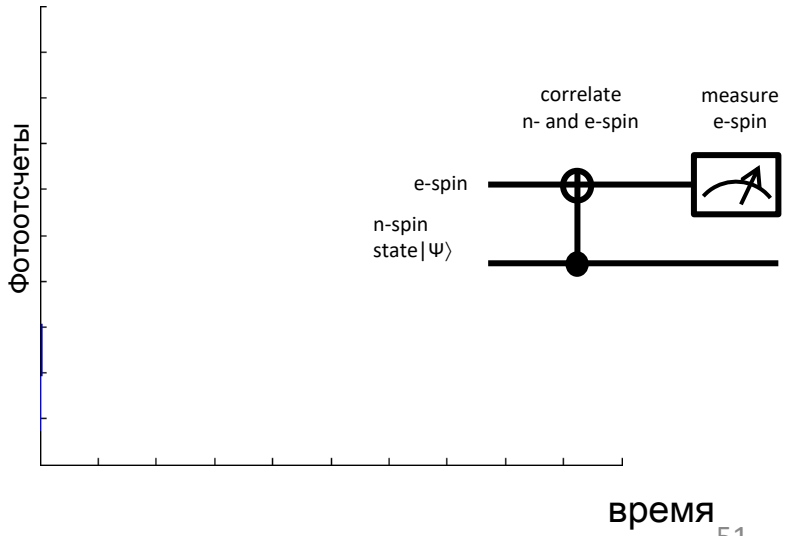

A. P. Nizovtsev, S. Y. Kilin, A. L. Pushkarchuk, V. A. Pushkarchuk, F. Jelezko, New J Phys 16, (2014).
A. P. Nizovtsev, S. Y. Kilin, P. Neumann, F. Jelezko, J. Wrachtrup, Opt Spectrosc. 108, 239 (2010).

Квантовые корреляции (entanglement)
Neumann et al., Science 320, 1326 (2008)
QND measurements
Neumann et al., Science 329, 542 (2010)
Время когерентности 1 секунда
Meurer et al., Science, 336, 1283 (2012)

THEORY

QUANTUM OPEN SYSTEMS

QUANTUM MEASUREMENTS & CONTROL

QUANTUM CHEMISTRY

ERROR COR. CODES

NV

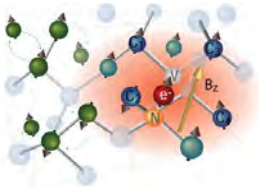

QUANTUM SENSORS

QUANTUM COMMUNICATIONS

QUANTUM COMPUTATIONS

P#1 HYBRID QUANTUM REGISTERS

ELECTRON AND NUCLEAR SPINS

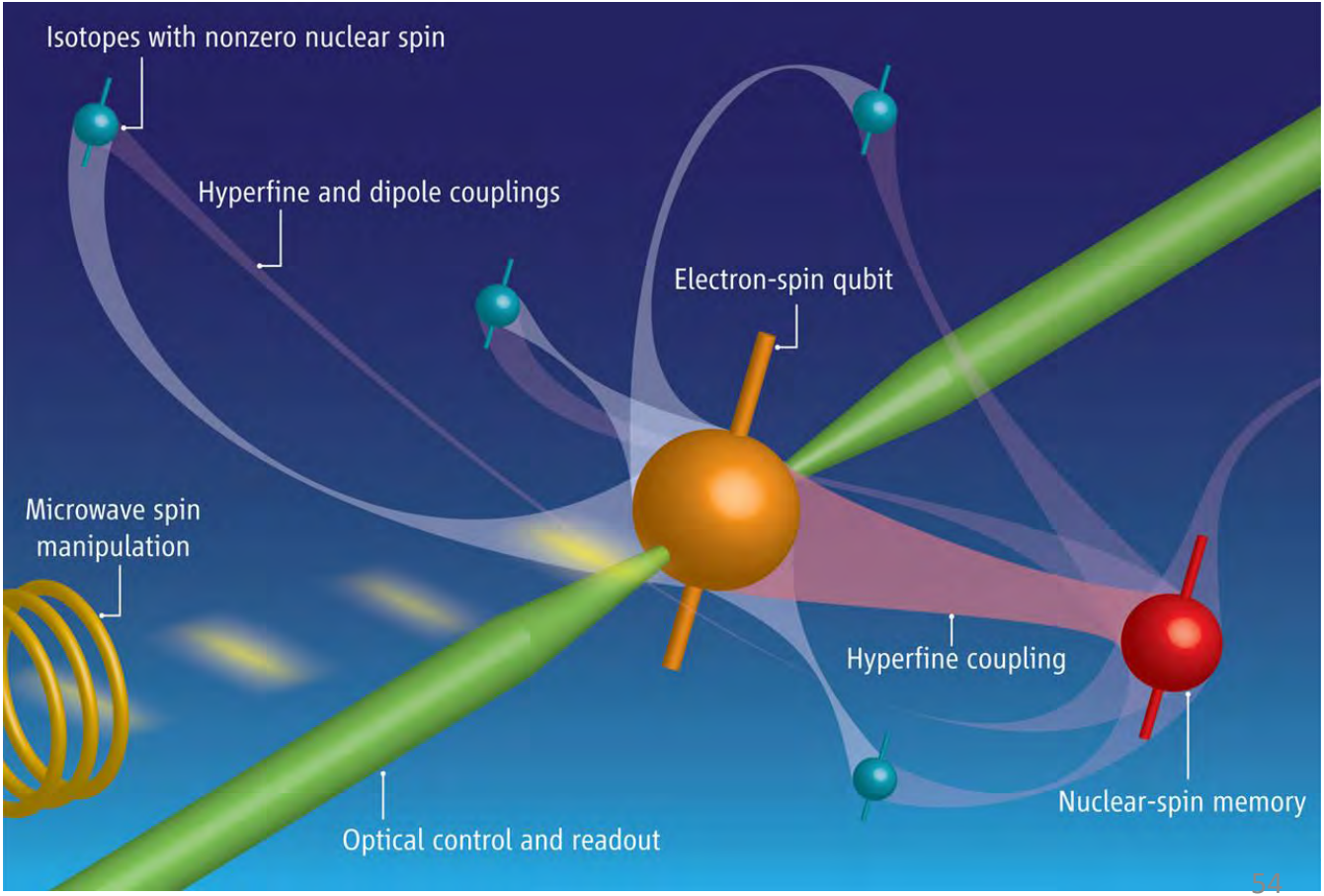

DANE R. MCCAMEY AND CHRISTOPH BOEHME, Science 2012

P#2 VISION WITH ATOMIC RESOLUTION

Супер Микроскоп:

Чувствительность: отдельные атомы

Разрешение: Å

Разрешение по времени: <мксек

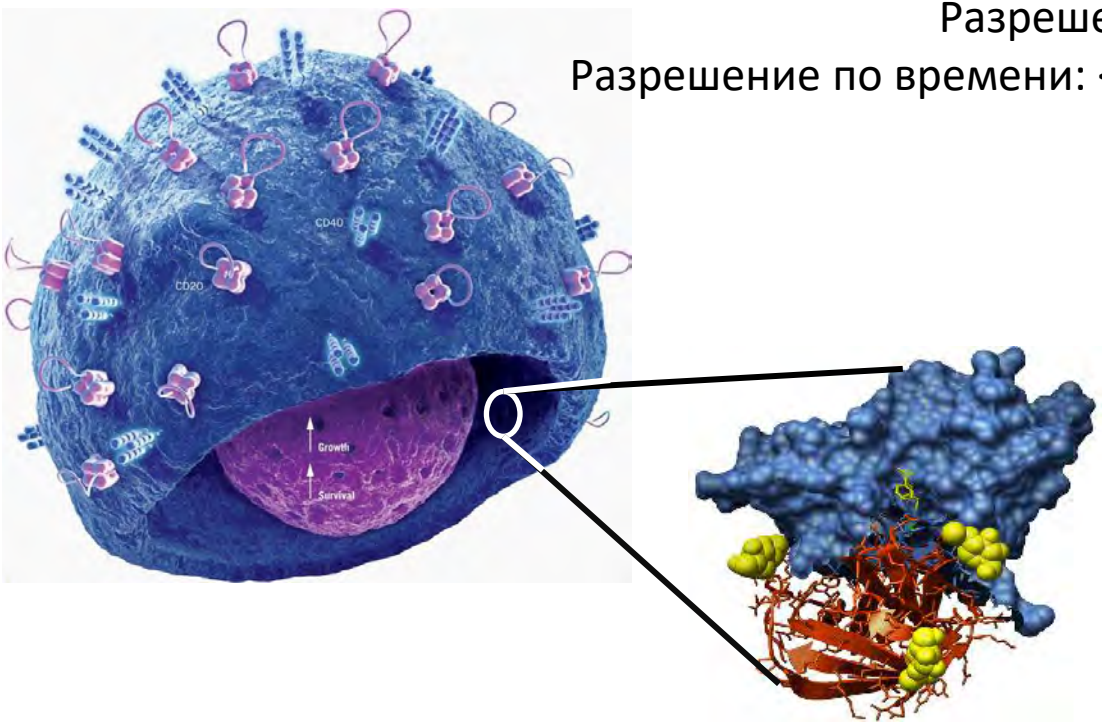

P#3 SENSORS WITH NV ENSAMBLE

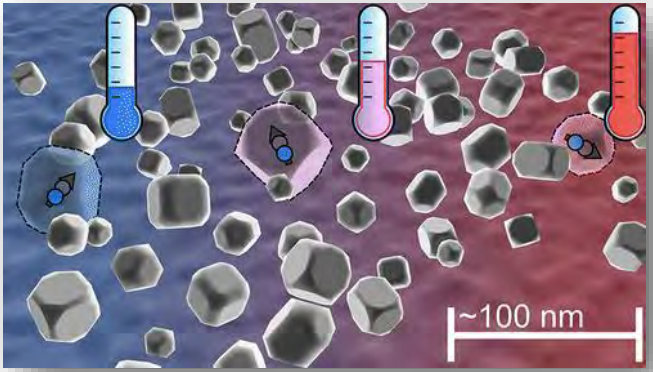

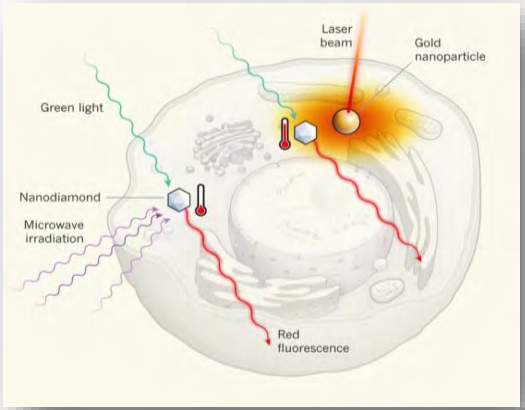

COHERENT CONTROL & USAGE OF NUCLEAR SPIN BATH

NV plus “BATH” of NUCLEAR SPINS

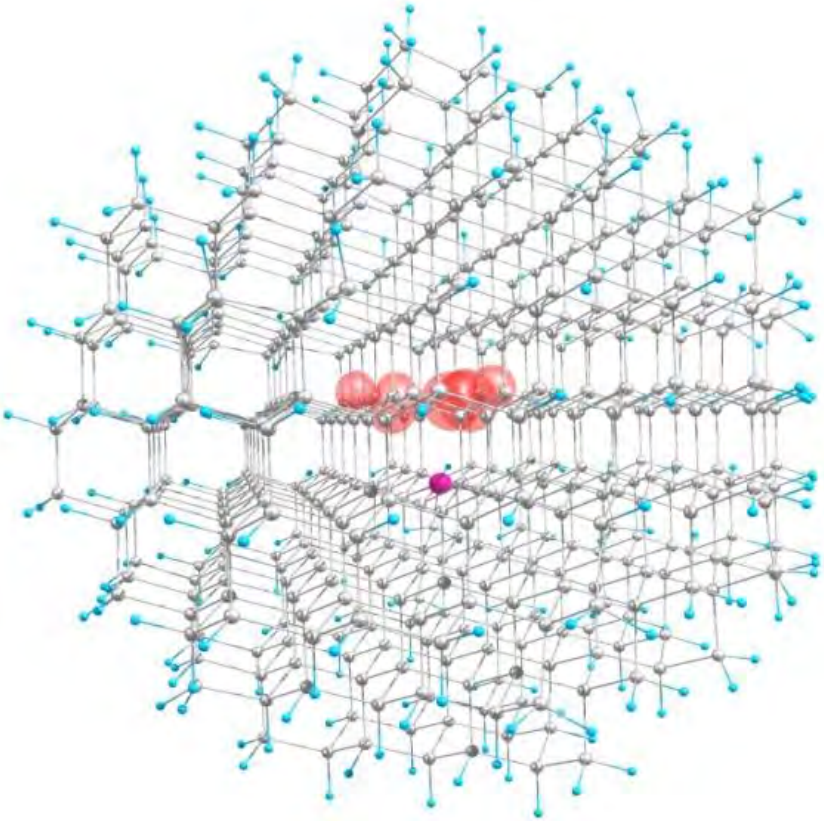

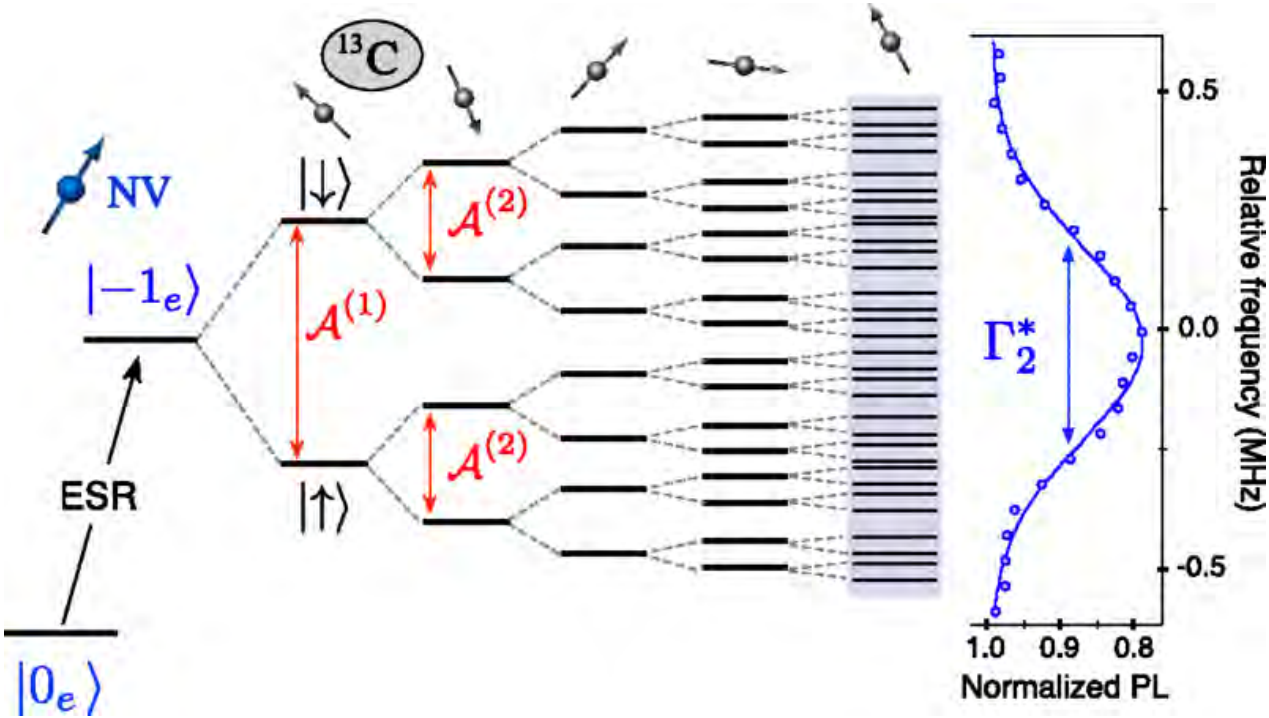
^{13}C
NV
$|-1_e\rangle$
ESR
$|0_e\rangle$
$|\downarrow\rangle$
$|\uparrow\rangle$
$\mathcal{A}^{(1)}$
$\mathcal{A}^{(2)}$
$\mathcal{A}^{(2)}$
Γ_2^*
0.5
0.0
-0.5
Relative frequency (MHz)
1.0
0.9
0.8
Normalized PL

USAGE OF SPIN “BATH”

DYNAMICAL ISOLATION OF COUPLED SPINS

DYNAMICAL METHODS TO SUPPRESS DEPHASING

Two-pulse echo

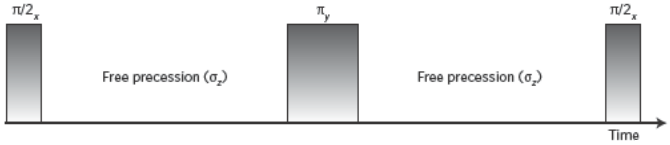

Remove inhomogeneous broadening

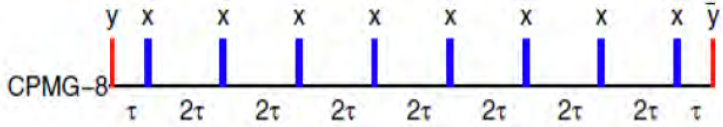

Carr-Purcell-Meiboum-Gibbs sequence

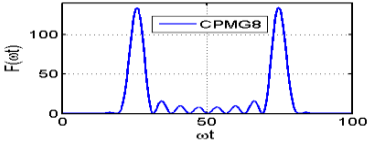

Filter function for CPMG-8

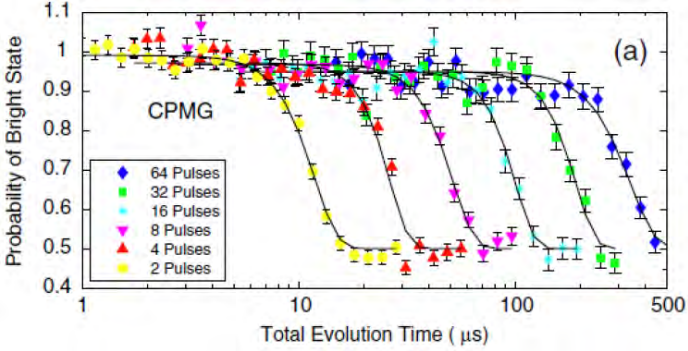

The method allows to demonstrate T2 dephasing time for NV approaching to 1 second !!!!

Room-Temperature Quantum Bit Memory Exceeding One Second

P. C. Maurer,[1*] G. Kucsko,[1*] C. Latta,[1] L. Jiang,[2] N. Y. Yao,[1] S. D. Bennett,[1] F. Pastawski,[3] D. Hunger,[3] N. Chisholm,[4] M. Markham,[5] D. J. Twitchen,[5] J. I. Cirac,[3] M. D. Lukin[1]†

Science 33 (2012) 1283

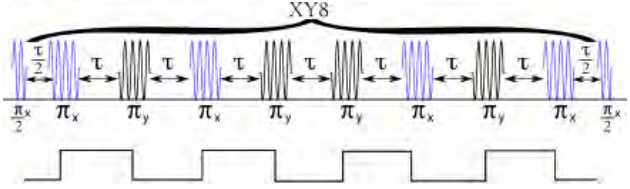

$$\tau = \frac{2n\pi}{\omega_L}$$

INDIVIDUAL CONTROL OF INDIVIDUL ^{13}C BATH SPINS (sensing sequences)

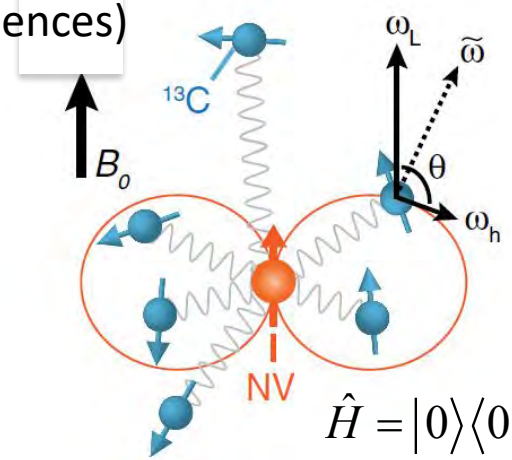

$$H = \omega_L I_z + A_{\parallel} S_z I_z + A_{\perp} S_z I_x,$$

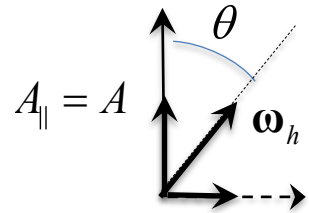

$A_{\parallel} = A$

$A_{\perp} = B$

$$\hat{H} = |0\rangle\langle 0|\hat{H}_0 + |1\rangle\langle 1|\hat{H}_1$$

$$\hat{H}_0 = \omega_L \hat{I}_z,$$

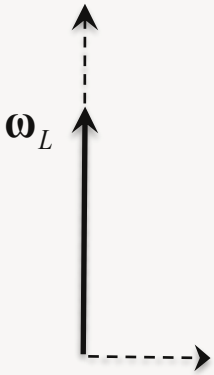

$$\hat{H}_1 = (A_{\parallel} + \omega_L)\hat{I}_z + A_{\perp}\hat{I}_x$$
$$= \tilde{\omega}(\cos\tilde{\theta}\hat{I}_z + \sin\tilde{\theta}\hat{I}_x)$$

$$\tilde{\omega} = \sqrt{(A + \omega_L)^2 + B^2}$$

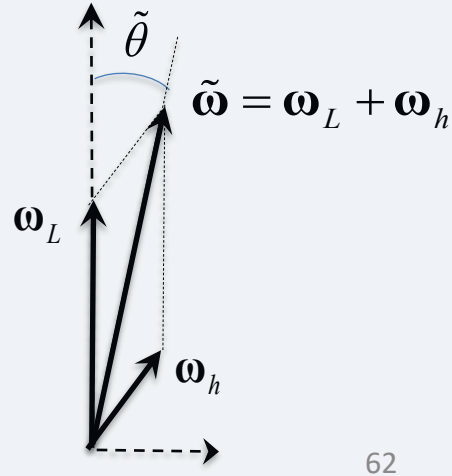

$$\left[\left(\tau-\pi-2\tau-\pi-\tau\right)^{N/2}\right]$$

$$\hat{H}=|0\rangle\langle 0|\hat{H}_0+|1\rangle\langle 1|\hat{H}_1$$

$$N=2$$

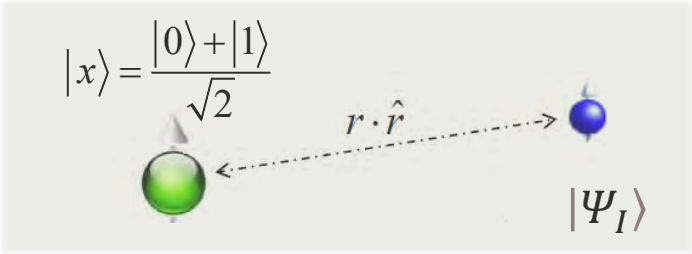

$$|\psi(t)\rangle_{en}=e^{-iHt}|x\rangle|\Psi_I\rangle=e^{-iHt}\frac{|0\rangle+|1\rangle}{\sqrt{2}}|\Psi_I\rangle=\frac{|0\rangle\hat{V}_0|\Psi_I\rangle+|1\rangle\hat{V}_1|\Psi_I\rangle}{\sqrt{2}}$$

$|\psi(t)\rangle_{en}$ - entangled state

$$\begin{aligned}\hat{V}_0 &= \exp\left[-i\hat{H}_0\tau\right]\exp\left[-i\hat{H}_1 2\tau\right]\exp\left[-i\hat{H}_0\tau\right]\\ \hat{V}_1 &= \exp\left[-i\hat{H}_1\tau\right]\exp\left[-i\hat{H}_0 2\tau\right]\exp\left[-i\hat{H}_1\tau\right].\end{aligned}$$

ПЕРЕПУТАННОЕ СОСТОЯНИЕ

$$|\Psi_I(T)\rangle_x=\langle x|e^{-iHt}|x\rangle|\Psi_I\rangle=\frac{\hat{V}_0+\hat{V}_1}{2}|\Psi_I\rangle$$

$$P_x=\left|{}_x\langle\Psi_I(T)|\Psi_I(T)\rangle_x\right|^2=\frac{1+\langle\Psi_I|\hat{V}_0\hat{V}_1^{\dagger}|\Psi_I\rangle}{2}$$

$$\left[\left(\tau-\pi-2\tau-\pi-\tau\right)^{N/2}\right]$$

$$P_x^{(N)} = \frac{1+\langle\Psi_I|\hat{V}_0^{\frac{N}{2}}(\hat{V}_1^{\dagger})^{\frac{N}{2}}|\Psi_I\rangle}{2} = \frac{1+M}{2}$$

$$\begin{aligned}\hat{V}_0 &= \exp\left[-i\phi(\hat{\mathbf{I}}\cdot\hat{\mathbf{n}}_0)\right]\\ \hat{V}_1 &= \exp\left[-i\phi(\hat{\mathbf{I}}\cdot\hat{\mathbf{n}}_1)\right],\end{aligned}$$

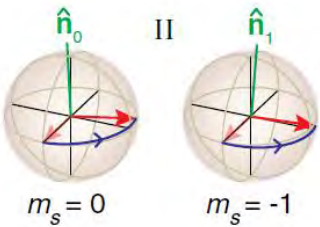

$$M = 1-(1-\hat{\mathbf{n}}_0\cdot\hat{\mathbf{n}}_1)\sin^2\frac{N\phi}{2}.$$

$$\cos\phi = \cos\alpha\cos\beta - m_z\sin\alpha\sin\beta \qquad \alpha = \tilde{\omega}\tau$$

$$1-\hat{\mathbf{n}}_0\cdot\hat{\mathbf{n}}_1 = m_x\frac{(1-\cos\alpha)(1-\cos\beta)}{1-\cos\phi} \qquad \beta = \omega_L\tau$$

$$m_x = \sin\tilde{\theta} = A_\perp/\tilde{\omega} \sim \omega_h/\omega_L \ll 1 \qquad m_z = \cos\tilde{\theta} = (A_\parallel+\omega_L)/\tilde{\omega} \sim 1$$

$$\left[(\tau-\pi-2\tau-\pi-\tau)^{N/2}\right]$$

$$M = 1 - (1 - \hat{\mathbf{n}}_0 \cdot \hat{\mathbf{n}}_1)\sin^2\frac{N\phi}{2}.$$

$$1-\hat{\mathbf{n}}_0\cdot\hat{\mathbf{n}}_1 = m_x\frac{(1-\cos\alpha)(1-\cos\beta)}{1-\cos\phi}$$

$$\tan\frac{\alpha}{2}\tan\frac{\beta}{2} = \frac{1}{m_z}.$$

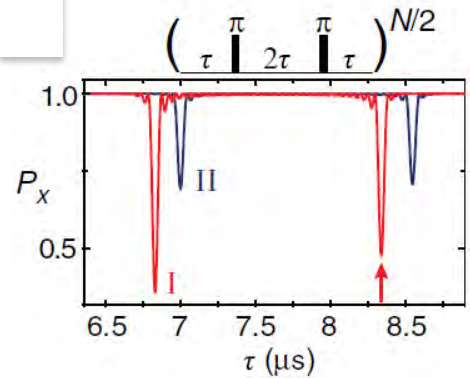

$$\tau_k = \frac{(2k-1)\pi}{2\omega_L + A},$$

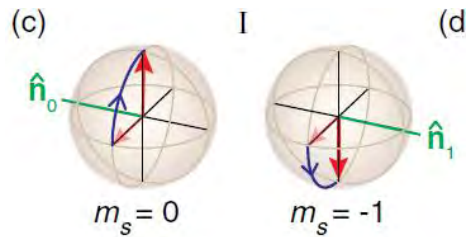

PRL **109,** 137602 (2012)

DECOUPLING & POLARIZATION & REGISTRATION

- Прямые flip-flops между электронным и ядерным спинами подавляются рассогласованием энергии.

- Как привести два спина в резонанс

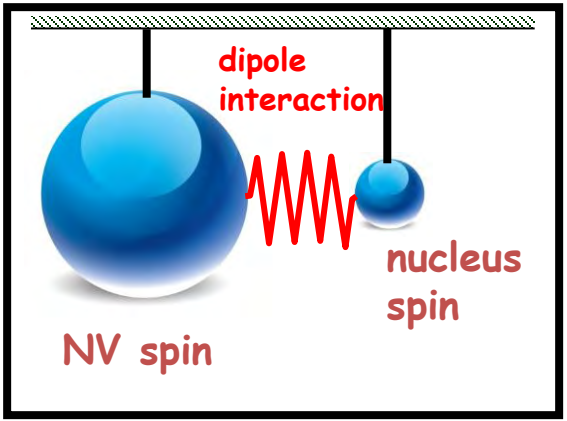

HARTMANN-HAHN CONDITION, DOUBLE RESONANCE

- Возбуждение электронных спинов.

$$\Omega_{Rabi} = \left| \gamma_N B + A_{hyp} \right|$$

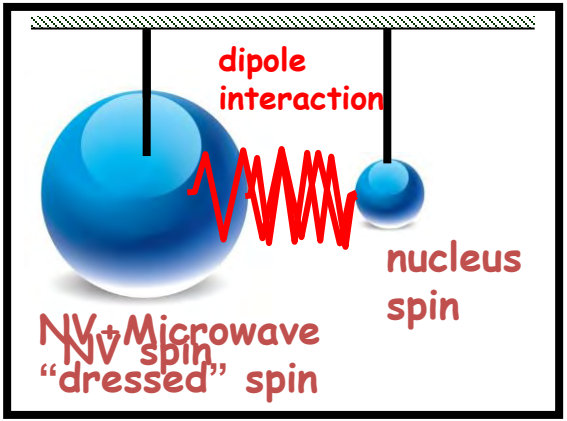

London et al., Phys. Rev. Lett. 111, 067601 (2013)

S. R. Hartmann and E. L. Hahn, "Nuclear Double resonance in the rotating frame", Physical Review 125, 5 (1962)

A. Henstra et al., Journal of Magnetic Resonance 77,389 (1988)

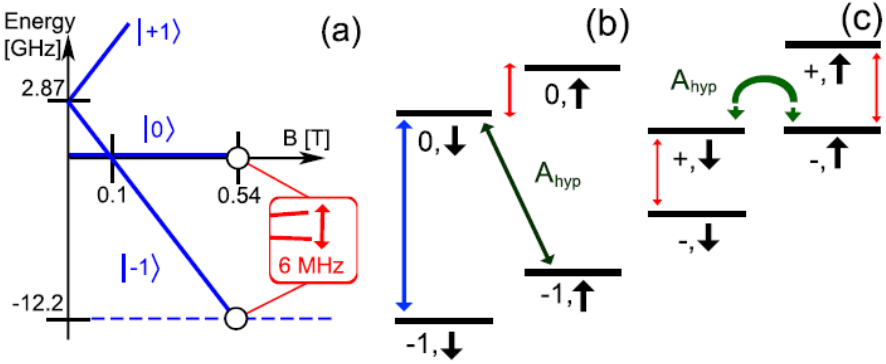
Energy
[GHz]
|+1⟩
(a)
2.87
|0⟩
B [T]
0.1
0.54
6 MHz
|-1⟩
-12.2
(b)
0,↑
0,↓
A_hyp
-1,↑
-1,↓
(c)
A_hyp
+,↑
+,↓
-,↑
-,↓

Concatenated Continuous Dynamical Decoupling

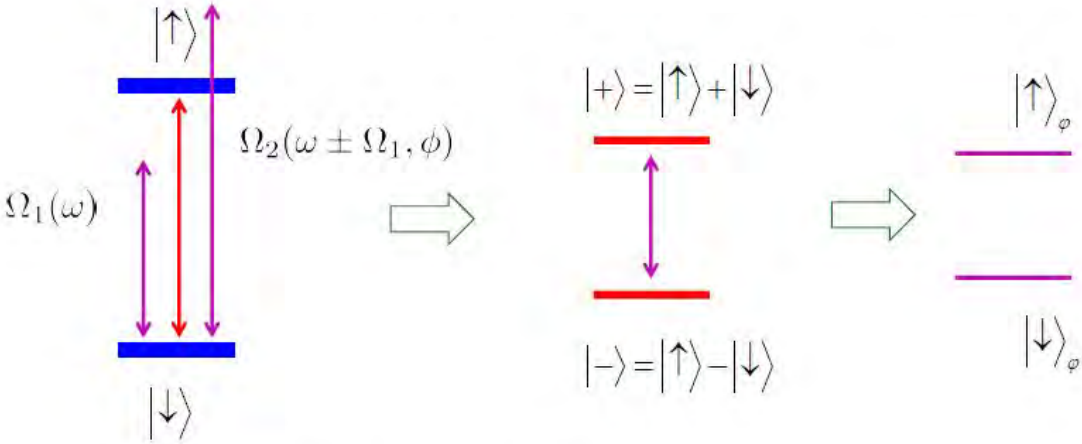

$$H = \hbar\Omega_1 \cos(\omega t)\sigma_x + \frac{\hbar}{2}\omega\sigma_z + 2\hbar\Omega_2 \sin(\omega t)\cos(\Omega_1 t)\sigma_x$$

$$\cong \hbar\Omega_1 \cos(\omega t + \frac{\Omega_2}{\Omega_1}\cos\Omega_1 t)\sigma_x$$

$$H = \frac{\hbar}{2}\Omega_1\sigma_x + \hbar\Omega_2\cos(\Omega_1 t)\sigma_y$$

$$H = \frac{\hbar}{2}\Omega_2\sigma_y$$

Theory & Experiment Bulk Diamonds: NJP 14, 113023 (2012)

Robust polarization sequences

Integrated Solid Effect (ISE)

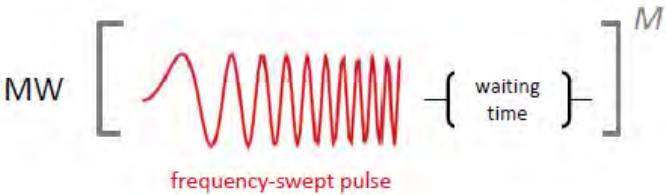

Henstra, A., *et al.*, Physics Letters A, 134(2), 134–136.

PulsePOL, sequences using high power pulses

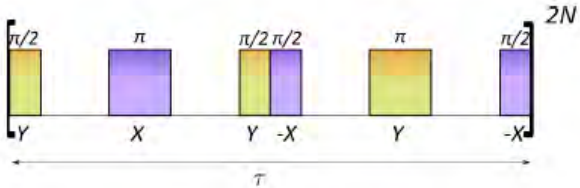

I. Schwartz *et al.*, Science Advances, 4(8) (2018)

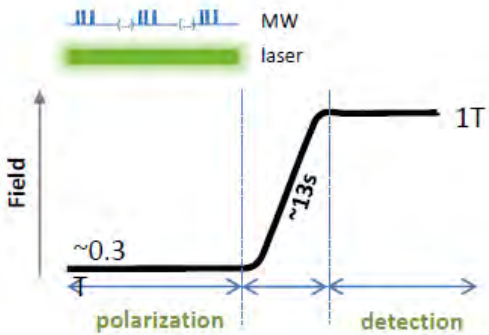

X/Q-band EPR magnet

NV Measurement Protocols & Sequences

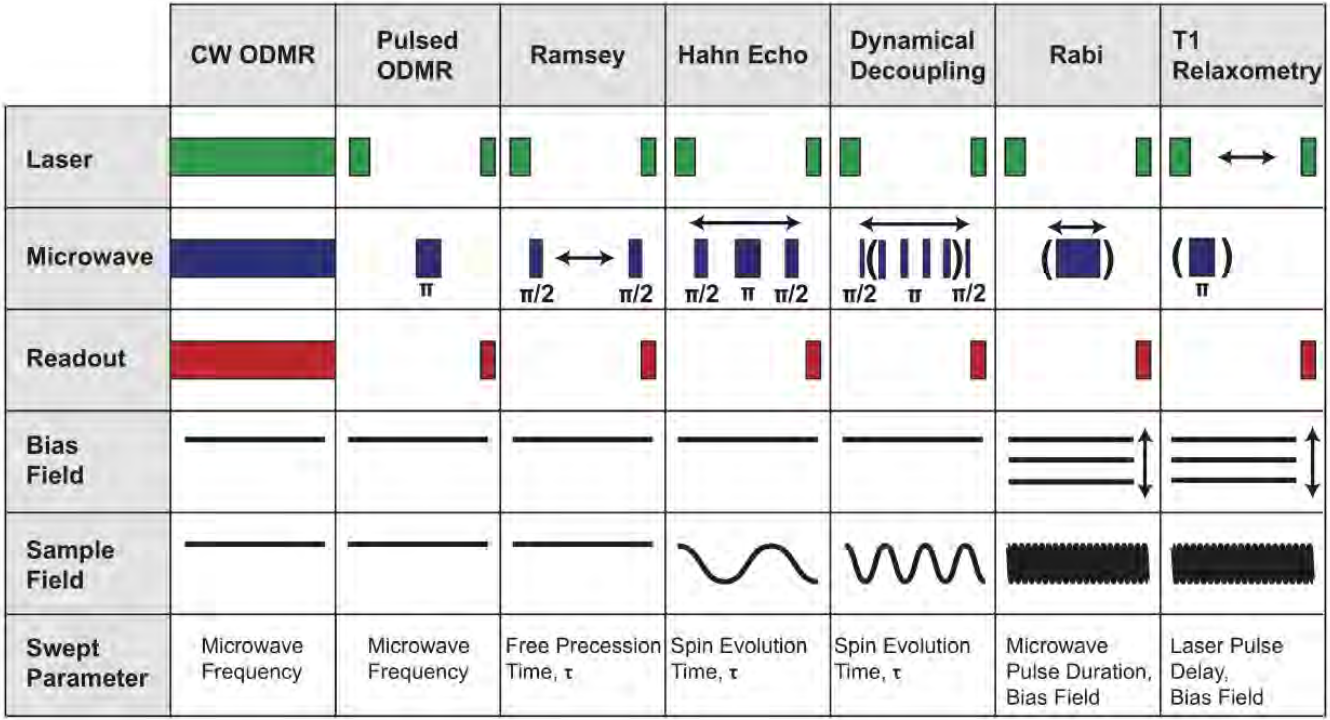

Levine, Edlyn V. et.al *Nanophotonics*, vol. 8, no. 11 (2019) pp. 1945-1973

P#2 VISION WITH ATOMIC RESOLUTION

Супер Микроскоп:

Чувствительность: отдельные атомы

Разрешение: Å

Разрешение по времени: <мксек

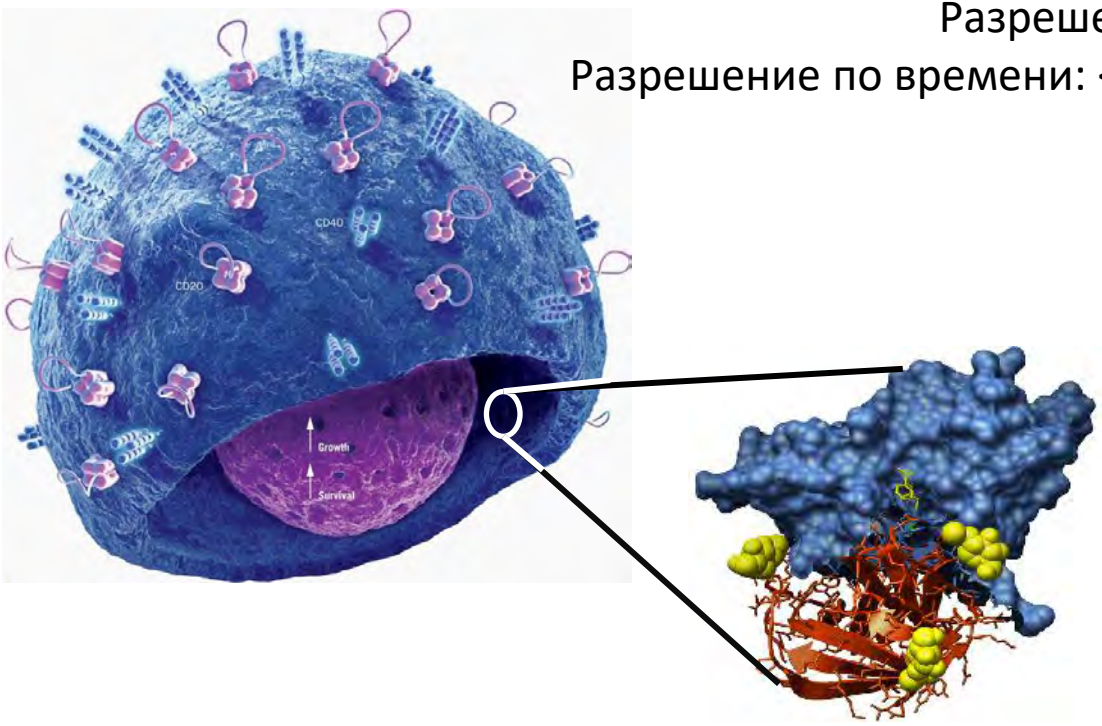

Magnetic Field Sensing with NV Qubits

Ramsey interferometry

$$\Delta\phi = \frac{g\mu_B}{\hbar} B\tau$$

$$e^{-i\phi\tau}$$

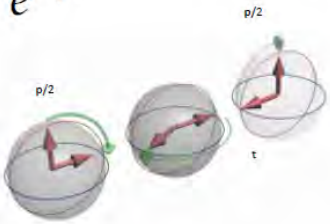

$$\delta B \simeq \frac{1}{g\mu_B} \frac{\hbar}{\sqrt{N\tau T}}$$

(standard quantum limit)

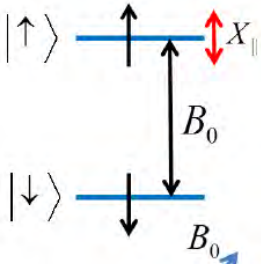

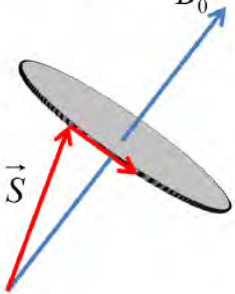

Sensitivity improvement strategies

The longer T_2*, the more precisely you can estimate δ

Increase number of NV centers, ensembles

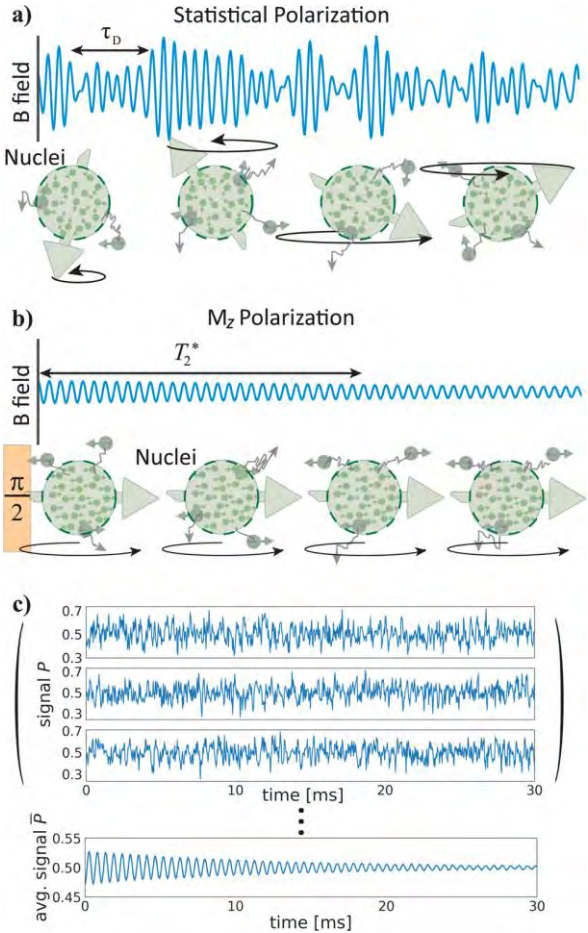

NV CENTERS IN A DUAL ROLE OF NMR DETECTOR AND OPTICAL HYPERPOLARIZATION SOURCE TO INCREASE S/N

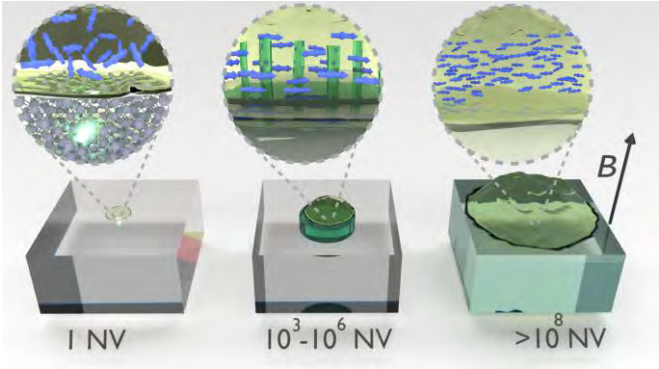

Schwartz, I., Rosskopf, J., Schmitt, S. *et al.* Blueprint for nanoscale NMR. *Sci Rep* **9**, 6938 (2019). https://doi.org/10.1038/s41598-019-43404-2

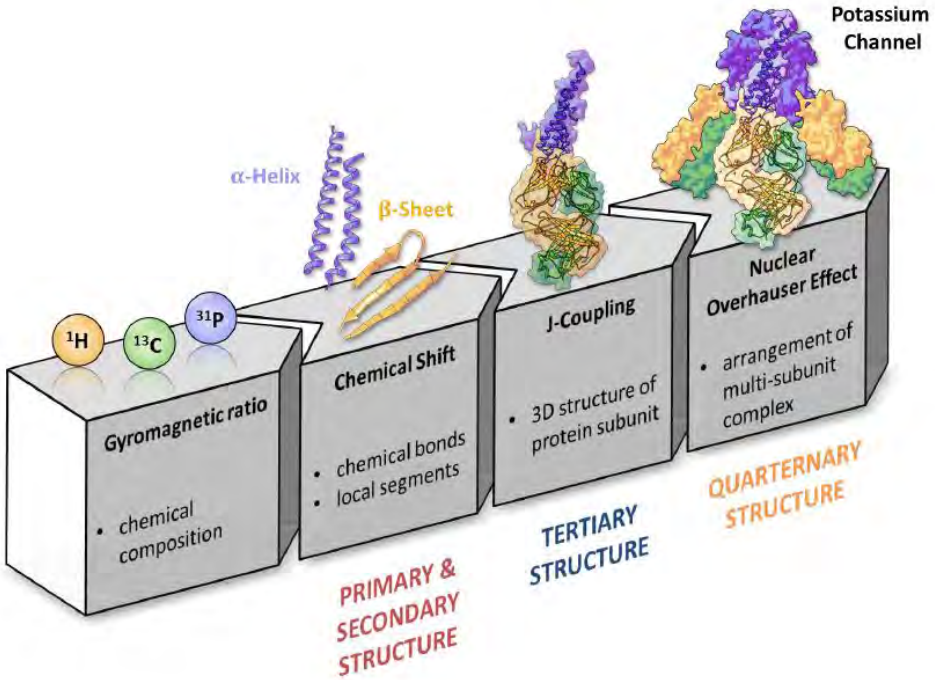
Potassium Channel
α-Helix
β-Sheet
^{1}H
^{13}C
^{31}P
Gyromagnetic ratio
• chemical composition
Chemical Shift
• chemical bonds
• local segments
J-Coupling
• 3D structure of protein subunit
Nuclear Overhauser Effect
• arrangement of multi-subunit complex
PRIMARY & SECONDARY STRUCTURE
TERTIARY STRUCTURE
QUARTERNARY STRUCTURE

ОПРЕДЕЛЕНИЕ СТРУКТУРЫ ОДНОЙ МОЛЕКУЛЫ

ДВУМЕРНЫЙ ЯМР ВЫСОКОГО РАЗРЕШЕНИЯ

Цель: Разрешение структуры и динамики одиночных биомолекул

Задача 1: чувствительность (*sub nT*)
Задача 2: спектральное разрешение (*sub Hz*)

JOHN C. KENDREW

Myoglobin and the structure of proteins

Nobel Lecture, December 11, 1962

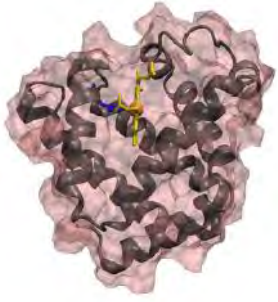

Квантовые инструменты для метрологии:
Квантовая память
Квантовая коррекция ошибок

Unden et al., Phys. Rev. Lett. 116, 230502 (2016)

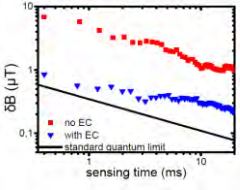

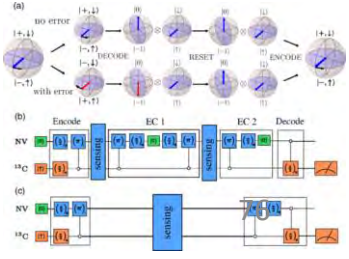

БИОСТРУКТУРНЫЙ АНАЛИЗ

СПЕКТРОСКОПИЯ ОДИНОЧНЫХ МОЛЕКУЛ VS NMR

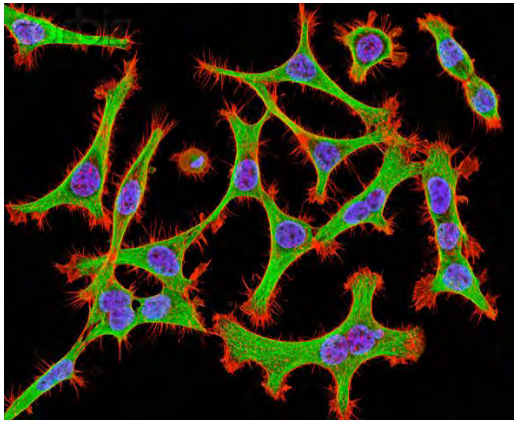

Чувствительность: уровень одиночной молекулы
Высокое **пространственное** разрешение: 10 нм (STED)

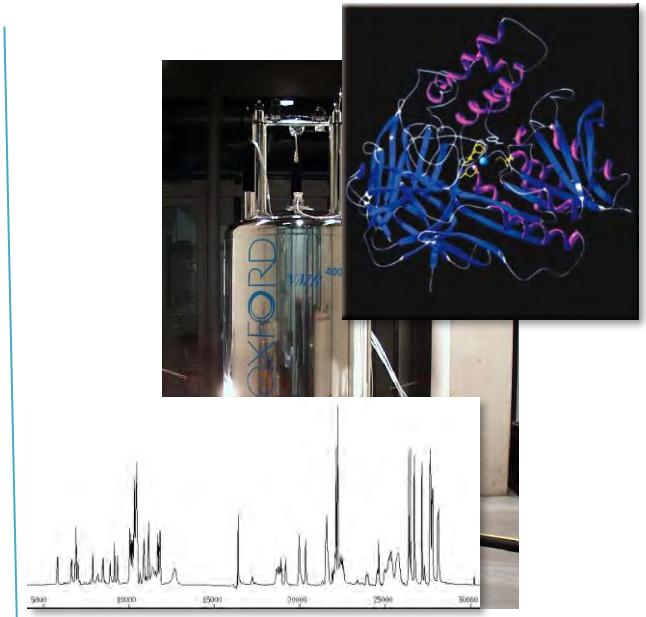

количественный
Label free

Высокое **спектральное** разрешение
Низкая чувствительность

АЛМАЗНЫЕ МАГНИТОМЕТРЫ

Balasubramanian, G.; et.al, Nature 2008, 455, 648-651.
Maze, J. et. Al, Nature 2008, 455, 644-647.

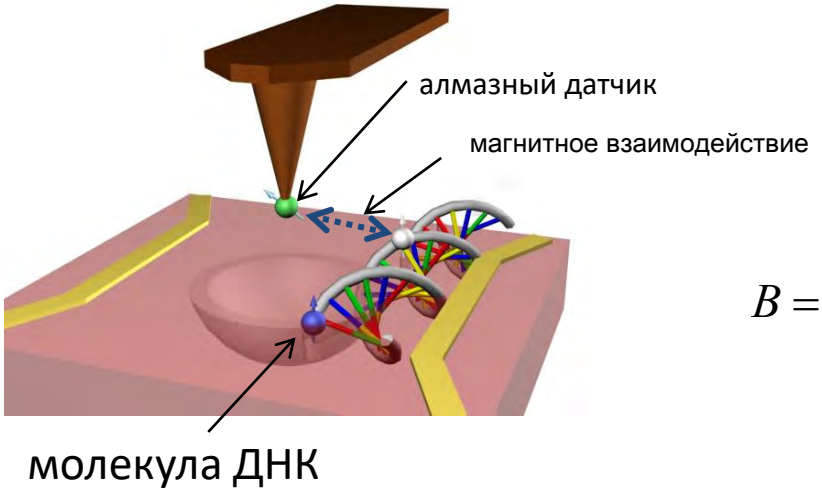

$$B = \frac{\mu_0 \hbar \gamma_e}{r^3}\left[1 - 3\cos^2(\theta)\right] S_z$$

Новый алмазный датчик позволяет измерять магнитные поля с высоким пространственным разрешением

ЯМР ОДИНОЧНОЙ МОЛЕКУЛЫ

Lovchinsky et al., Science 351, 836-840 (2016)

Ubiquitin
Регуляторный белок (8,5 кДа)

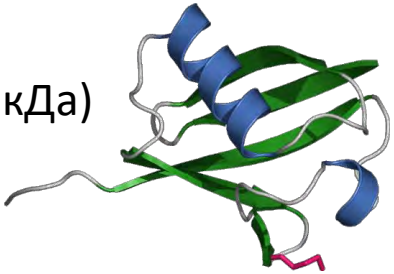

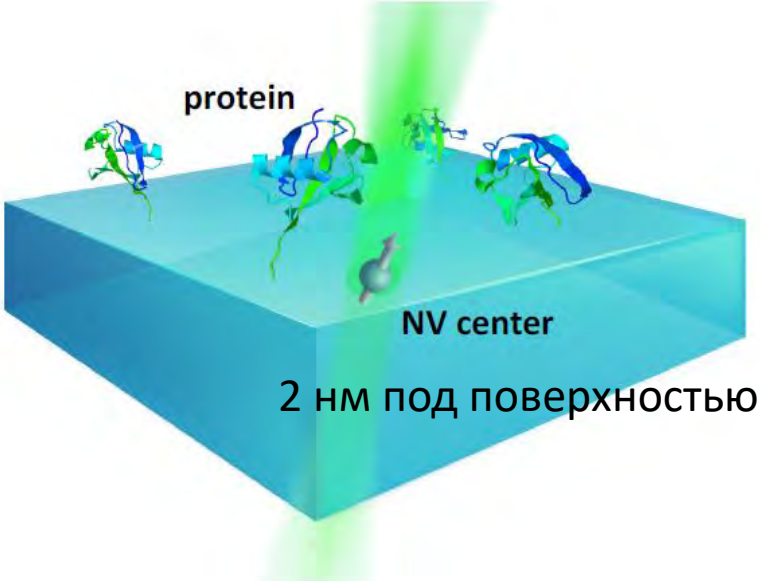

2 нм под поверхностью

НАНОЧАСТИЦЫ АЛМАЗОВ

Wu et al., Ang. Chemie Int Ed 2016 55(23):6586-98

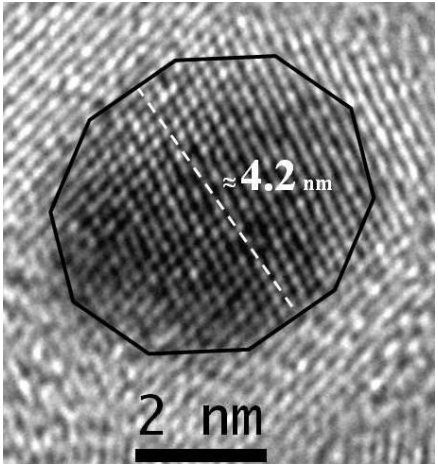

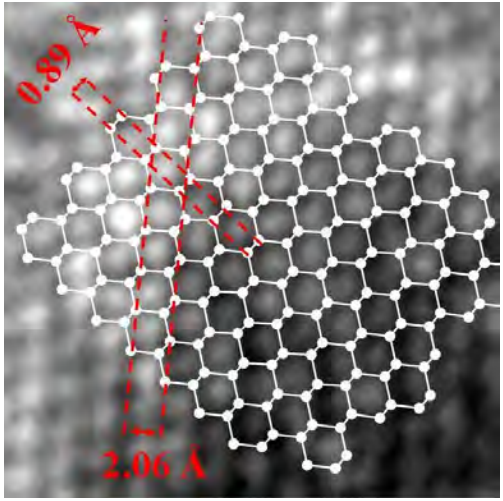

ЭКСПЕРИМЕНТЫ В КЛЕТКАХ

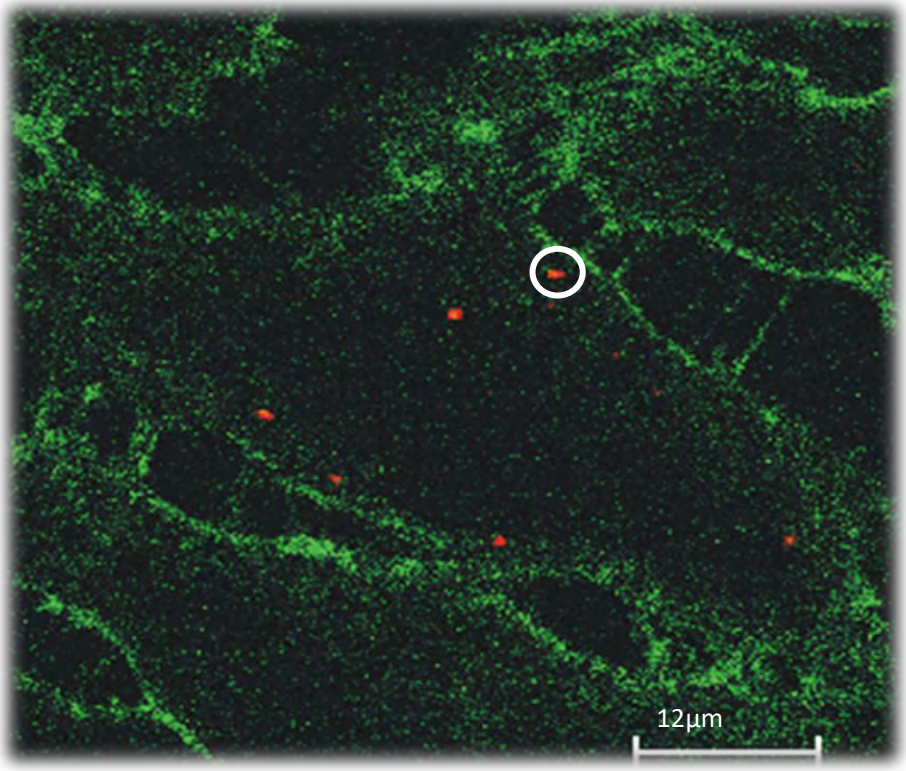

green: Plasma membrane,
red: Diamonds

ГИПЕРПОЛЯРИЗАЦИЯ ДЛЯ МРТ И ЯМР

ЯДЕРНАЯ МАГНИТНО-РЕЗОНАНСНАЯ ТОМОГРАФИЯ (МРТ)

Хорошее пространственное разрешение в тканях.

Недостаточная чувствительность для обнаружения отдельных молекул или клеток.

Увеличение поляризации путем увеличения поля.
Результат - «умеренное» увеличение чувствительности и разрешения
Увеличение стоимости магнита

ГИПЕРПОЛЯРИЗАЦИЯ ДЛЯ МРТ И ЯМР

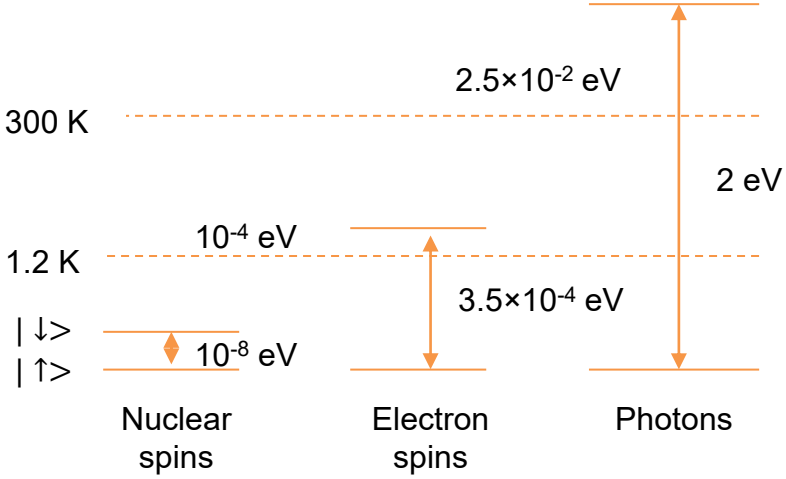

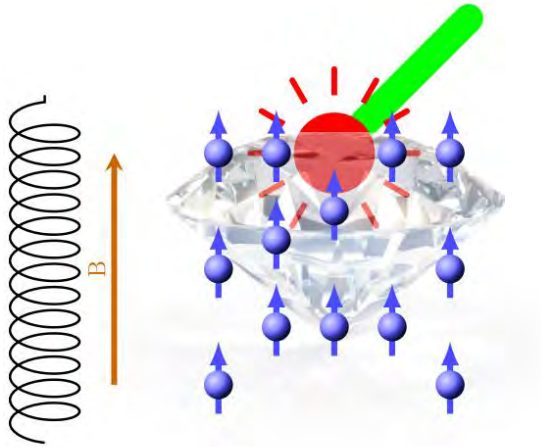

Hyperpolarized nanodiamonds

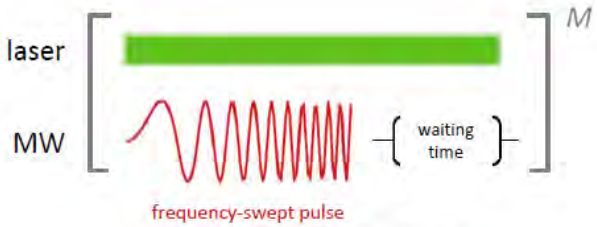

Integrated solid effect (ISE)

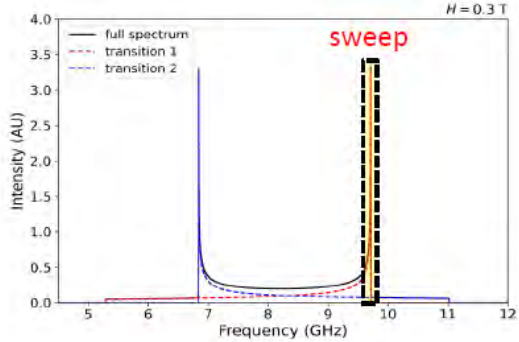

Outcome:

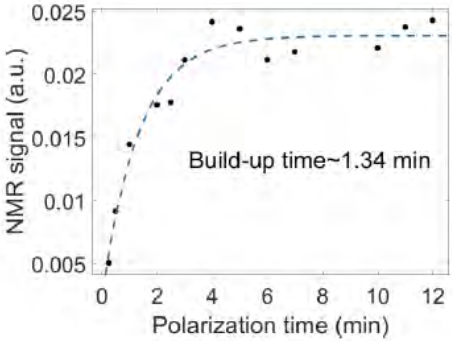

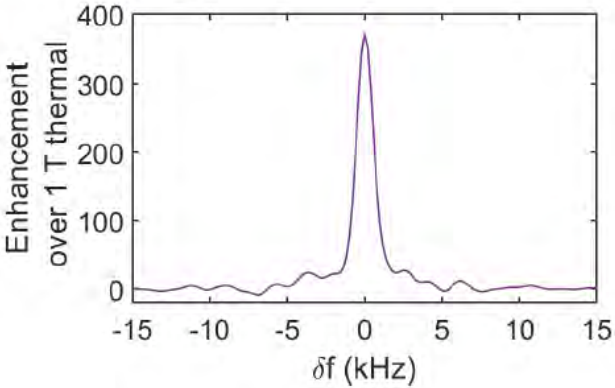

Enhancement over 1T thermal

x380

thermal = calculated from proton ref.

Hyperpolarization of proton spins with ensembles of shallow NV centers

Collaboration: NVISION (Ulm)

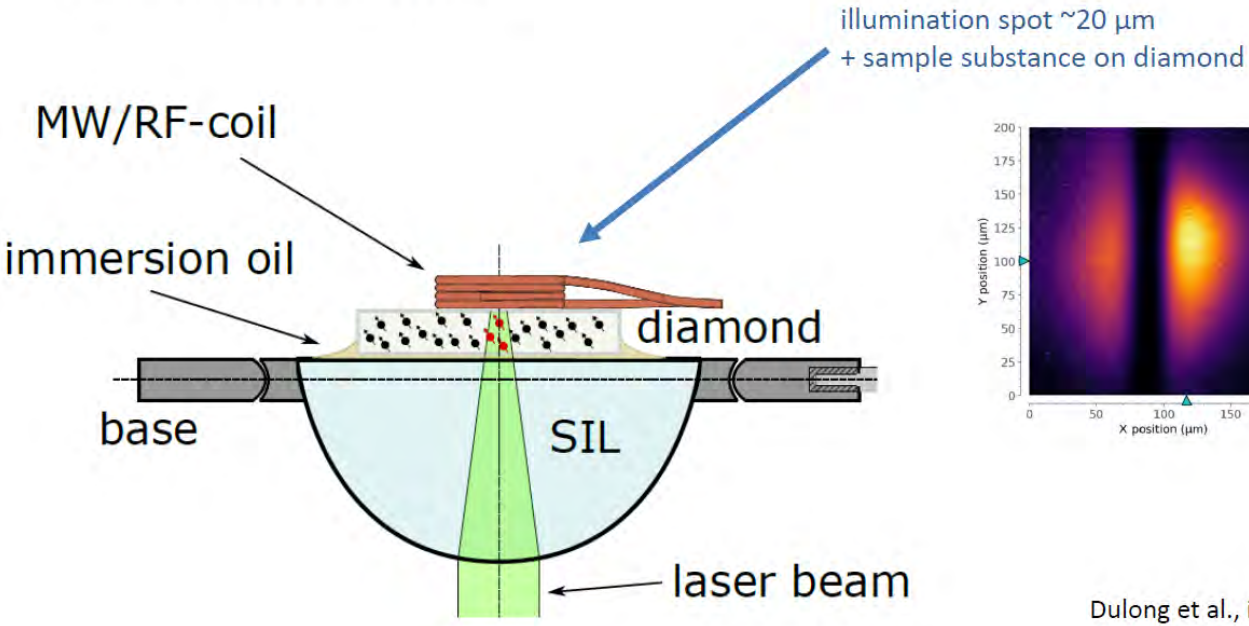

Dulong et al., in preparation

NANO-MRI USING MAGNETIC COATED SCANNING PROBES

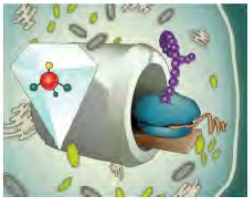

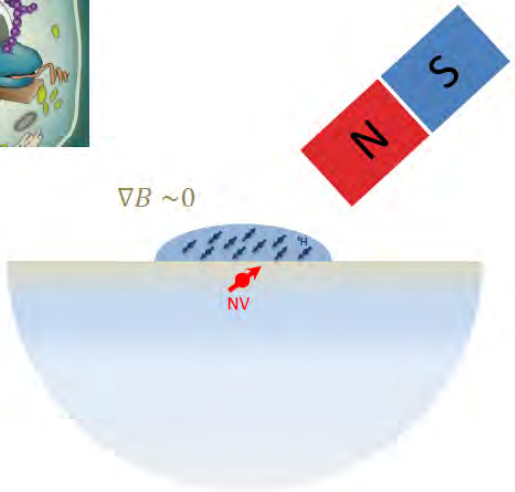

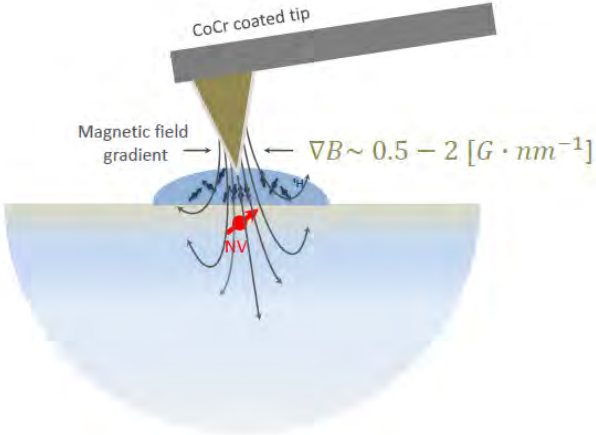

- Statistically polarized volume for both cases
- The tip-field gradient increases the spatial resolution

Room temperature optically induced dynamic nuclear polarization in diamond

Hyperpolarized and functionalized nanodiamonds

tracers in Magnetic Resonance Imaging (MRI)

Source of polarization for external bio-molecules

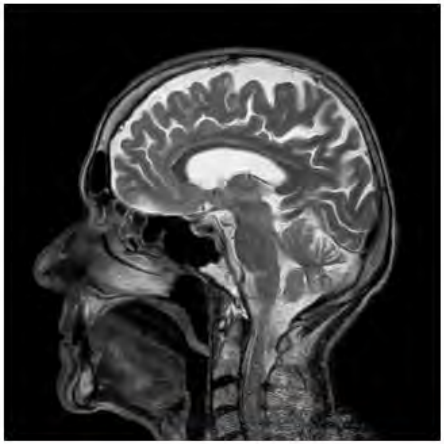

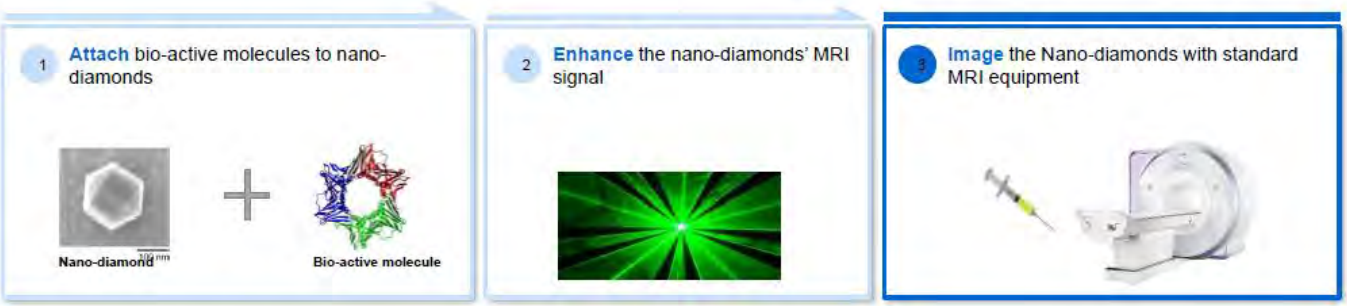

ГИПЕРПОЛЯРИЗАЦИЯ ДЛЯ МРТ

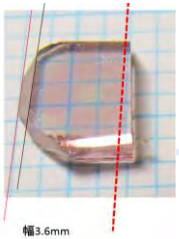

EPR

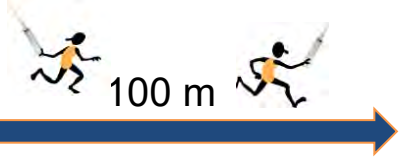

NMR

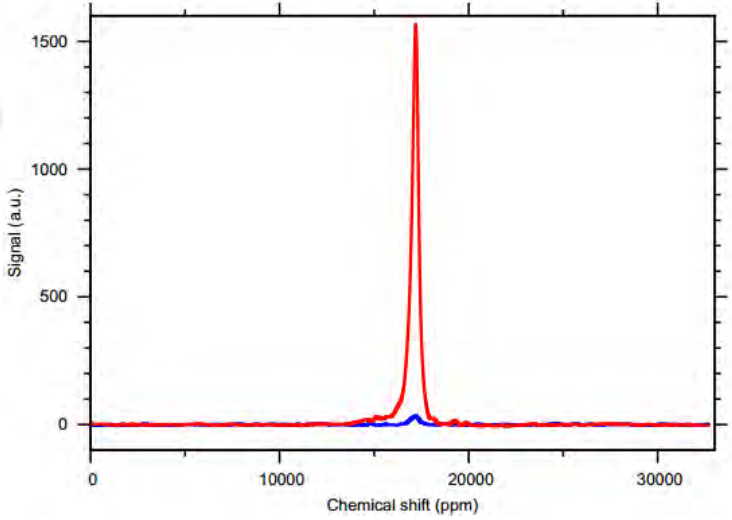

Preclinical PET and MR Evaluation

^{89}Zr- and ^{68}Ga-Labeled Nanodiamonds in Mice

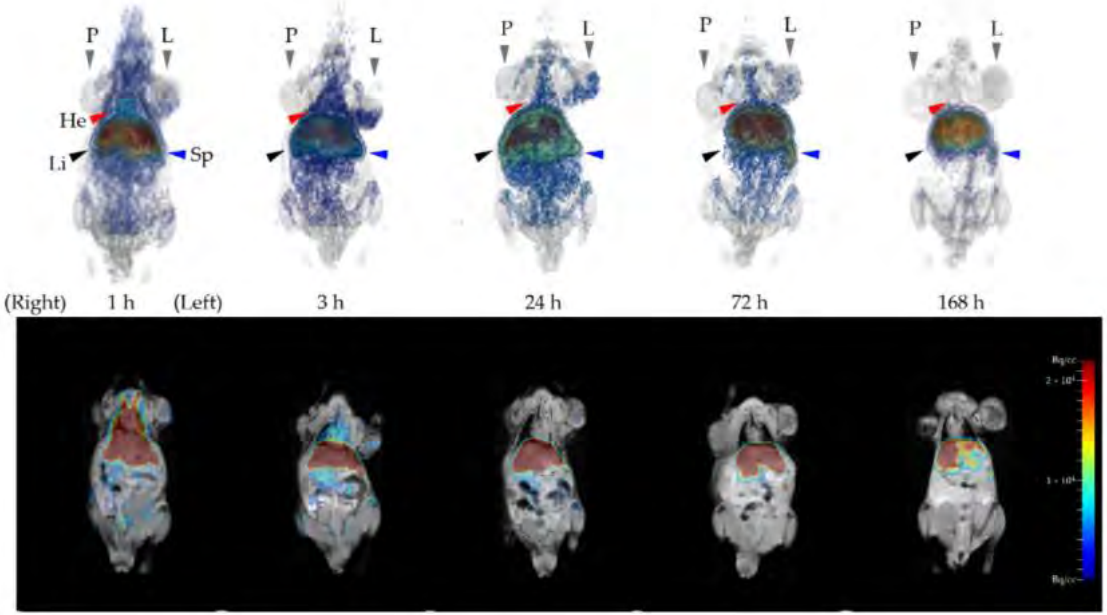

Winter et al., Nanomaterials **2022**, *12*(24), 4471

Design of nanoparticles for efficient polarization transfer to external nuclear spins

Collaboration: V. Agafonov (Tours University)

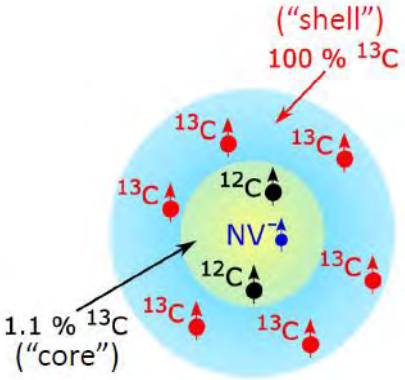

"Core" hosting NV center:

Natural ^{13}C content 1,1 %

Irradiated nanodiamonds with NV centers

"Shell" allowing spin diffusion:

With additional ^{13}C enrichment (50-100%)

As low as possible nitrogen concentration

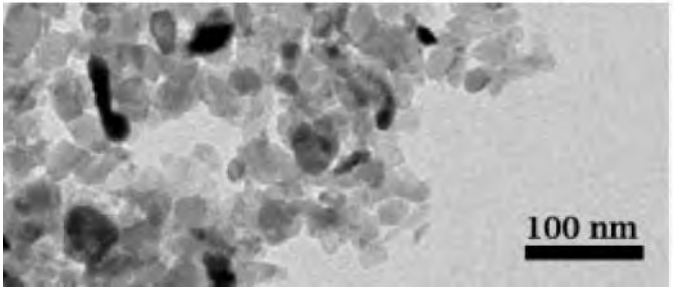

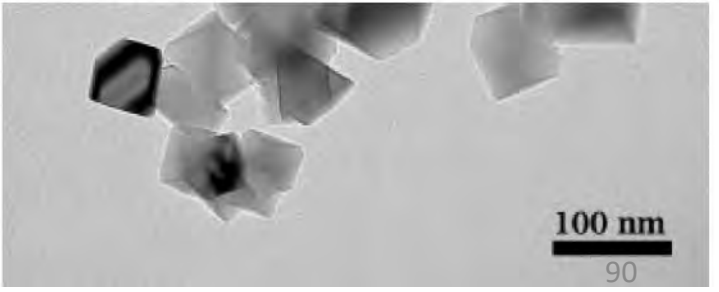

Core-shell diamond nanoparticles

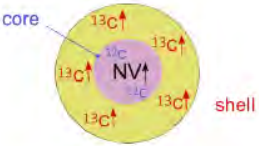

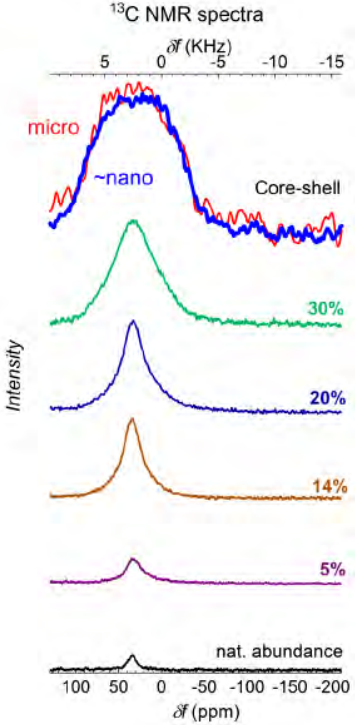

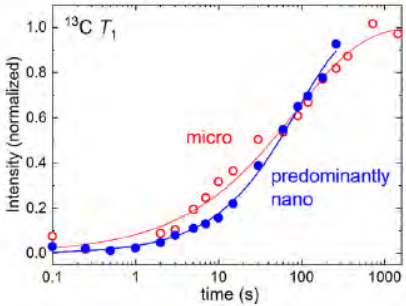

T_1 (spin relaxation time) ~ 90 sec

Diffusion length:

$$L = \sqrt{DT_1} = 24\ nm$$

where the nuclear spin diffusion constant D $=6.53 \times 10^{-14}$ cm^2 s^{-1} for 100% ^{13}C abundance

Y. Mindarava et. al *J. Phys. Chem. C* 125, 27647 (2021)

Quantum sensing with NV centers

Applications:
Single protein NMR
Zero-field NMR

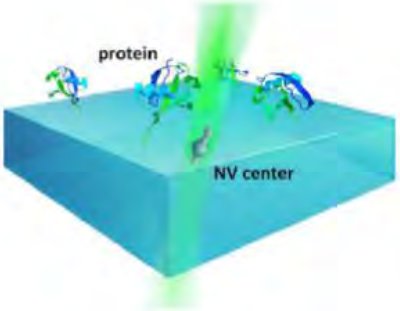

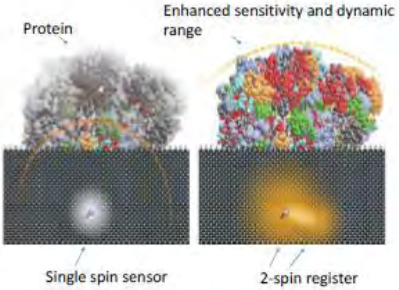

Hyperpolarized nanodiamonds as MRI tracers

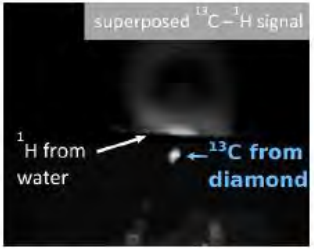

Minute magnetic fields are everywhere in life

Membrane pores:
I:10 pA
B field ~ 0.1nT

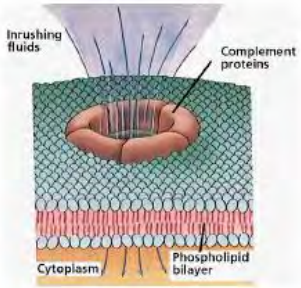

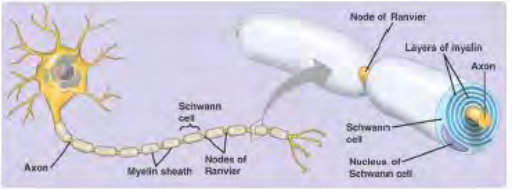

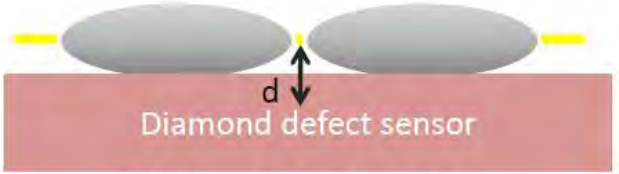

d=100nm; B field ~ 1 nT

Catalytic centers in enzymes:

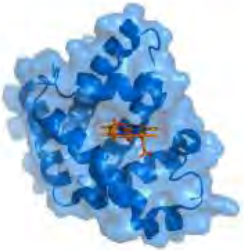

B field ~ 1μT@10nm

P#1 HYBRID QUANTUM REGISTERS

ELECTRON AND NUCLEAR SPINS

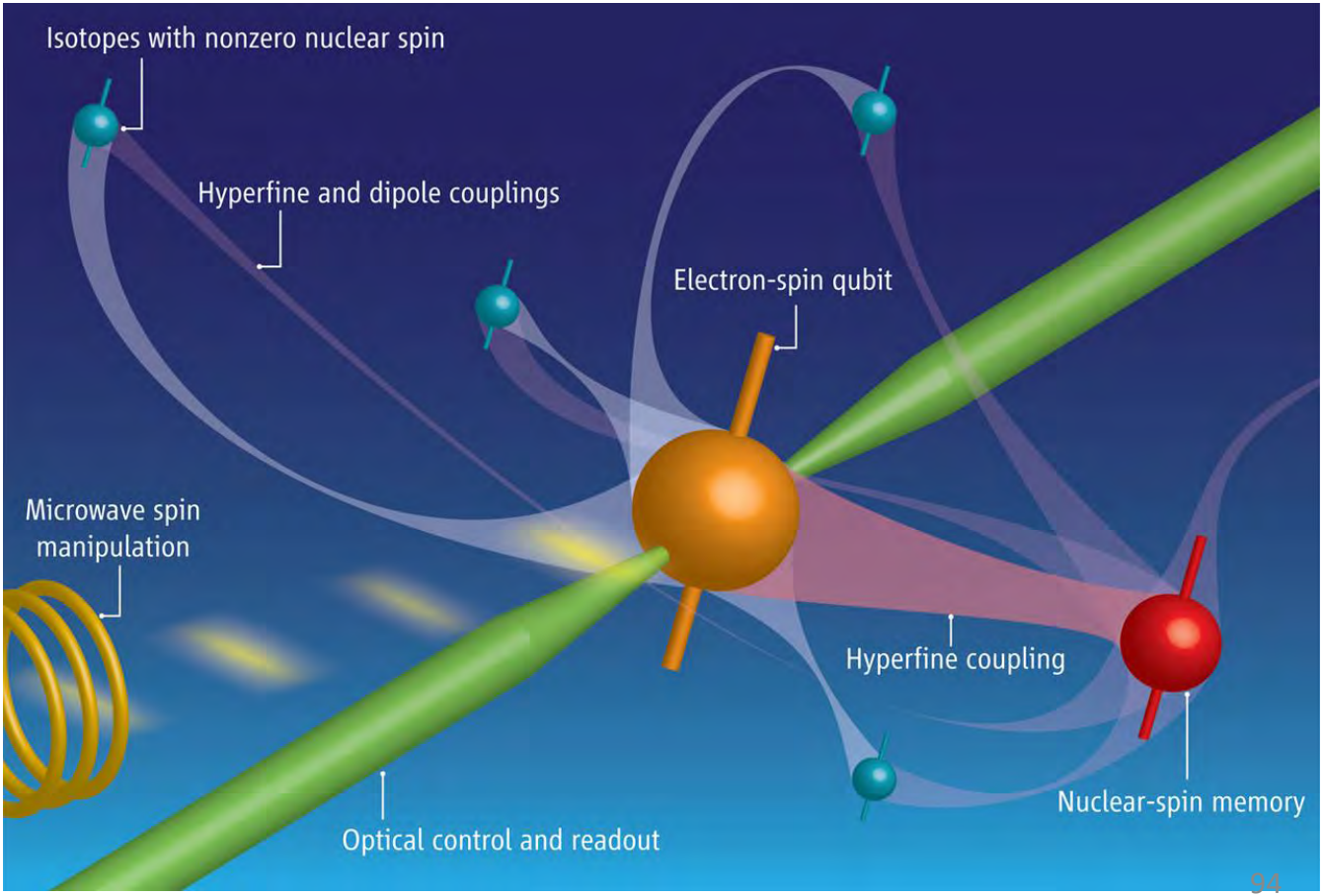

DANE R. MCCAMEY AND CHRISTOPH BOEHME, Science 2012

NV PLUS ^{13}C SPINS QUANUM REGITERS

SCALABLE NV BASED QUANTUM REGISTER

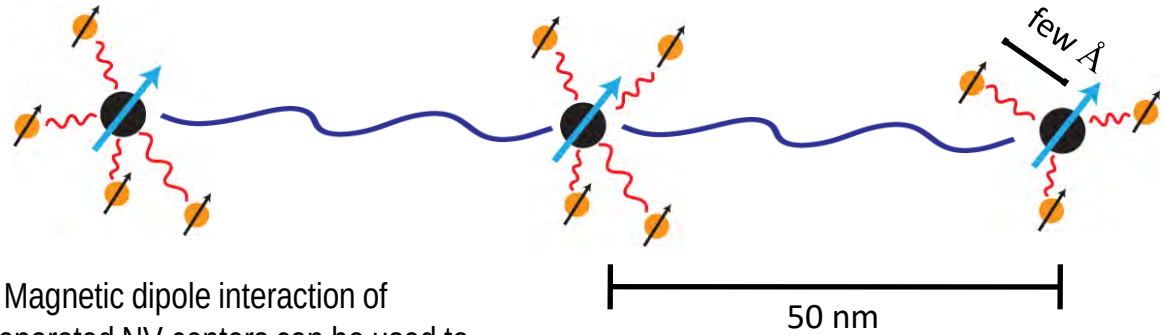

- Magnetic dipole interaction of separated NV centers can be used to increase the number of qubits
- Each NV is a small quantum register itself

For a distance of about = 50 nm is interaction is roughly 0.45 kHz - within T_2 time

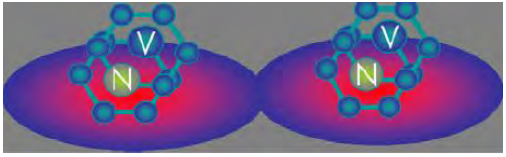

Challenges

Addressing single qubits

Create single spins with high accuracy

Magnetic dipole coupled spin arrays

$$B^{dip} = \left(\frac{\mu_0}{4\pi}\mu\right)\sqrt{3\cos^2\theta - 1}\Big/ r^3$$

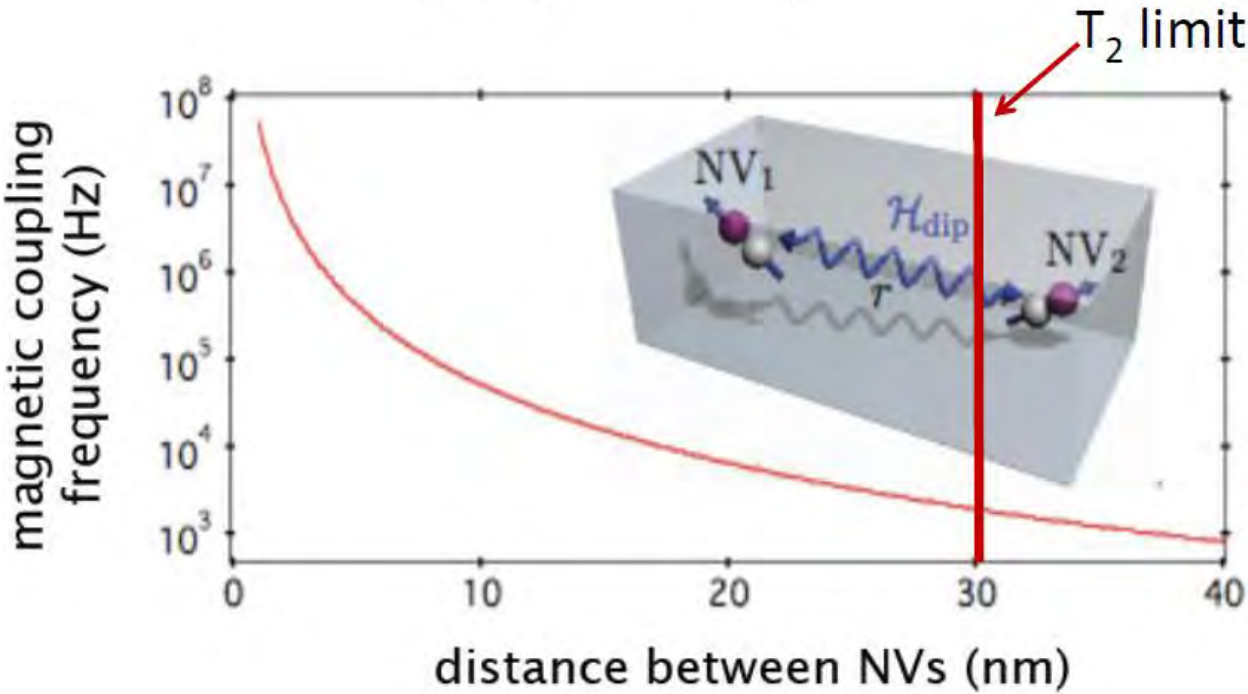

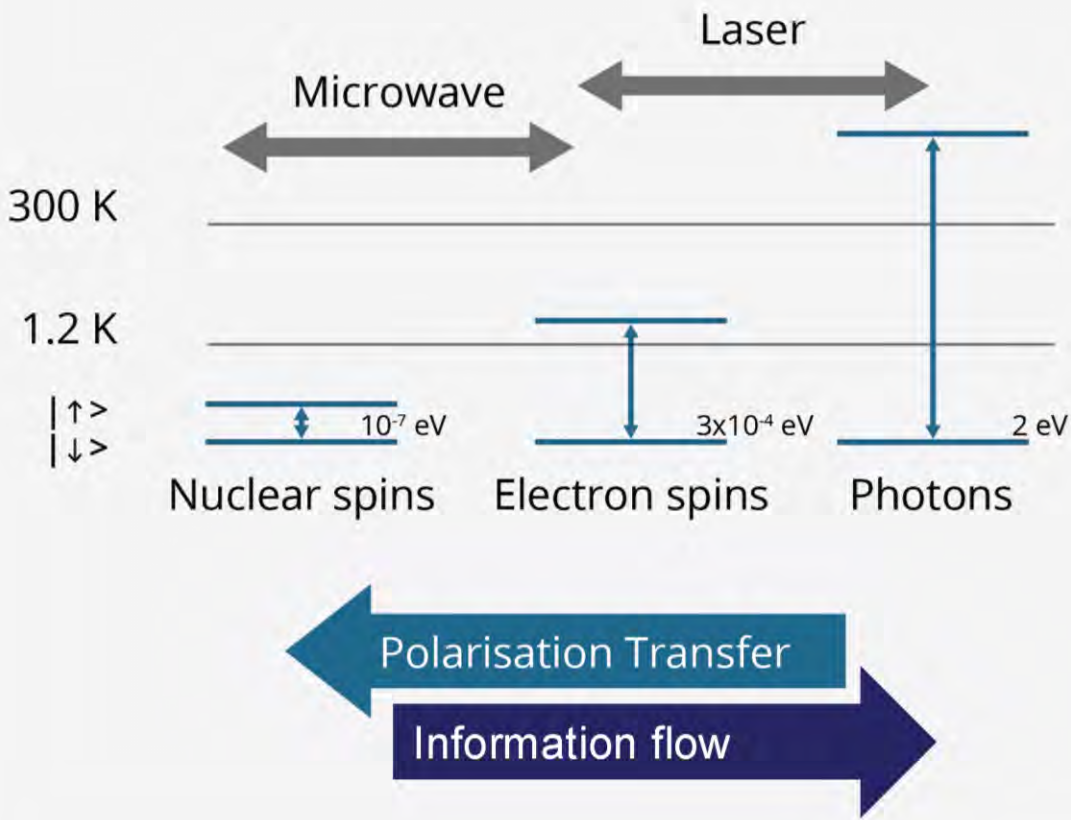
Laser
Microwave
300 K
1.2 K
|↑>
|↓>
10-7 eV
3x10-4 eV
2 eV
Nuclear spins
Electron spins
Photons
Polarisation Transfer
Information flow

A TEN-QUBIT SOLID-STATE SPIN REGISTER WITH QUANTUM MEMORY UP TO ONE MINUTE

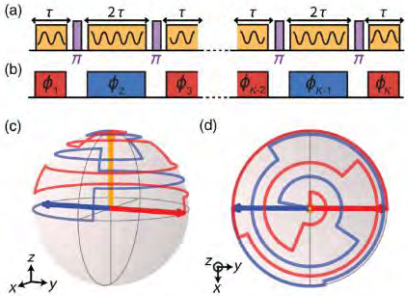

FIG. 2. (a) Illustration of the pulse sequence employed to realize a DDrf gate. Dynamical decoupling pulses on the electron

$$H = |0\rangle\langle 0| \otimes (\omega_L - \omega_1) I_z + |1\rangle\langle 1| \otimes \Omega[\cos(\phi) I_x + \sin(\phi) I_y],$$

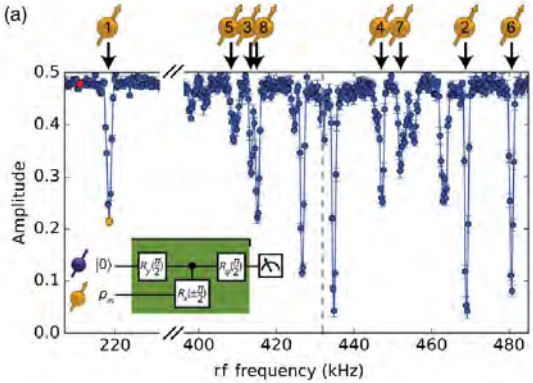

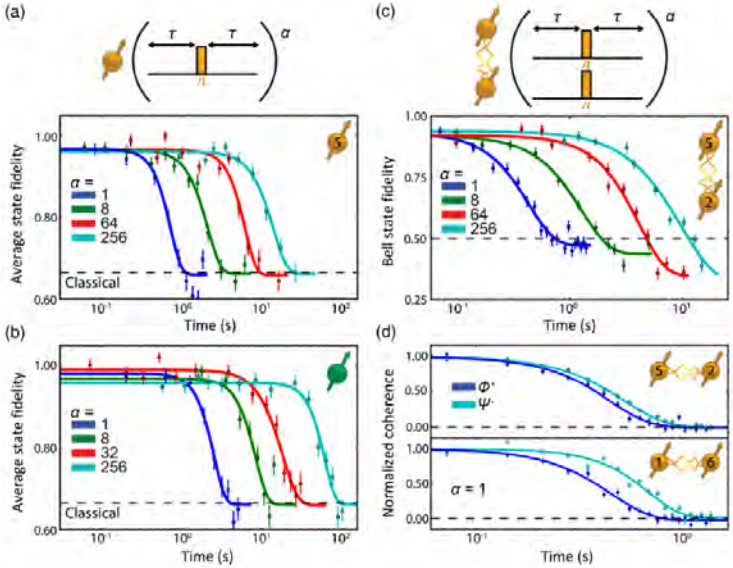

C. E. BRADLEY et al. PHYS. REV. X 9, 031045 (2019)

ATOMIC-SCALE IMAGING OF A 27-NUCLEAR-SPIN CLUSTER USING A QUANTUM SENSOR

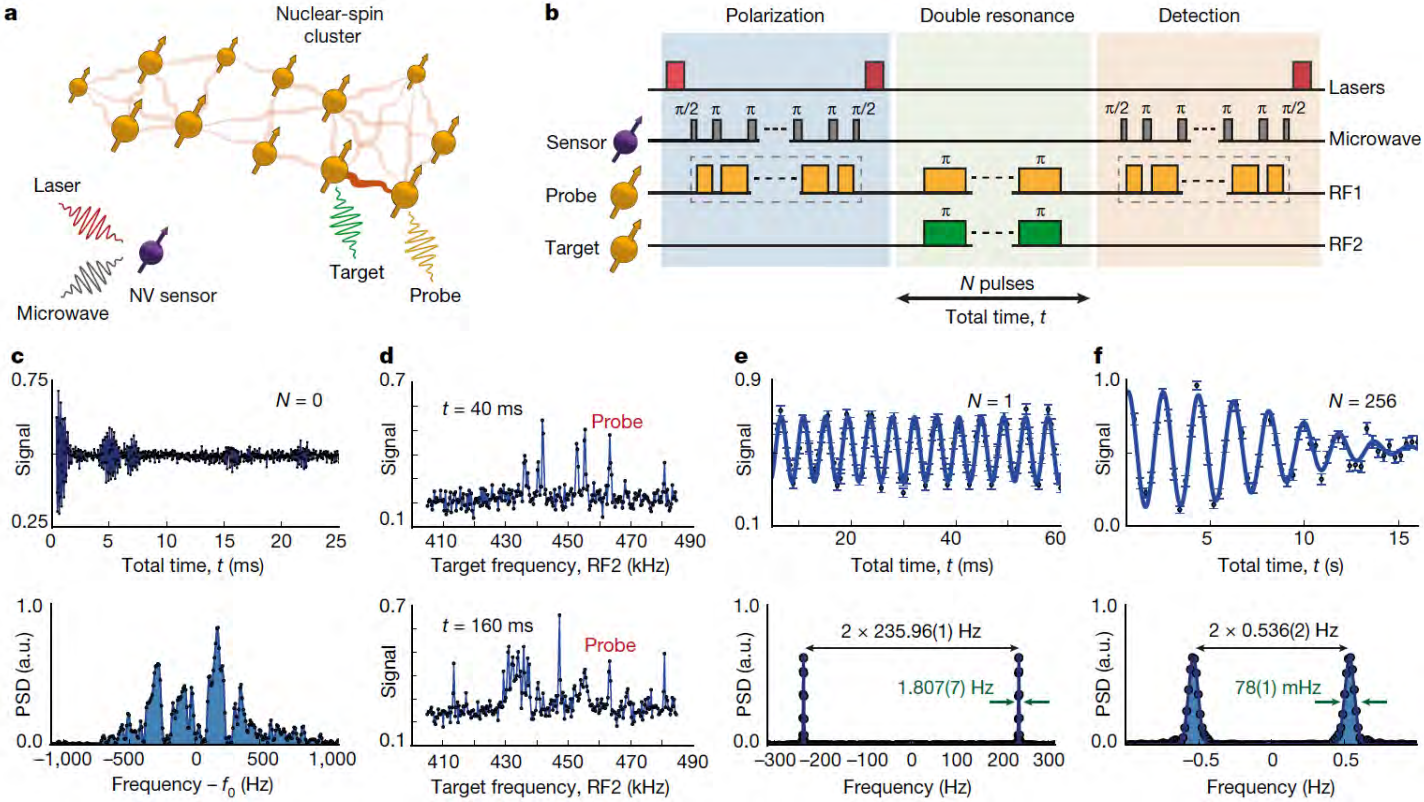

T. H. Taminiau, Nature | Vol 576 | 19/26 December 2019 | **413**

ATOMIC-SCALE IMAGING OF A 27-NUCLEAR-SPIN CLUSTER USING A QUANTUM SENSOR

Additionally, we determine the position of the NV sensor relative to the cluster. Although not required to reconstruct the cluster, this provides a control experiment. We measure the coupling of the 14N nuclear spin to 12 of the 13C spins (Extended Data Fig. 4). This unambiguously determines the location of both the 14N atom and the vacancy (fit uncertainties <0.3 A). We can now compare the electron–13C hyperfine couplings to previous density functional theory (DFT) calculations for 5 of our spins [33]. All 5 couplings agree with the DFT calculations (Extended Data Fig. 4), providing an independent corroboration of the extracted structure, as well as a direct test of the DFT calculations.

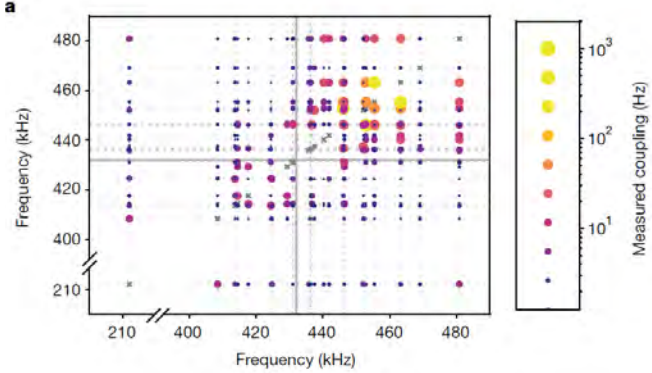

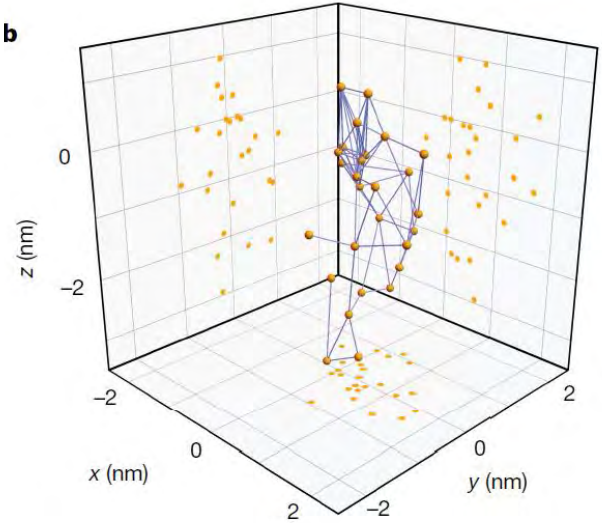

33. Nizovtsev, A. P. et al. Non-flipping 13C spins near an NV center in diamond: hyperfine and spatial characteristics by density functional theory simulation of the C510[NV]H252 cluster. *New J. Phys*. 20, 023022 (2018).

T. H. Taminiau, Nature | Vol 576 | 19/26 December 2019 | **413**

Three-dimensional localization spectroscopy of individual nuclear spins with sub-Angstrom resolution

J. Zopes[1], K.S. Cujia[1], K. Sasaki[1,2], J.M. Boss[1], K.M. Itoh[2] & C.L. Degen[1]

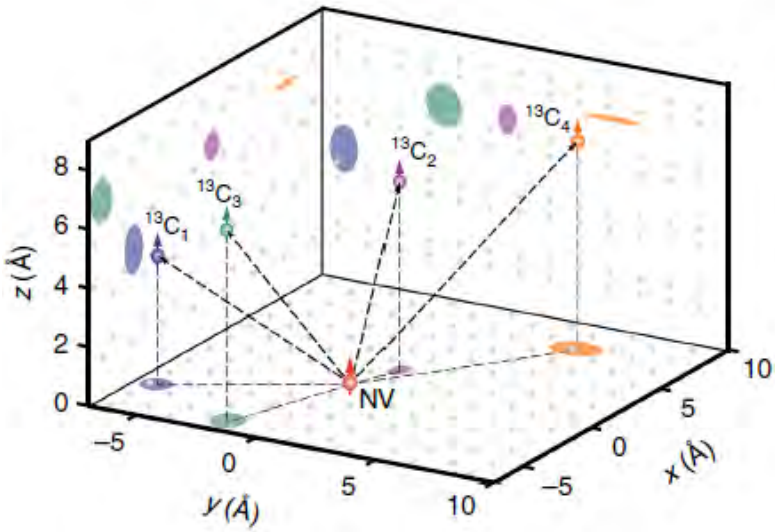

NATURE COMMUNICATIONS | (2018)9:4678 | DOI: 10.1038/s41467-018-07121-0

^{13}C SPIN CARTOGRAPHY (3D LOCALIZATION SPECTROSCOPY OF INDIVIDUAL NUCLEAR SPINS WITH SUB-ANGSTROM RESOLUTION) & HFI CHARACTERIZATION

SIMULATION OF THE CLUSTER $C_{510}[NV]H_{252}$: STABLE NON-FLIPPING ^{13}C NUCLEAR SPINS

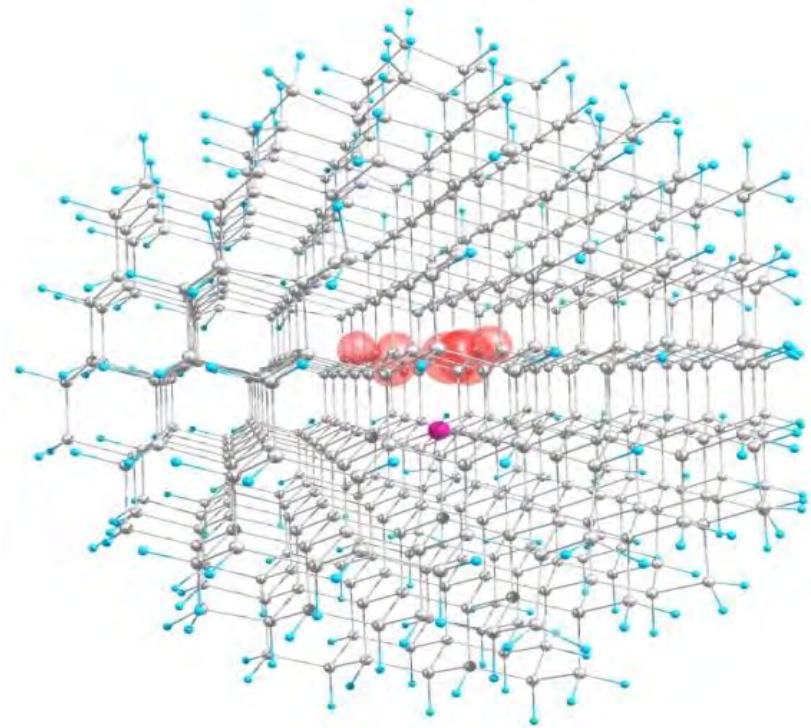

We simulated hfi matrices for all possible positions of ^{13}C in the cluster and used them in spin-Hamiltonian of NV-^{13}C spin systems to calculate the observable.

Here we are interested in the search of hfi characteristics and positions for stable (or near-stable) systems NV-^{13}C.

$$\mathbf{A} = \begin{pmatrix} \mathbf{A_{XX}} & \mathbf{A_{XY}} & \mathbf{A_{XZ}} \\ \mathbf{A_{YX}} & \mathbf{A_{YY}} & \mathbf{A_{YZ}} \\ \mathbf{A_{ZX}} & \mathbf{A_{ZY}} & \mathbf{A_{ZZ}} \end{pmatrix}$$

$$\tau_0 = 1/\gamma_0 \sim 1 + A_{ZZ}^2 / A_{nd}^2$$

Nizovtsev et.al. New journal of Physics, 20 (2018) 023022

SIMULATED "LIFETIMES" OF ALL POSSIBLE ^{13}C NUCLEAR SPINS IN THE $C_{510}[NV]H_{252}$ CLUSTER

^{13}C spin "lifetime"

$$\tau_0 = 1/\gamma_0 \sim 1 + A_{ZZ}^2 / A_{nd}^2$$

Keep in mind the log scale !!!!

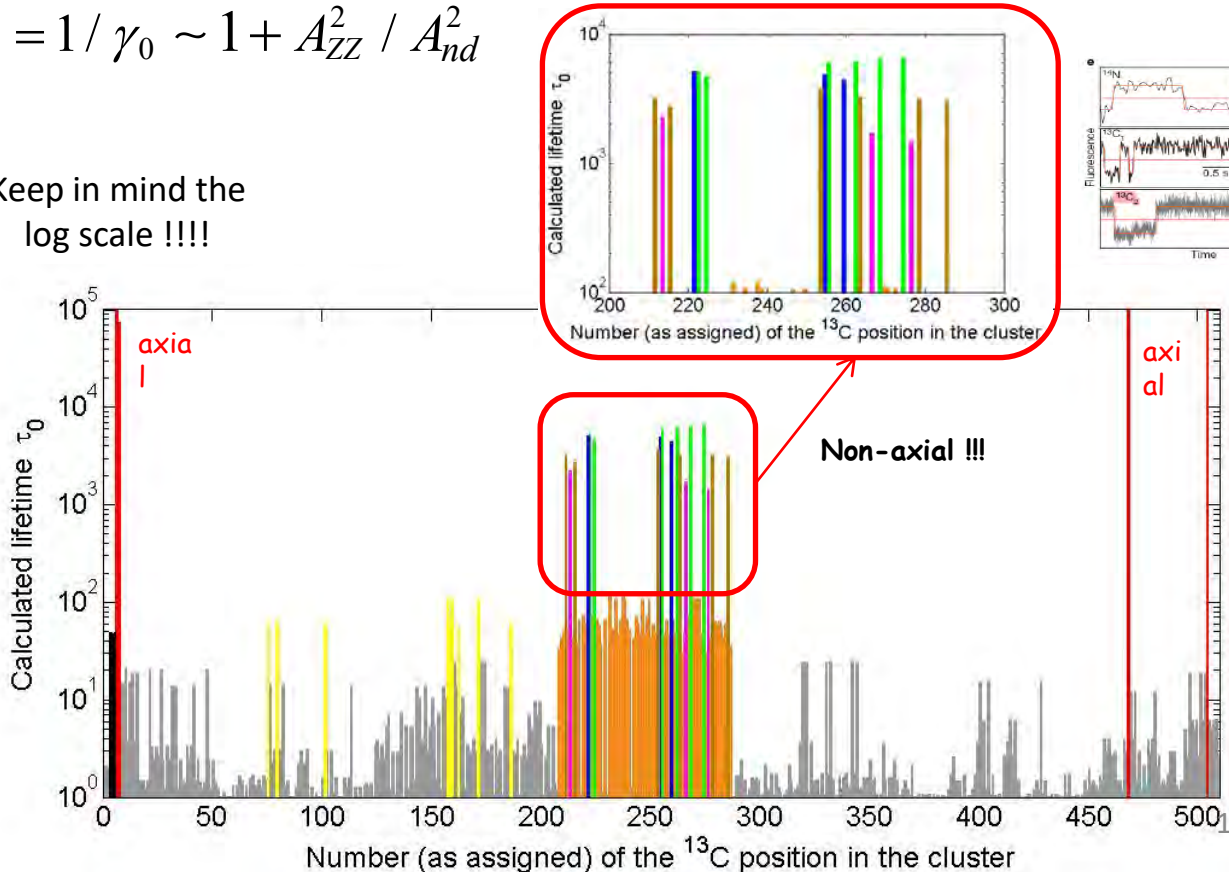

SPATIAL LOCATIONS OF NEAR-STABLE NON-AXIAL SYSTEMS NV-^{13}C IN THE CLUSTER

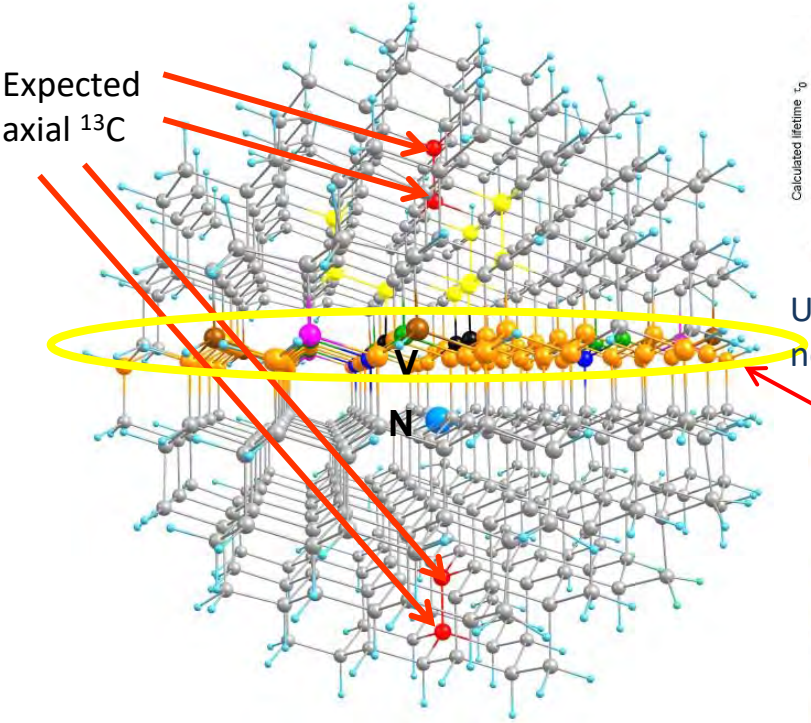

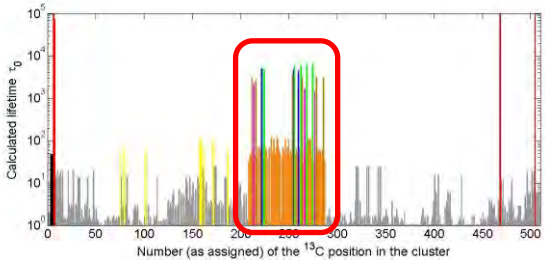

Unexpected
non-axial ^{13}C

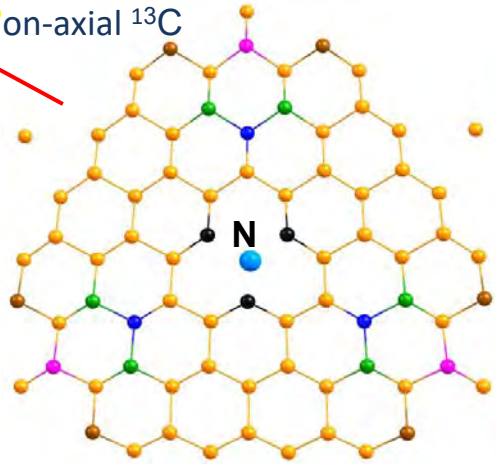

side view

top view

SPIN DENSITY DISTRIBUTION NEAR STABLE POSITIONS IS SYMMETRIC!

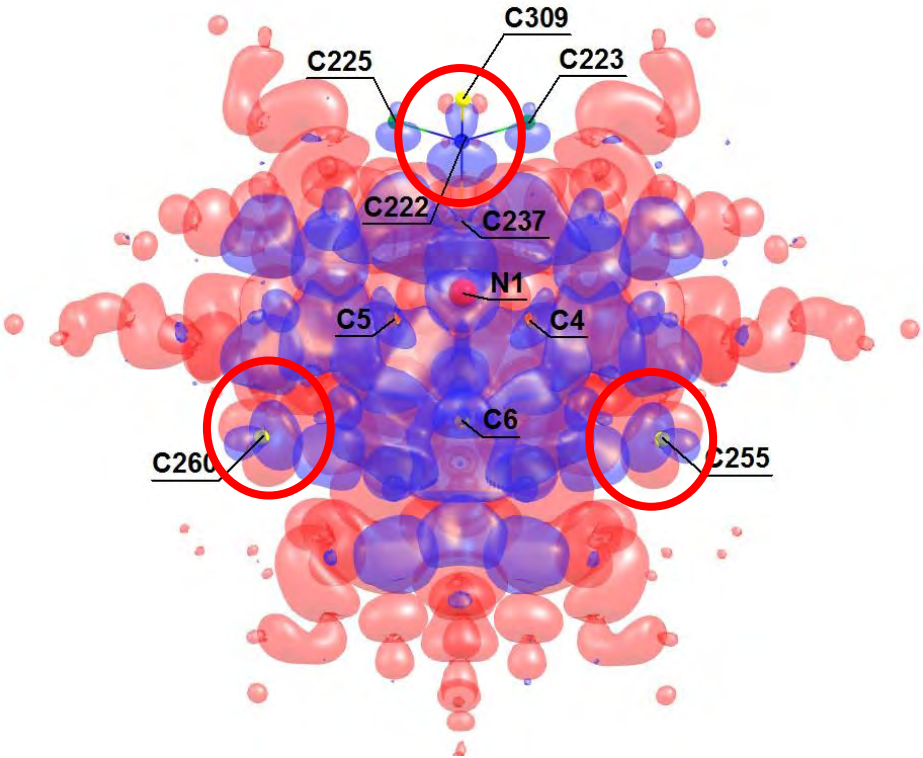

Top view

Red – positive spin density distribution contour with small value (~0.0001) over the cluster.
Blue – negative spin density.

View is chosen so to visualize symmetric negative spin density distributions **at stable positions C222, C225 and C223.**

Positions C222, C255 and C260 belongs to the St1(K2) family, positions C225, C223 – to the St2(Y) family.

SPIN DENSITY DISTRIBUTION
NEAR ONE SPECIFIC STABLE POSITION C222

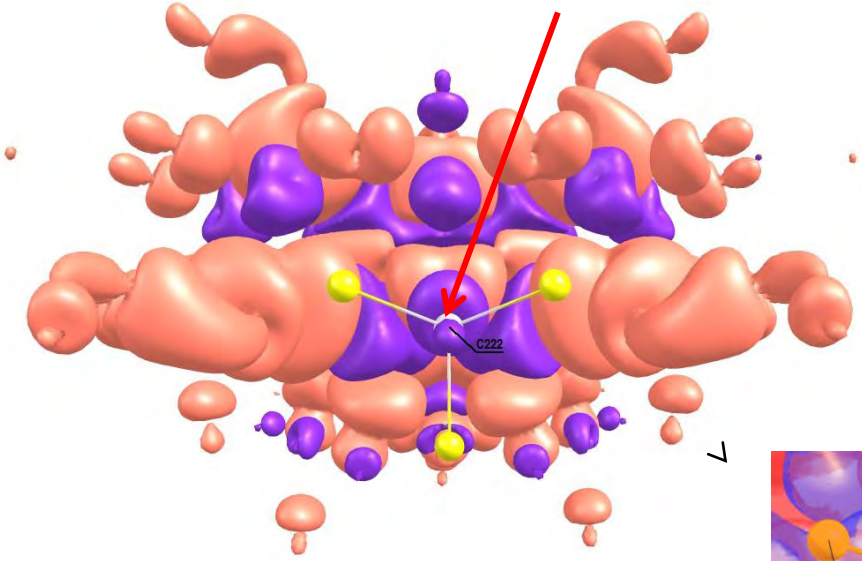

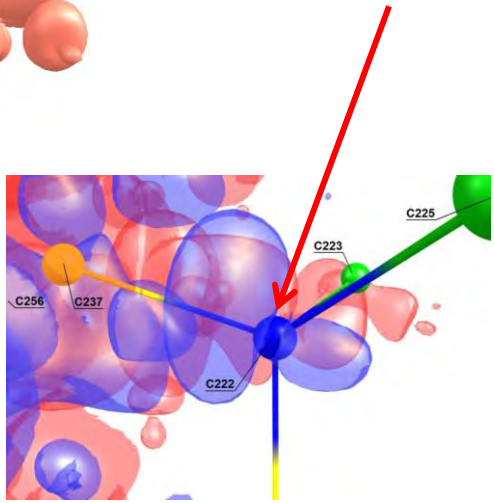

INTERPRETATION OF STABLE ^{13}C

Stable (or near-stable) NV-^{13}C spin systems have small off-diagonal elements A_{ZX} and A_{ZY} in their hfi matrices $A_{KL,}$ resulted from anisotropic (dipole-dipole) part of hfi. They are expressed in terms of spin density

$$\rho_\sigma = \rho_\uparrow - \rho_\downarrow$$

$$A_{aniso} = \frac{\mu_0}{4\pi}(g_e\mu_e)(g_n\mu_n)\int T(r)\rho_\sigma(r+r_n)dr$$

- Anisotropic (dipolar) part

$$T(r) = \frac{1}{r^5}\begin{pmatrix} 3x^2 - r^2 & 3xy & 3xz \\ 3xy & 3y^2 - r^2 & 3yz \\ 3xz & 3yz & 3z^2 - r^2 \end{pmatrix}$$

-dipole-dipole interaction tensor (traceless)

If the local spin density distribution in the location of certain ^{13}C is symmetric with respect to the sign change of x and y then the integrals will be zero !!! So, we need just to visualize the spin density….

EXPERIMENTAL CONFIRMATION (ULM)

They re-investigated the very stable NV-^{13}C spin system of the article [PRL 116, 230502 (2016)] undergoing B=340 gauss (||OZ) and exhibiting the hfi-induced splitting of the state m_S=-1 of Δ~50 kHz.

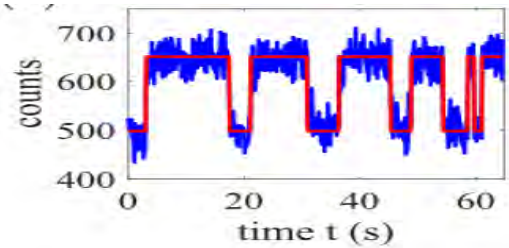

and measure Zeeman+hfi splittings of both involved NV substates m_S=0 and m_S=-1

m_S=-1

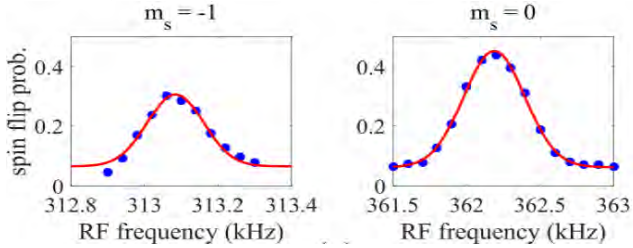

m_S=0

peaked at Δ^-=313.1 kHz

<

peaked at δ=362.1 kHz

FIVE-QUBIT CODE WITH A FLAG PROTOCOL THAT ENABLES FAULT TOLERANCE USING A TOTAL OF SEVEN QUBITS

Chao, R. & Reichardt, B. W. Quantum error correction with only two extra qubits. *Phys. Rev. Lett.* 121, 050502 (2018).

Chao, R. & Reichardt, B. W. Flag fault-tolerant error correction for any stabilizer code. *PRX Quantum* 1, 010302 (2020).

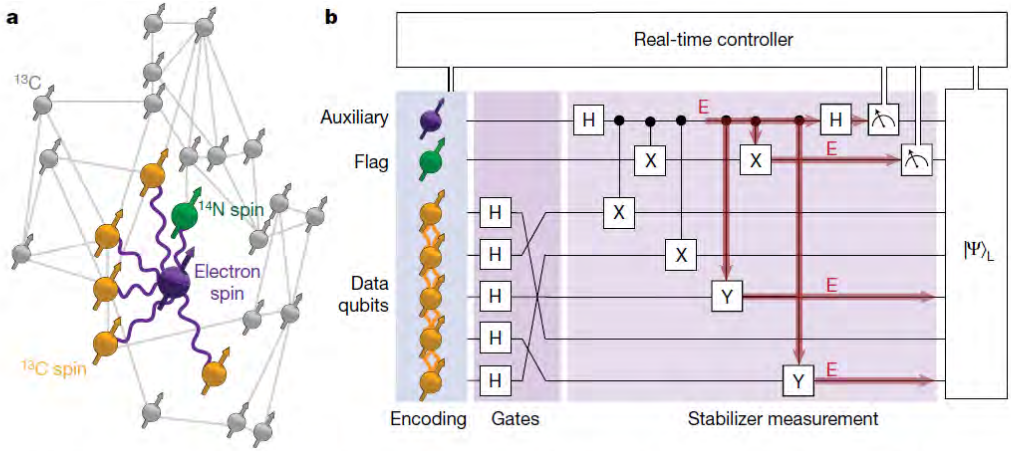

Fig. 1 | Diamond quantum processor, logical qubit and fault tolerance. **a**, Our processor consists of a single NV centre and 27 ^{13}C nuclear-spin qubits, for which the lattice sites and qubit–qubit interactions are known[38]. We select five ^{13}C qubits as data qubits that encode the logical state (yellow). The other qubits (grey) are not used here. We use the NV electron spin (purple) as an auxiliary qubit for stabilizer measurements and the NV ^{14}N nuclear spin (green) as a flag qubit to ensure fault tolerance. Purple lines indicate the electron–nuclear two-qubit gates used here (Methods). Grey lines indicate dipolar nuclear–nuclear couplings greater than 6 Hz. **b**, Illustration of the main components of the experiment. We realize fault-tolerant encoding, gates and stabilizer measurements with real-time processing on a logical qubit of the five-qubit quantum error-correction code. To ensure that any single fault does not cause a logical error, an extra flag qubit is used to identify errors that would propagate to multi-qubit errors and corrupt the logical state[28]. An illustration of such an error E is shown in red.

T. H. Taminiau at.el

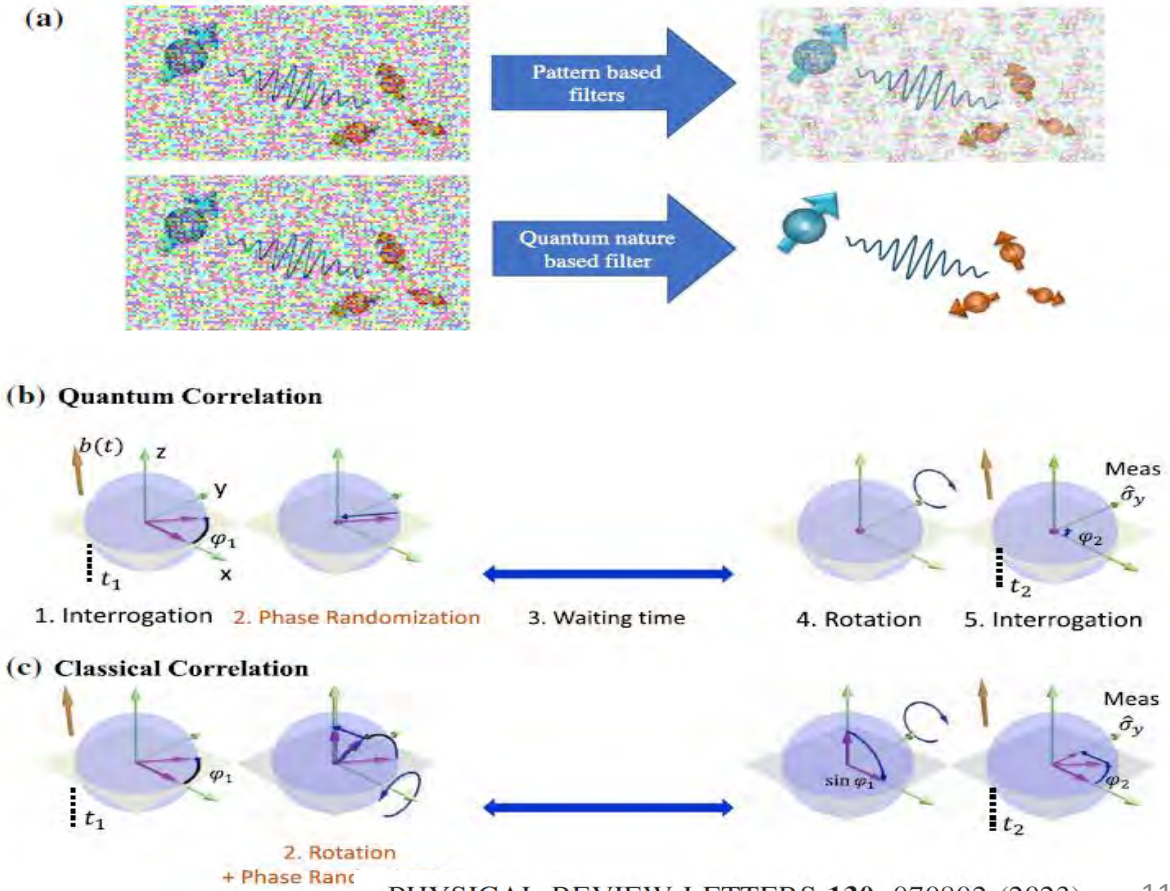

PHYSICAL REVIEW LETTERS **130,** 070802 (2023)

NEW OBJECTS FOR QC

NEW STABLE QUBITS: ^{13}C - ^{13}C DIMERS

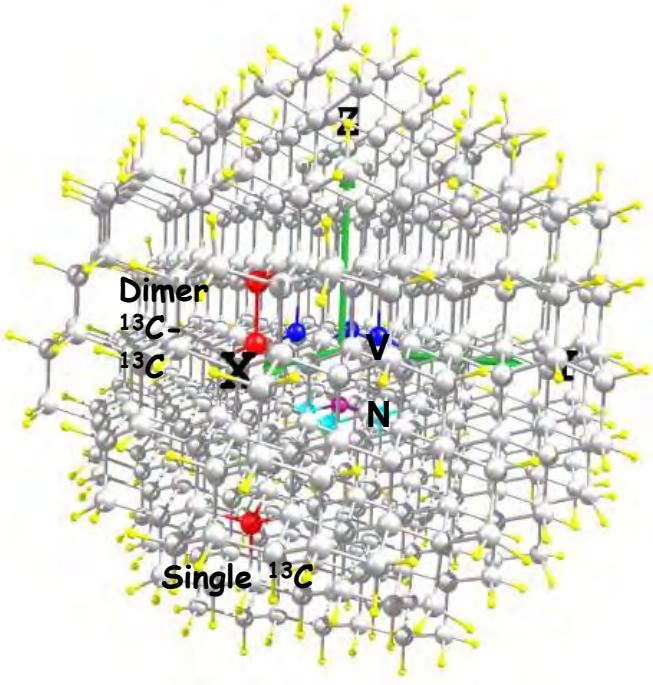

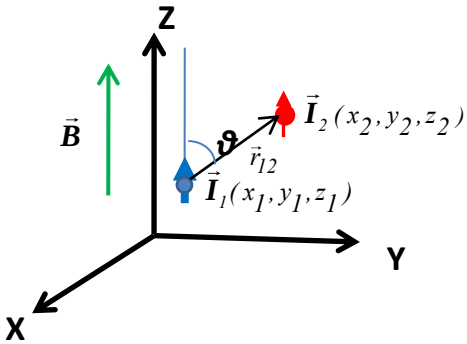

$$|T_-\rangle = |\uparrow\uparrow\rangle$$

$$|T_0\rangle = \frac{|\uparrow\downarrow\rangle + |\downarrow\uparrow\rangle}{\sqrt{2}}$$

$$|T_+\rangle = |\downarrow\downarrow\rangle$$

$$|S_0\rangle = \frac{|\uparrow\downarrow\rangle - |\downarrow\uparrow\rangle}{\sqrt{2}}$$

Simulation of Indirect ^{13}C–^{13}C J-Coupling Tensors in Diamond Clusters Hosting the NV Center Nizovtsev et. al (2022) elhttps://doi.org/10.3390/materproc2022009004

ВЗАИМОДЕЙСТВИЕ ЯДЕРНЫХ СПИНОВ

Диполь-дипольное

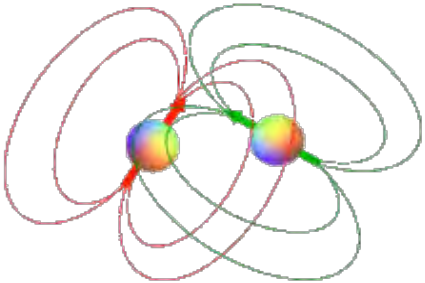

$$\hat{\mathcal{H}}_{DD} = -\frac{\mu_0 \gamma_1 \gamma_2 \hbar^2}{4\pi} \left(\frac{3(\hat{\boldsymbol{I}}_1 \cdot \boldsymbol{r}_{12})(\hat{\boldsymbol{I}}_2 \cdot \boldsymbol{r}_{12})}{r_{12}^5} - \frac{\hat{\boldsymbol{I}}_1 \cdot \hat{\boldsymbol{I}}_2}{r_{12}^3} \right),$$

Величина вз. двух ^{13}C на расстоянии 1.54 Å ~ 2 кГц

Непрямое (J-couping)

$$\hat{\mathcal{H}}_J = \hat{\boldsymbol{I}}_1 \cdot \hat{J} \cdot \hat{\boldsymbol{I}}_2. \qquad \mathbf{J} = \begin{pmatrix} J_{xx} & J_{xy} & J_{xz} \\ J_{yx} & J_{yy} & J_{yz} \\ J_{zx} & J_{zy} & J_{zz} \end{pmatrix}.$$

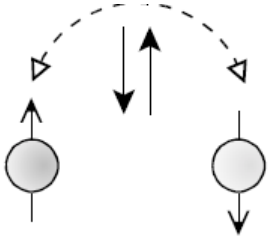

Обычно измеряют только изотропную константу Jiso=Sp(J)/3.
Типичные величины ~ 10-200 Гц

SPIN-HAMILTONIAN OF ^{13}C-^{13}C DIMER IN MAGNETIC FIELD

$$H = -\gamma^{13C}(\vec{I}_1 + \vec{I}_2)\vec{B} + \vec{I}_1 \bullet (D^{(1,2)} + J^{(1,2)}) \bullet \vec{I}_2$$

where γ=1.07084 kHz/G – gyromagnetic ratio, I_1, I_2 – operators of spin I=1/2 with spatial components:

$$I_x = \begin{pmatrix} 0 & 1 \\ 1 & 0 \end{pmatrix} / 2, \quad I_y = \begin{pmatrix} 0 & -i \\ i & 0 \end{pmatrix} / 2, \quad I_z = \begin{pmatrix} 1 & 0 \\ 0 & -1 \end{pmatrix} / 2$$

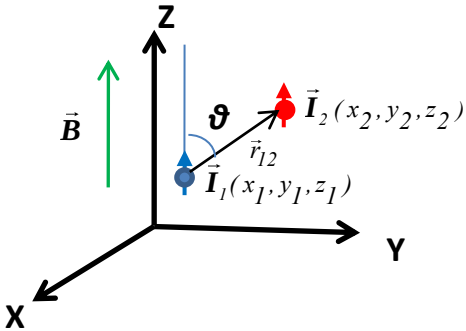

$D^{(1,2)}$ and $J^{(1,2)}$ - dipole-dipole and indirect coupling tensors

R.E,Wasylishen. Dipolar and Indirect Coupling Tensors in Solids.

eMagRes, Online © 2007 John Wiley & Sons, Ltd.
This article is © 2007 John Wiley & Sons, Ltd.
This article was previously published in the *Encyclopedia of Magnetic Resonance* in 2007 by John Wiley & Sons, Ltd.
DOI: 10.1002/9780470034590.emrstm0125

To simulate NMR spectra of C-C dimers we will use the total spin-Hamiltonian with total D and J tensors calculated for the above cluster. Numerical diagonalization of the spin-Hamiltonian gives energy levels and eigenstates of the coupled C-C spin system and allows to predict frequencies and amplitudes of lines in the NMR spectrum of any specific ^{13}C-^{13}C dimer. We did such analysis for few exemplary ^{13}C-^{13}C dimers (see below) and compare the results with simplified analytical formulas.

EPR SPECTRA OF ^{13}C-^{13}C DIMERS

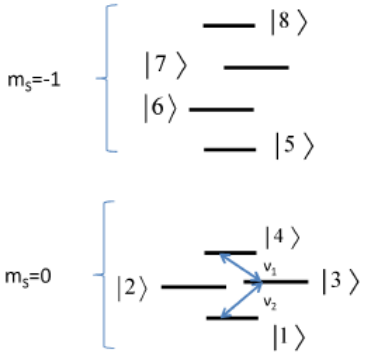

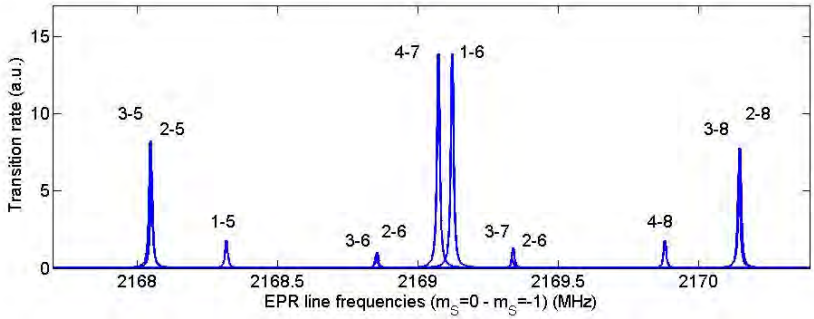

SINGLET EXITATION →

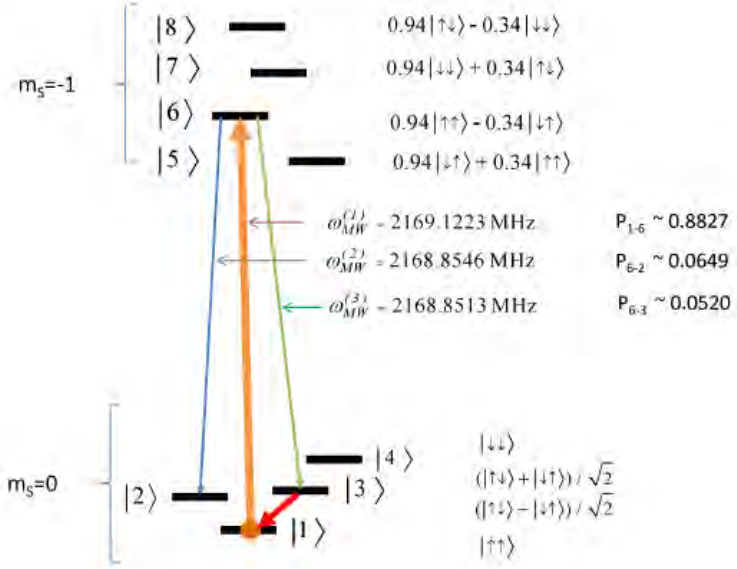

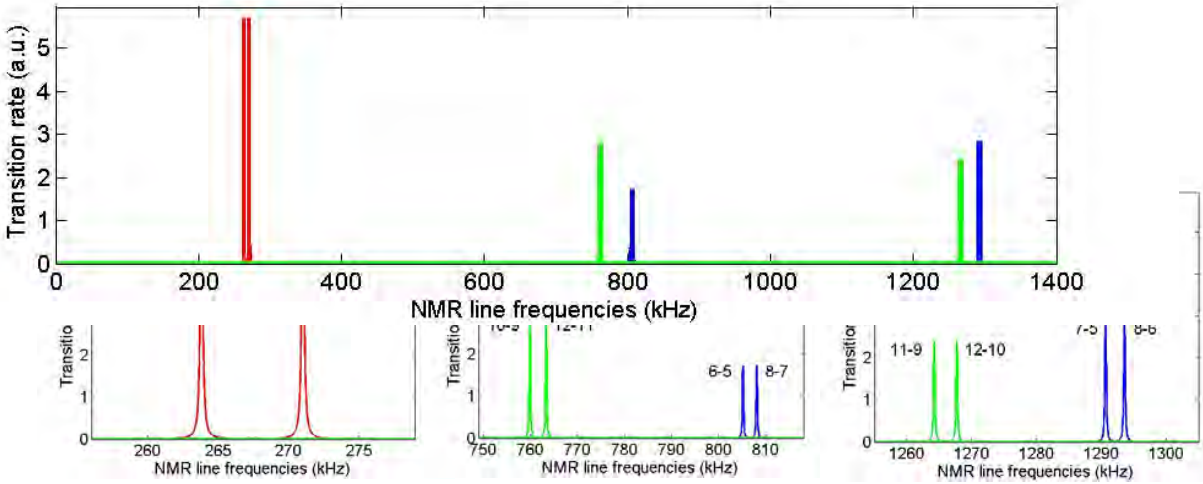
Transition rate (a.u.)
NMR line frequencies (kHz)
6-5
8-7
11-9
12-10

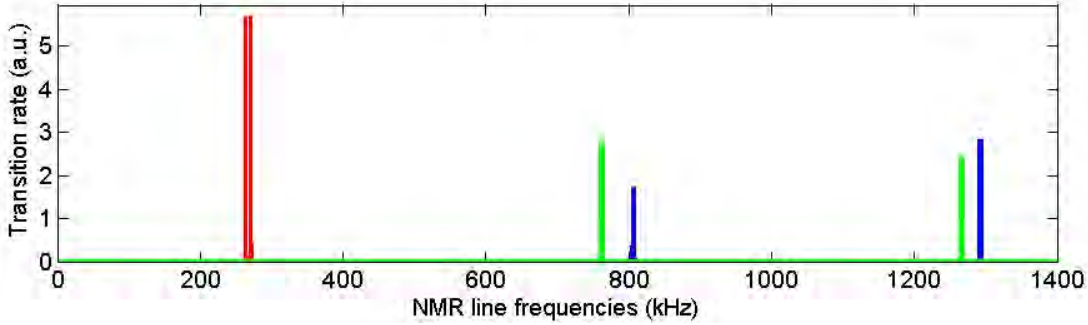
Transition rate (a.u.)
NMR line frequencies (kHz)

ENTANGLEMENT OF SPIN-PAIR QUBITS WITH INTRINSIC DEPHASING TIMES EXCEEDING A MINUTE

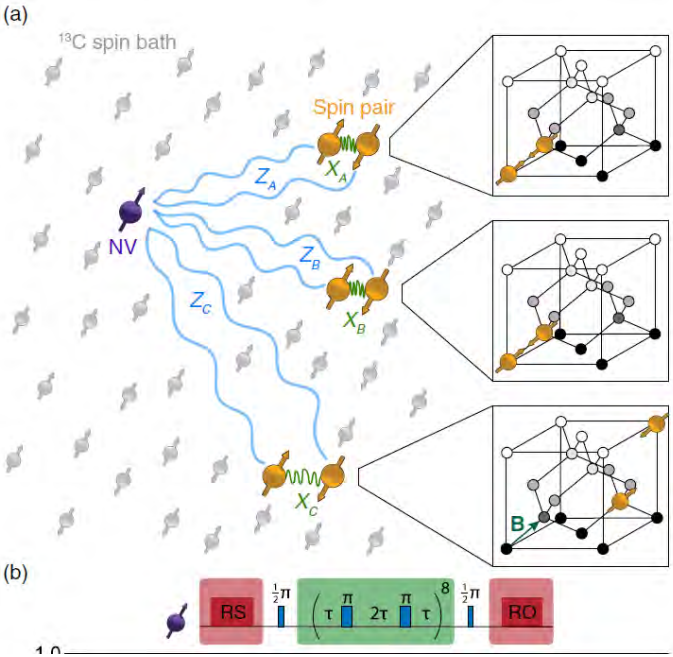

Inhomogeneous dephasing time

$$T_2^* = 1.9(3)\ min$$

A combination of a decoherence-free subspace, a clock transition, and a motional narrowing effect

The NV electron spin has a dephasing time of T^*_2 =4.9 µs and a spin echo time of T_2 =1.182 ms.

H. P. BARTLING et al. PHYS. REV. X 12, 011048 (2022)

P#3: SENSORS WITH NV ENSAMBLE

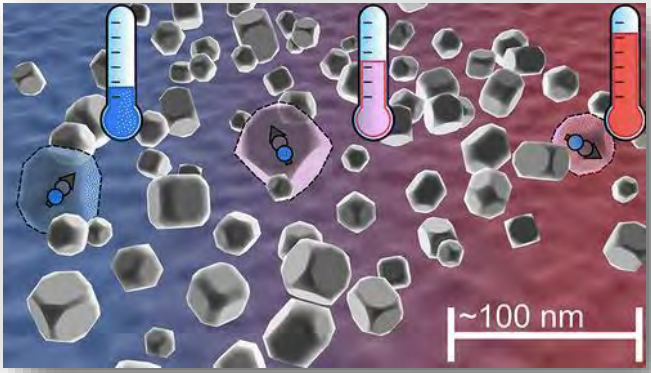

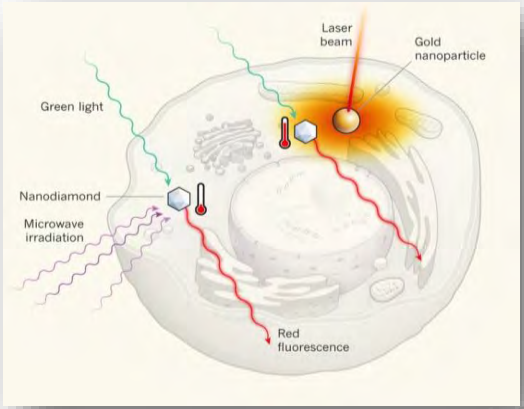

NV FOR NANOSCALE LOCAL MEASUREMENTS

Magnetic fields

NMR spectr on a $(5\ nm)^3$ volume →

Staudacher et al., (2014)

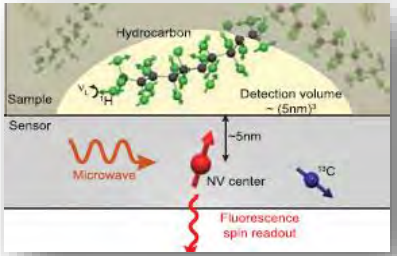

Temperature

Acosta at.el (2010)

Shift: dD(T)/dP = 74 KHz/K

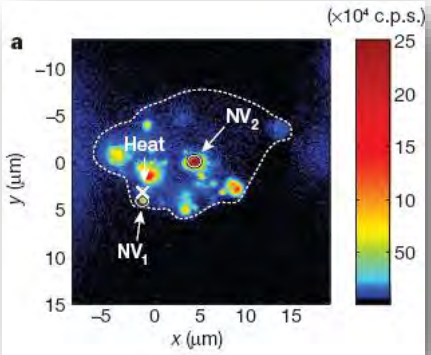

←In living cell
Kucsko at.el (2013)

Pressure

Doherty et al., (2014)

ZPL, ODMR shift:

dD(P)/dP = 14.58 MHz/GPa

Single charge nanoscale detection (electrometer)

Dolde et al, (2014)→

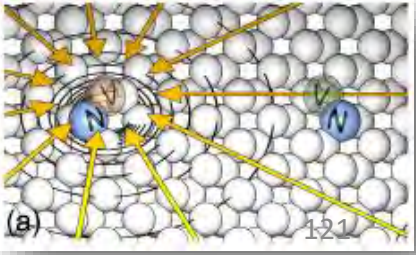

STRUCTURES FOR SINGLE PHOTON SOURCE

Photonic-crystal-fiber-coupled photoluminescence interrogation of nitrogen vacancies in diamond nanoparticles

I.V. Fedotov[1], N.A. Safronov[1], Yu.A. Shandarov[1], A.Yu. Tashchilina[1], A.B. Fedotov[1], A.P. Nizovtsev[2], D.I. Pustakhod[2], V.N. Chizevski[2], K. Sakoda[3], S.Ya. Kilin[2], A.M. Zheltikov[1,4,*]

Article first published online: 2 DEC 2011

DOI: 10.1002/lapl.201110112

Issue

Laser Physics Letters
Volume 9, Issue 2, pages 151–154, February 2012

(а)

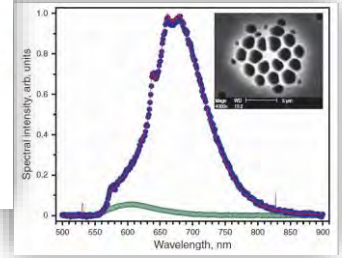

(б)

Фотонно-кристаллический волоконный источник света с порами, заполненными нанокристалами алмаза с NV центрами (а). Спектр фотолюминесценции такого источника (б)

122

FIBER-OPTIC MAGNETIC-FIELD IMAGING

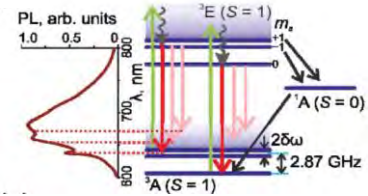

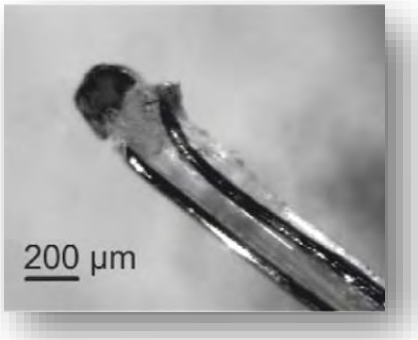

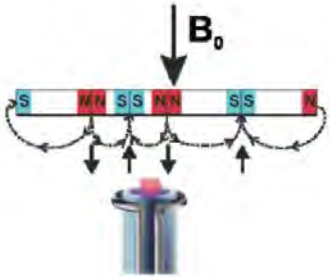

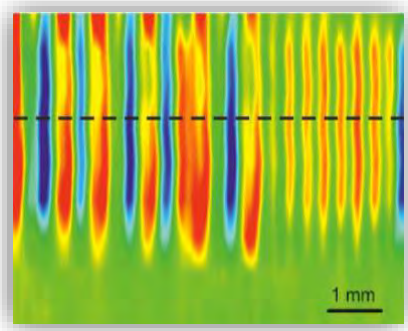

The sensitivity of magnetic field measurements

$\eta \approx 300\ \mathrm{nT} \cdot \mathrm{Hz}^{-1/2}$ → $10\ \mathrm{pT} \cdot \mathrm{Hz}^{-1/2}$

Fedotov et al. OPTICS LETTERS / Vol. 39, No. 24 / December 15, 2014

123

NV

Fiber-optic magnetic-field imaging, I. V. Fedotov, et.al, Opt. Lett. 39, 6954 (2014).

Fiber-optic vectorial magnetic-field gradiometry S. M. Blakley, et.al, Opt. Lett. 41, 2057 (2016).

Room-temperature magnetic gradiometry with fiber-coupled NV centers in diamond S. M. Blakley, et.al, Opt. Lett. 40, 3727 (2015).

All-Optical Brain Thermometry in Freely Moving Animals

Ilya V. Fedotov, Maxim A. Solotenkov, Matvey S. Pochechuev, Olga I. Ivashkina, Sergei Ya. Kilin, Konstantin V. Anokhin, and Aleksei M. Zheltikov*

Cite This: *ACS Photonics* 2020, 7, 3353–3360

Read Online

GeV

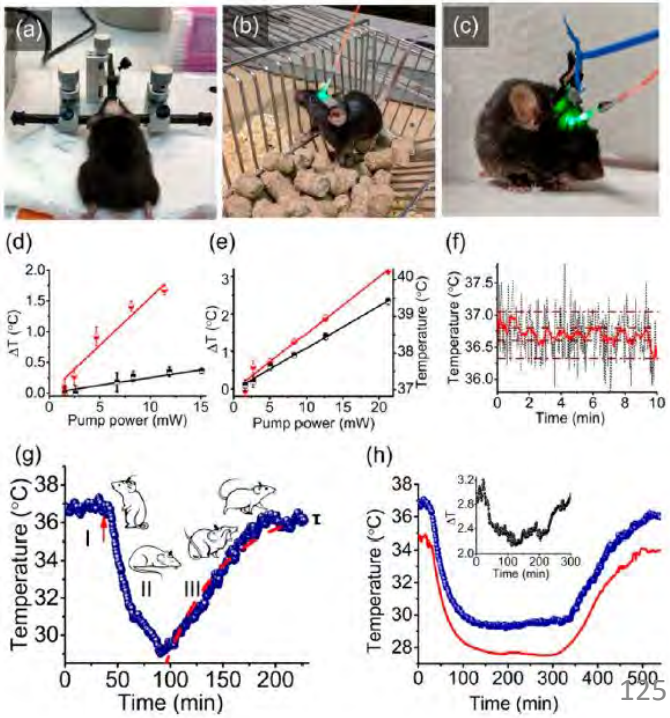

THE ZERO-FIELD-LEVEL ANTICROSSING (ZFLAC) MICROWAVE-FREE SENSOR

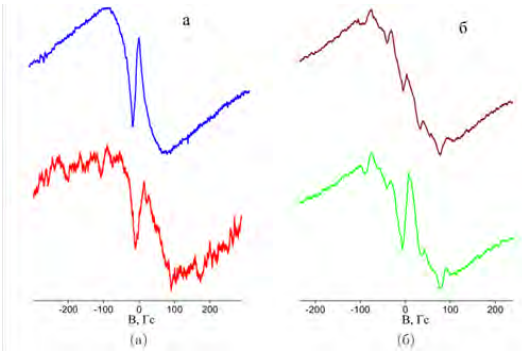

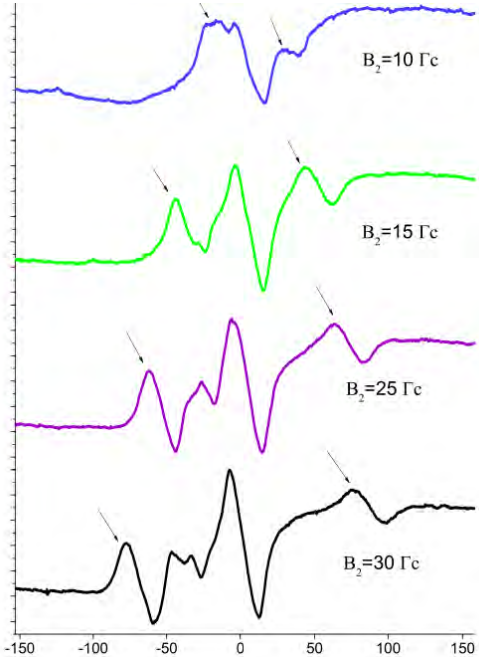

D. S. Filimonenko, V. M. Yasinskii, A. P. Nizovtsev, S. Y. Kilin, F. Jelezko, J. Appl. Spectrosc. 2022, 88, 1131.

WHAT NEXT ?

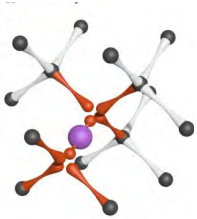

H3 (NVN), SiV, GeV, SnV

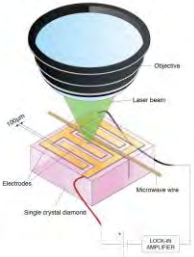

PHOTOELECTRICAL DETECTION

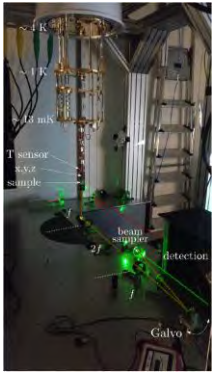

EXPERIMENTS @ mK

FLAG PROTOCOL

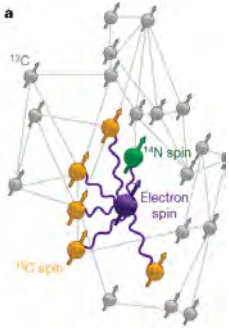

QUNTUM DATA ANALISIS

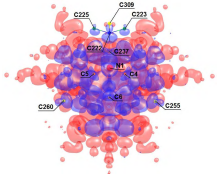

SPIN CARTOGRAPHY

THANK YOU!